



RESEARCH MEMORANDUM

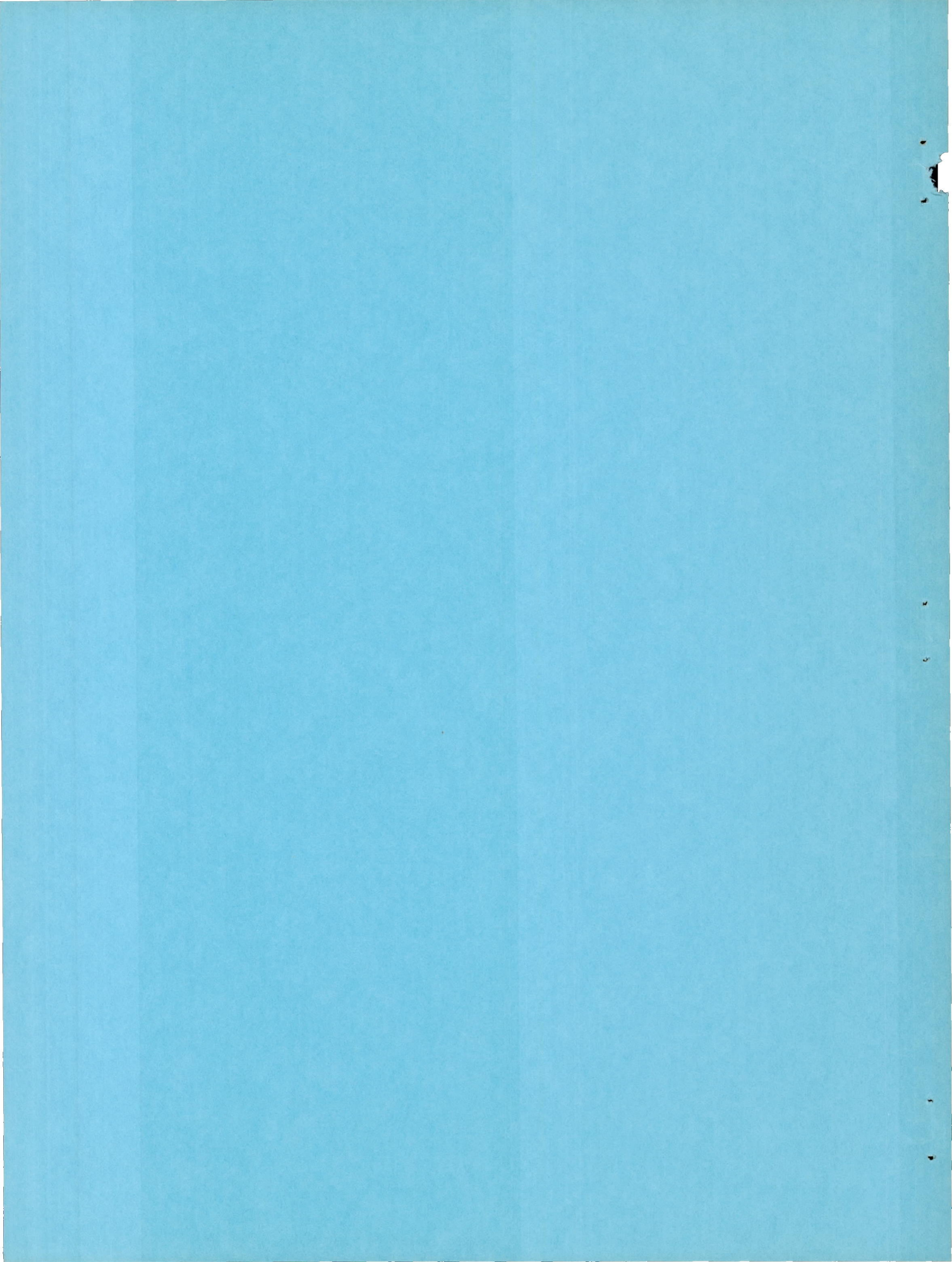
AN INVESTIGATION AT LOW SPEED OF A LARGE-SCALE TRIANGULAR
WING OF ASPECT RATIO TWO.- III. CHARACTERISTICS OF
WING WITH BODY AND VERTICAL TAIL

By Adrien E. Anderson

Ames Aeronautical Laboratory
Moffett Field, Calif.

NATIONAL ADVISORY COMMITTEE
FOR AERONAUTICS
WASHINGTON

October 14, 1949
Declassified June 11, 1953



NATIONAL ADVISORY COMMITTEE FOR AERONAUTICS

RESEARCH MEMORANDUMAN INVESTIGATION AT LOW SPEED OF A LARGE-SCALE TRIANGULAR
WING OF ASPECT RATIO TWO.- III. CHARACTERISTICS OF
WING WITH BODY AND VERTICAL TAIL

By Adrien E. Anderson

SUMMARY

An investigation has been made to determine the aerodynamic characteristics in sideslip of a triangular wing of aspect ratio 2.04 in combination with a body of fineness ratio 12.5 and a vertical tail surface. The airfoil section was a modified symmetrical double wedge with a maximum thickness of 4.76 percent. Force and moment data were obtained at several angles of sideslip for various deflections of constant-chord split flaps, semispan split-flap-type ailerons, and a constant-chord rudder. The Reynolds number, as based on the mean aerodynamic chord, was approximately 15.4×10^6 and the Mach number 0.13.

The results of this investigation show that the body combined with the triangular plan-form wing caused no sizable changes in the lift characteristics of the wing and caused only a 1-percent decrease in the static margin. Flap lift and pitching-moment effectiveness decreased proportional to the decrease in flap area caused by the addition of the body. The wing with body and vertical tail exhibited positive dihedral effect throughout the lift range. Directional stability, however, decreased with increasing lift and the model became directionally unstable at high lift coefficients. In contrast, rudder effectiveness remained nearly constant throughout the lift range. The contribution of the vertical tail to the directional stability and the rudder yawing effectiveness could be predicted with reasonable accuracy at zero wing lift.

INTRODUCTION

A general study of triangular-plan-form wings has been undertaken in the Ames 40- by 80-foot wind tunnel to determine their characteristics at low speed and large scale. The study of such a plan form having a symmetrical double-wedge airfoil section was reported in reference 1. An investigation into the effects on the longitudinal characteristics of airfoil-section modifications was carried out and reported in reference 2. This report, the third of the series, contains

the results of the investigation into the effects of sideslip on the characteristics of the wing alone, the wing plus body, and the wing plus body and vertical tail.

NOTATION

The standard NACA coefficients and symbols used within this report are defined as follows and in figure 1:

- A aspect ratio $\left(\frac{b^2}{S}\right)$
- b wing span, feet
- c wing chord, measured parallel to air stream, feet
- \bar{c} mean aerodynamic chord, measured parallel to air stream
- $$\left(\frac{\int_0^{b/2} c^2 dy}{\int_0^{b/2} c dy}\right), \text{ feet}$$
- C_L lift coefficient $\left(\frac{\text{lift}}{qS}\right)$
- C_D drag coefficient $\left(\frac{\text{drag}}{qS}\right)$
- (Drag, as used herein, is defined as the component of the resultant force acting along the X axis, fig. 1.)
- C_{DT} increment of drag coefficient due to wind-tunnel-wall interference
- C_Y side-force coefficient $\left(\frac{\text{side force}}{qS}\right)$
- (Side force, as used herein, is defined as the component of the resultant force acting along the Y axis, fig. 1.)
- C_m pitching-moment coefficient $\left(\frac{\text{pitching moment}}{qS\bar{c}}\right)$
- C_l rolling-moment coefficient $\left(\frac{\text{rolling moment}}{qSb}\right)$
- C_n yawing-moment coefficient $\left(\frac{\text{yawing moment}}{qSb}\right)$

$C_{l\beta}$	rate of change of rolling-moment coefficient with sideslip, per degree
$C_{n\beta}$	rate of change of yawing-moment coefficient with sideslip, per degree
$C_{n\beta t}$	rate of change with sideslip of yawing-moment coefficient contributed by the vertical tail, per degree
$C_{Y\beta}$	rate of change of side-force coefficient with sideslip, per degree
$C_{N\alpha_t}$	rate of change of tail normal-force coefficient with tail angle of attack, per degree
F	ratio of exposed rudder area to total rudder area
l	tail length, feet
L/D	lift-drag ratio
q	free-stream dynamic pressure, pounds per square foot
q_t	dynamic pressure at tail surface, pounds per square foot
S	wing area, square feet
S_t	vertical tail area to the body center line, square feet
V	free-stream velocity, feet per second
V_y	velocity component at tail due to separation vortices, feet per second
V_R	resultant velocity at tail, feet per second
y	spanwise distance, outboard from wing center line, feet
α	free-stream angle of attack, degrees
α_T	increment of angle of attack due to wind-tunnel-wall interference, degrees
α_t	angle of attack of vertical tail surface, degrees
β	angle of sideslip, degrees
δ_a	split-flap-type aileron deflection, measured perpendicular to hinge line, degrees (Subscripts L and R designate left and right aileron, respectively.)

δ_f	split-flap deflection, measured perpendicular to hinge line, degrees
δ_r	rudder deflection, measured perpendicular to hinge line, degrees
$\frac{d\alpha_t}{d\delta_r}$	rate of change of angle of attack of the vertical tail with rudder deflection for constant tail normal-force coefficient
σ	increment of tail angle of attack above that due to the angle of sideslip, produced by sidewash at the tail, degrees

EQUIPMENT

The principal dimensions of the model are given in figure 2(a) and table I. The airfoil section of the wing, taken in the streamwise direction, was developed from a symmetrical double-wedge airfoil section as described in figure 2(b). Coordinates for the body of fineness ratio 12.5 used in this investigation are presented in table II. The vertical tail had a symmetrical double-wedge airfoil section with a maximum thickness of 5-percent chord at 50-percent chord. Split-flap-type control surfaces were used on the wing, negative flap deflections being obtained by placing the flaps on the upper surface of the wing. A gap was produced in the span of the flaps by the presence of the tail boom used with the wing-alone model.

The photographs of figure 3 show the model as mounted in the Ames 40- by 80-foot wind tunnel.

TESTS AND CORRECTIONS TO DATA

Force and moment data were obtained through the angle-of-attack range at various angles of sideslip for the wing alone, wing plus body, and wing plus body and vertical-tail configurations as outlined in table III. The investigation was conducted at a dynamic pressure of 25 pounds per square foot, which corresponds to a Mach number of approximately 0.13 and a Reynolds number of approximately 15.4×10^6 based on the mean aerodynamic chord.

The force and moment data are presented with reference to the stability axes with the origin located at the half-chord station of the root chord of the modified wing. The latter point corresponds to the same longitudinal station as the quarter-chord station of the mean aerodynamic chord.

All of the force data have been corrected for air-stream inclination and for wind-tunnel-wall effect, the latter correction being that for a wing of the same span having elliptic loading but with an unswept plan form. The following corrections were applied:

$$\alpha_T = 0.719 C_L$$

$$C_{DT} = 0.01255 C_L^2$$

Drag and pitching-moment tares resulting from strut interference, based on tares obtained with a rectangular wing, were applied to the data.

RESULTS AND DISCUSSION

The basic results are presented in figures 4 to 19 and are summarized in figures 20 to 28.

The discontinuities which will be noted in the force and moment curves for the wing-alone model (figs. 4 to 6) correspond to those which were a characteristic of the model with the double-wedge airfoil section (reference 1). Discussion of these discontinuities and of the flow over triangular wings will be found in references 1, 2, and 3.

Longitudinal Characteristics

Lift.— The body added to the triangular wing supported a lift equal to the lift normally carried by the wing area it covered. That this was the case can be seen by a comparison of the lift curve for the flaps-undeflected condition of the wing alone (fig. 4(a)) with the lift curve for the flaps-undeflected condition of the wing plus body (fig. 7(a)). The lift-curve slope through zero lift in each case was 0.039 per degree. The value of $C_{L_{max}}$ for the wing-alone model was 1.34. Interference of the body nose with the top of the wind-tunnel test section made it impossible to reach the angle of attack for $C_{L_{max}}$ of the wing-body model. However, the near coincidence of the two lift curves up to within 2° or 3° of the angle for maximum lift (of the wing alone) makes it appear likely that there was little or no change in the value of $C_{L_{max}}$ when the body was added.

Pitching moment.— The addition of the body to the wing caused only a slight forward shift of the aerodynamic-center location. The slopes of the pitching-moment curves (slopes taken over the lift-coefficient range between 0 and 0.4 in figs. 4(c) and 7(c)) indicate a shift of the aerodynamic center from 38.5 to 37.2 percent of the mean aerodynamic chord. This shift is about one-quarter the amount computed by adding body-alone data, obtained in the Ames 40- by 80-foot wind tunnel, to the wing-alone data.

Split-flap effectiveness.— In general, the flaps produced 20 percent less lift with the body on than with the body off. It is of interest to note that the decrease in flap effectiveness was in proportion to the decrease in flap area (20 percent) rather than to the

decrease in wing area influenced by the flap (a 32-percent decrease). It has been noted also, from the data in reference 4, that a decrease occurred in flap lift effectiveness proportional to the decrease in flap area for a plain flap on a wing of triangular plan form.

It is believed that there was no carry-over of flap lift effectiveness across the body. The incremental span load distribution due to deflecting a plain flap was found, from an investigation conducted in the Ames 40- by 80-foot wind tunnel, to be nearly elliptic in form for a wing-alone model. The portion of the loading for that region of the wing which would be occupied by the body was removed from the loading diagram. The change in the load was found to be very nearly 20 percent of the total load. This agrees with the change found by the force test reported herein and would indicate little or no carry-over of lift due to flap deflection.

It should also be noted that, as reported in reference 1, the variation of lift with flap deflection was nonlinear, and the variation was found to be dependent upon the flow conditions over the wing; for example, whether the angle of attack was above or below the angle for the break in the lift curve. (In fig. 20, the angles of attack of 0° and 8° represent values below the break while the angles of 19° and 24° represent those above.)

It appears from the lift curves of figure 4(a) that split flaps are of little or no value as a means of increasing $C_{L_{max}}$. Large flap deflections resulted in a reduced value of $C_{L_{max}}$.

The pitching-moment effectiveness of the flaps is represented in figure 21 by the increments of pitching-moment coefficient due to a given flap deflection for the same angles of attack at which the lift increments were presented in figure 20. The change in the increment of pitching moment, due to the addition of the body, was also found to be nearly proportional to the change in flap area.

Lift-drag ratios.— Adding the body to the wing reduced the $(L/D)_{max}$ value from 11 to 8.5. (See fig. 22(a).) At the same time the lift coefficient for $(L/D)_{max}$ was raised from 0.15 to 0.20. Both these effects would be expected due to the added drag of the body. The effect of flap deflection on the L/D values for the wing plus body model is presented in figure 22(b). With the controls deflected up, as needed for trim, there was an appreciable loss in L/D throughout the entire lift range.

Lateral and Directional Characteristics

Lateral and directional stability.— The stability derivatives presented in figure 23 represent the slope through zero angle of sideslip of the curves of C_l , C_n , and C_y as functions of β (C_L constant). It

was pointed out in reference 1 that the variation of these coefficients with sideslip was not always linear for the triangular wing with the sharp leading edge, particularly at the higher lift coefficients. Sample curves of C_L , C_n , and C_y versus sideslip angle for the models reported herein are presented in figure 24. While some nonlinearities exist, they are not as severe as for the wing with sharp leading edge.

All three model configurations had a positive dihedral effect as will be seen from figure 23. When the body was added, $C_{L\beta}$ became more negative, particularly at the higher values of C_L . On the other hand, $C_{L\beta}$ became more negative at the lower values of C_L with the addition of the vertical tail.

The wing alone was directionally stable up to the stall and the addition of the vertical tail overcame, up to a C_L of 0.7, the directional instability caused by the body. Between a C_L of 0.7 and 1.1, however, the directional stability of the model with body and tail decreased to zero and, by the time wing stall was reached, was considerably negative. This loss in directional stability is traceable to the increments of yawing-moment coefficient contributed by the vertical tail. Above a C_L of 0.7 these increments decreased to nearly zero at a rate which increased with angle of sideslip. (See fig. 25.) Such a loss in directional stability is apparently connected with the effect on the vertical tail of the separation-vortex type of flow which exists over this wing. (Consult reference 3 for a description of the separation vortices.) That it was not connected with a loss in dynamic pressure at the tail is indicated by the rudder-effectiveness data as will be discussed later.

The influence of the separation vortices on the angle of attack of the vertical tail may very well account for the loss in tail effectiveness. The pattern of the separation vortices over the wing in sideslip is shown in figure 26(a). The apparent point of origin of the separation vortices moves inboard with angle of attack. In side view, the vortices form an angle with respect to the chord plane of the wing. The magnitude of this angle is approximately one-third of the angle of attack of the wing. Thus, in the view looking upstream (fig. 26(b)) the vertical displacement of the vortices, back at the tail, increases with increase in wing angle of attack. The vortex on the right side moves closer to the plane of the vertical tail than does the vortex on the left, for the model is in positive sideslip and hence the vortices are under the influence of the free-stream air flow from the right. The effective angle of attack on the upstream panel of a triangular plan-form wing in sideslip is greater than that on the downstream panel. Consequently, the strength of the vortex on the right in figure 26(b) will be greater than that of the one on the left for a given wing angle of attack. Above the core of the vortices and in the plane of the vertical tail, then, there will be a velocity component to the left which is the resultant of the velocity vectors from the two vortex flows. Below the core of the vortices there will be a velocity component to the right.

Consideration is now given to the velocity vectors on two sections of the vertical tail: one near the top of the tail (fig. 26(c)) and one near the base (fig. 26(d)). The angle of attack of the section near the top of the tail increases with increases in the angle of attack of the wing. It is quite likely, therefore, that this section stalls, if it were not stalled initially. (It was shown in reference 3 that the tips of triangular plan-form wings stall at a very low angle of attack.) On the section near the base of the tail, the component of velocity contributed by the vortices reverses direction with increase in angle of attack of the wing. As a result the angle of attack of this section of the tail decreases with a consequent loss in side force produced by the tail. The influence of the separation vortices appears, therefore, to account for the loss in tail effectiveness with increasing lift coefficient.

Rudder effectiveness.— The increments of C_L , C_n , and C_Y per degree of rudder deflection were found, on the basis of a 10° rudder deflection, to be essentially independent of sideslip up to a C_L of 0.7 (fig. 27). Above this value of C_L , the curves for constant values of the sideslip angle are no longer coincident, particularly at the larger angles of sideslip. It is of interest to note that there was no loss in rudder effectiveness. This is in contrast to the loss of effectiveness of the vertical tail when the model was at high lift coefficients and would indicate that there was apparently no serious loss in dynamic pressure at the tail.

Aileron effectiveness.— Although adding the body to the wing reduced the flap area considerably, the moment of the flap area about the fuselage center line decreased only negligibly. Thus, the increment of rolling moment per degree of aileron travel was nearly the same for the wing plus body as for the wing alone. (See fig. 28.) In both cases the ailerons were deflected approximately equal amounts in the direction to give positive roll. Rolling effectiveness decreased with both increasing C_L and β . The yawing-moment curves of the same figure indicate the existence of a small amount of adverse yawing moment which increased with lift coefficient, but was little affected by sideslip below $0.9 C_L$. Certain of the curves of figure 28 exhibit nonlinearities near the stall, a characteristic similar to that reported in reference 1.

Estimation of Tail and Rudder Effectivenesses

It has already been pointed out that the tail on this model did not provide directional stability at high lift coefficients. It is of interest, however, to determine if the directional stability and rudder effectiveness can be predicted when the model is at zero lift.

The contribution of the vertical tail to the directional stability of the model can be expressed as follows:

$$C_{n_{\beta_t}} = C_{N_{\alpha_t}} \frac{S_t}{S} \frac{l}{b} \left(1 + \frac{d\sigma}{d\beta} \right) \frac{q_t}{q} \quad (1)$$

The equation to predict rudder effectiveness is

$$\frac{dC_n}{d\delta_r} = - C_{N_{\alpha_t}} \frac{d\alpha_t}{d\delta_r} F \frac{S_t}{S} \frac{l}{b} \frac{q_t}{q} \quad (2)$$

The major problem in applying these two equations is in selecting the effective area and aspect ratio of the vertical tail. For most conventional airplane designs the methods of selection have been fairly well established. These methods do not appear applicable, however, to designs similar to the type under discussion. For this type, it is believed that the effective tail area extends to the fuselage center line. With a complete end-plate effect, as in the case where the wing trailing edge extends beyond the tail trailing edge, the tail area covered by the fuselage should be fully effective. This is indicated by the fact that a similar area of the wing was found to be fully effective. With the present wing-tail arrangement, this area of the tail was probably somewhat less fully effective; that is, the effective aspect ratio was somewhat less than twice the geometric aspect ratio. The actual value could not be established without recourse to the experimental data. The increment of $C_{Y_{\beta}}$ due to the tail, expressed in terms of the tail lift-curve slope and compared with theoretical values for triangular wings (reference 5), indicates that the effective aspect ratio was 1.3.

With effective tail area and aspect ratio established, the values of the other factors in the two equations were then selected. The value of the tail length l in equation (1) was taken as the distance from the model moment center to the theoretical center of pressure of the tail (reference 5); for equation (2) the distance was to the rudder hinge line. The value of $d\sigma/d\beta$ was assumed zero and q_t/q was assumed to be unity, since the wing was at zero lift and the fuselage effect was considered negligible. The value of $d\alpha_t/d\delta_r$ was assumed to be the same as that measured on a triangular wing of aspect ratio 2 (reference 4), which had the same geometrical relation between flap and wing as between rudder and tail in the present case. This value was reduced by the factor F of equation (2) or the ratio of the exposed rudder area to the total rudder area.

The following values were thus substituted in the two equations:

$C_{N_{\alpha t}}$	0.027
$\frac{d\alpha_t}{d\delta_r}$.62
F	.845
S_t/S	.218
l/b (equation (1))	.525
l/b (equation (2))	.741
$\frac{d\sigma}{d\beta}$	0
q_t/q	1.00

The computed and experimental values compare as follows:

	$C_{n_{\beta t}}$	$dC_n/d\delta_r$
Computed	0.0031	-0.0023
Experimental	.0032	-.0025

The agreement between the computed and experimental values is thus satisfactory for zero angle of attack and would probably remain satisfactory until the angle of attack is reached at which the flow due to the separation vortices begins to have a strong influence upon the tail characteristics.

CONCLUDING REMARKS

The results of this investigation show that the body combined with the triangular plan-form wing caused no changes in the lift characteristics of the wing and caused only a 1-percent decrease in the static margin. Flap lift and pitching-moment effectiveness decreased proportional to the decrease in flap area caused by the addition of the body. The wing with body and vertical tail exhibited positive dihedral effect

throughout the lift range. Directional stability, however, decreased with increasing lift and the model became directionally unstable at high lift coefficients. Rudder effectiveness, on the other hand, remained nearly constant throughout the lift range. The contribution of the vertical tail to the directional stability and the rudder yawing effectiveness could be predicted with reasonable accuracy at zero wing lift.

Ames Aeronautical Laboratory,
National Advisory Committee for Aeronautics,
Moffett Field, Calif.

REFERENCES

1. Anderson, Adrien E.: An Investigation at Low Speed of a Large-Scale Triangular Wing of Aspect Ratio Two.- I. Characteristics of a Wing Having a Double-Wedge Section With Maximum Thickness at 20-Percent Chord. NACA RM A7F06, 1947.
2. Anderson, Adrien E.: An Investigation at Low Speed of a Large-Scale Triangular Wing of Aspect Ratio Two.- II. The Effect of Airfoil Section Modifications and the Determination of the Wake Downwash. NACA RM A7H28, 1947.
3. Anderson, Adrien E.: Chordwise and Spanwise Loadings Measured at Low Speed on Large Triangular Wings. NACA RM A9B17, 1949.
4. Stephenson, Jack D., and Amuedo, Arthur R.: Tests of a Triangular Wing of Aspect Ratio 2 in the Ames 12-Foot Pressure Wind Tunnel. II - The Effectiveness and Hinge Moments of a Constant-Chord Plain Flap. NACA RM A8E03, 1948.
5. DeYoung, John: Theoretical Additional Span Loading Characteristics of Wings with Arbitrary Sweep, Aspect Ratio, and Taper Ratio. NACA TN 1491, 1947.

TABLE I.— GEOMETRIC DATA OF MODEL USED IN THE INVESTIGATION

Item	Wing alone	Wing with body and vertical tail
Wing		
Span, feet	25.00	25.00
Area, square feet	307	307
Area exposed outside of fuselage, square feet	---	211
Mean aerodynamic chord, feet	16.37	16.37
Angle of incidence, degrees	---	0
Aspect ratio	2.04	2.04
Body		
Length, feet	---	56.16
Maximum diameter, feet	---	4.49
Fineness ratio	---	12.50
Ratio of maximum diameter to wing span	---	0.18
Split-flap-type controls		
Semispan, feet	10.83	8.70
Total area, square feet	57.80	46.46
Total wing area affected by control surface, square feet	301.5	205.5
Vertical tail		
Total area to body center line, square feet	---	66.90
Aspect ratio (total)	---	1.00
Rudder area (exposed), square feet	---	11.50
Rudder area (total), square feet	---	13.62
Tail length ($\bar{c}/4$ to tail center of pressure), feet	---	13.41
Tail length ($\bar{c}/4$ to rudder hinge line), feet	---	18.52



TABLE II.— BODY COORDINATES
[Stations and radii are in percent
of the total length.]

Station		Radius
0	100.00	0
.625	99.375	.26
1.25	98.75	.42
2.50	97.50	.70
5.00	95.00	1.15
7.50	92.50	1.54
10.00	90.00	1.86
15.00	85.00	2.41
20.00	80.00	2.86
25.00	75.00	3.22
30.00	70.00	3.51
35.00	65.00	3.73
40.00	60.00	3.88
45.00	55.00	3.97
50.00	— — —	4.00



TABLE III.- SUMMARY OF CONFIGURATIONS INVESTIGATED

Figure	Angle of sideslip (deg)	Deflection of split flaps (deg)	Deflection (deg)			Data presented
			Left aileron	Right aileron	Rudder	
Wing alone						
4	0.0	-22.0 0 21.2 44.0	---	---	---	CL vs α CD Cm CL CN CY
5	12.1	-22.0 0 21.2 44.0	---	---	---	
6	0.0 12.1	---	11.7	-11.3	---	
Wing + body						
7	0.0	-20.7 -10.8 0 20.4 45.4	---	---	---	CL vs α CD Cm
8	0.0 6.0 12.0 15.9	---	---	---	---	CL vs α CD Cm CL CN CY
9	0.0 6.0 12.0 15.9	-20.7	---	---	---	
10	0.0 6.0 12.0 15.9	20.4	---	---	---	
11	0.0 6.0 12.0 15.9	45.4	---	---	---	
12	0.0	---	10.8 0 0.0	0 0 -10.8	---	
13	0.0	---	10.8 0	-10.8 0	---	
14	12.0	---	-10.8 0 10.8	---	---	CL vs α CD Cm CL CN CY
15	12.0	---	---	-10.8 0 10.8	---	
16	12.0	---	10.8 0	-10.8 0	---	
Wing + body + vertical tail						
17	0.0 6.0 12.0 15.9	---	---	---	0	CL vs α CD Cm CL CN CY
18	0.0 6.0 12.0 15.9	---	---	---	10	
19	0.0 12.0	-20.7	---	---	10	

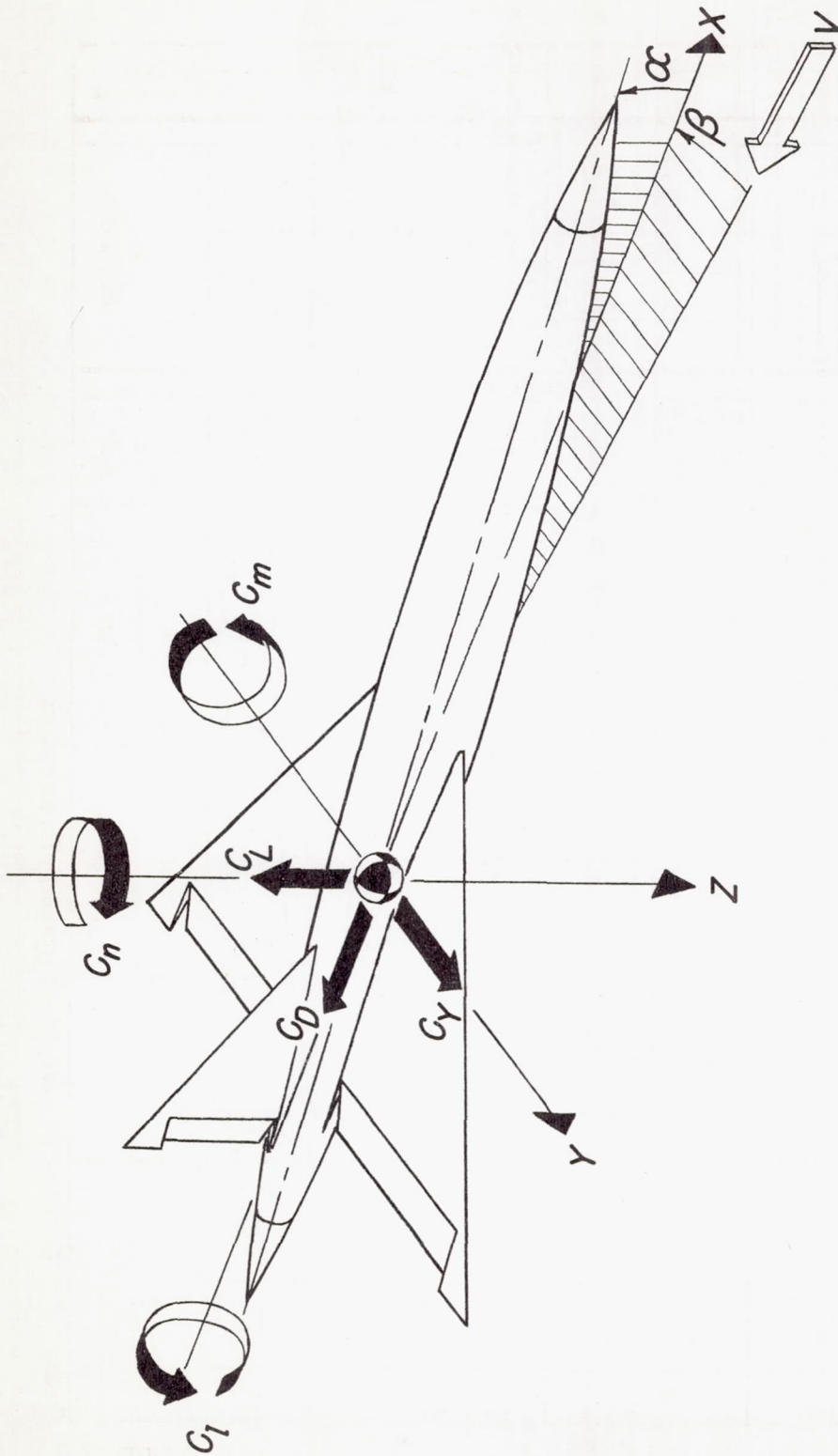
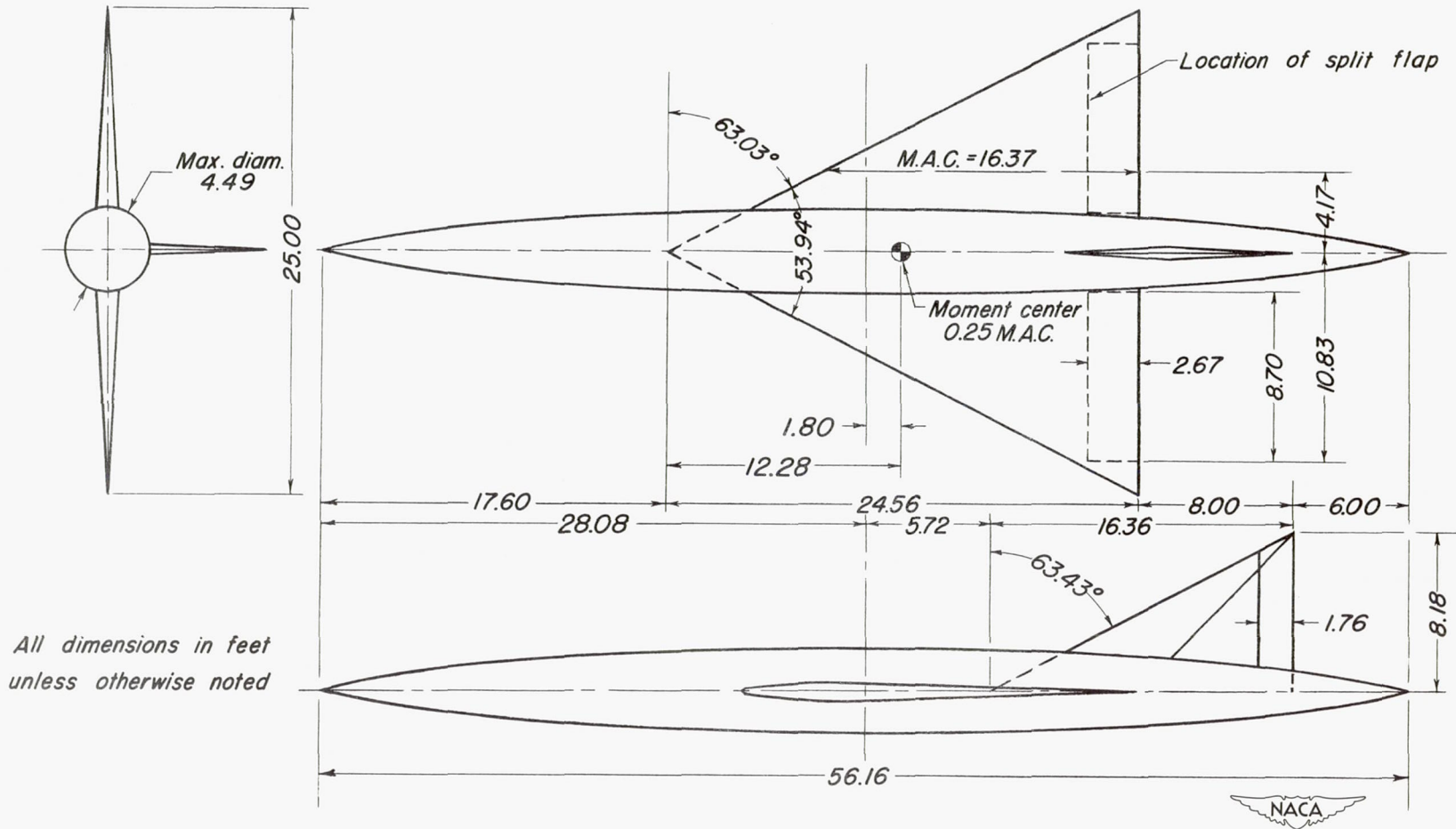


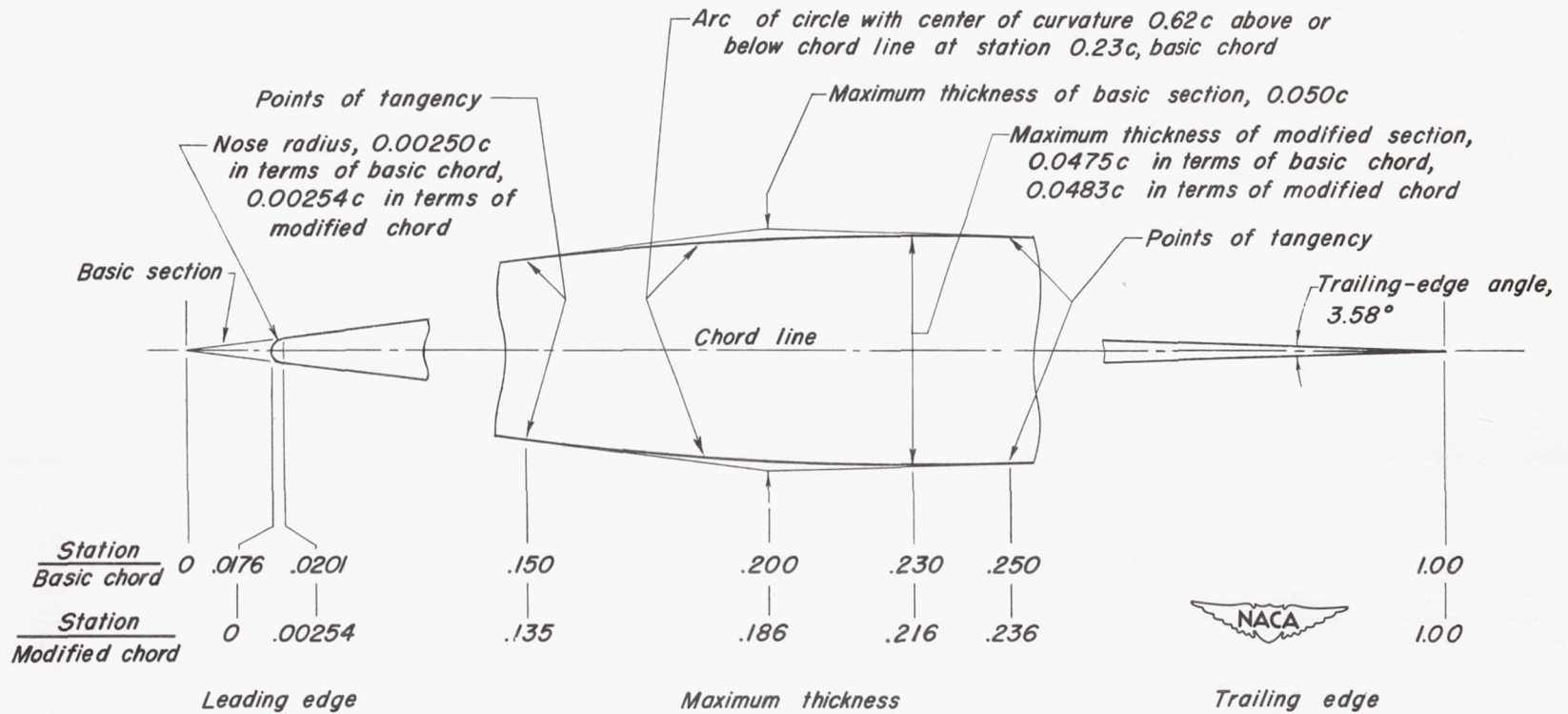
Figure 1.- Sign convention for force and moment coefficients. All forces, moments, angles, control-surface deflections, and axes are shown as positive.





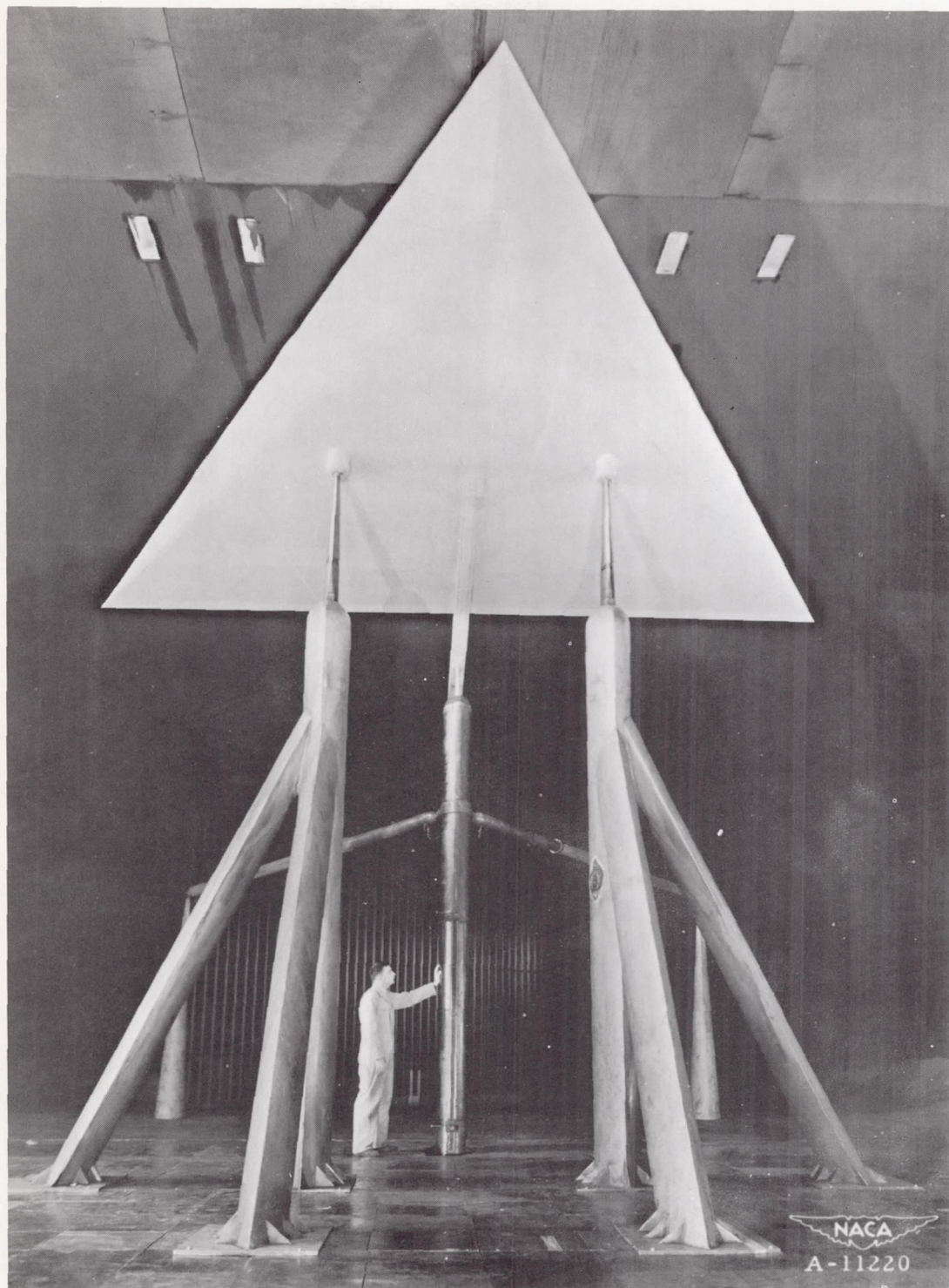
(a) General arrangement of model.

Figure 2.- Geometric details of model investigated.



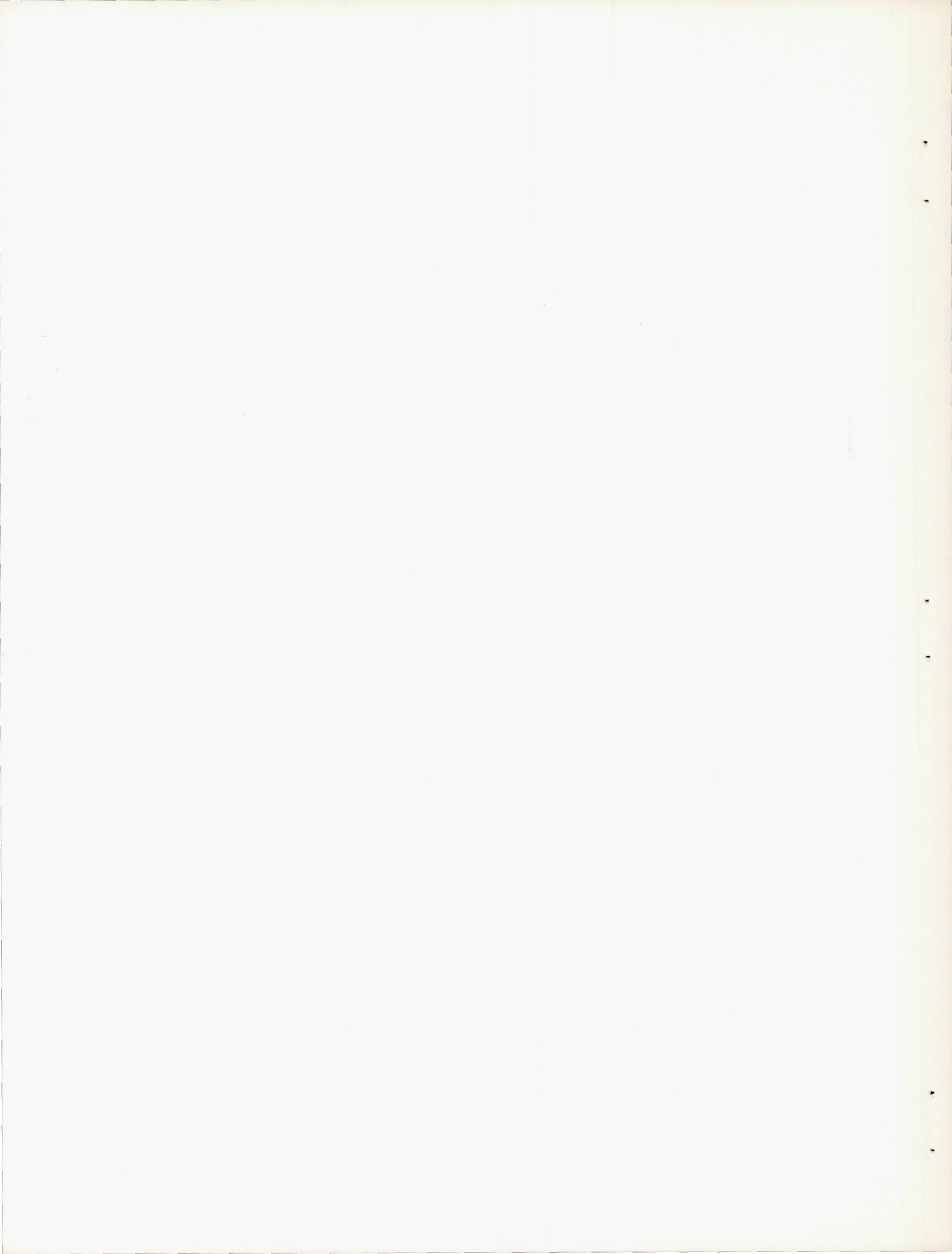
(b) Modified double-wedge airfoil section.

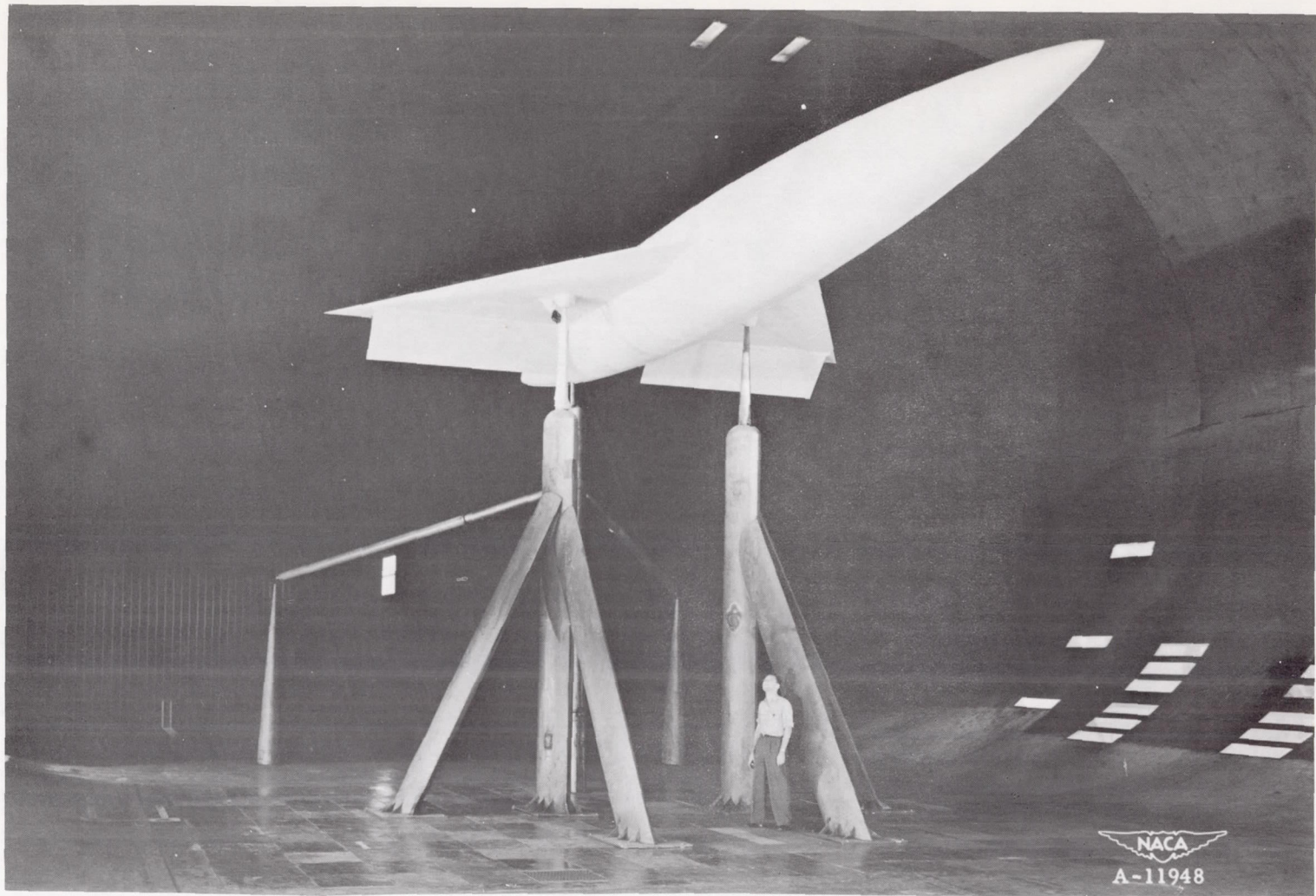
Figure 2.- Concluded.



(a) Wing alone.

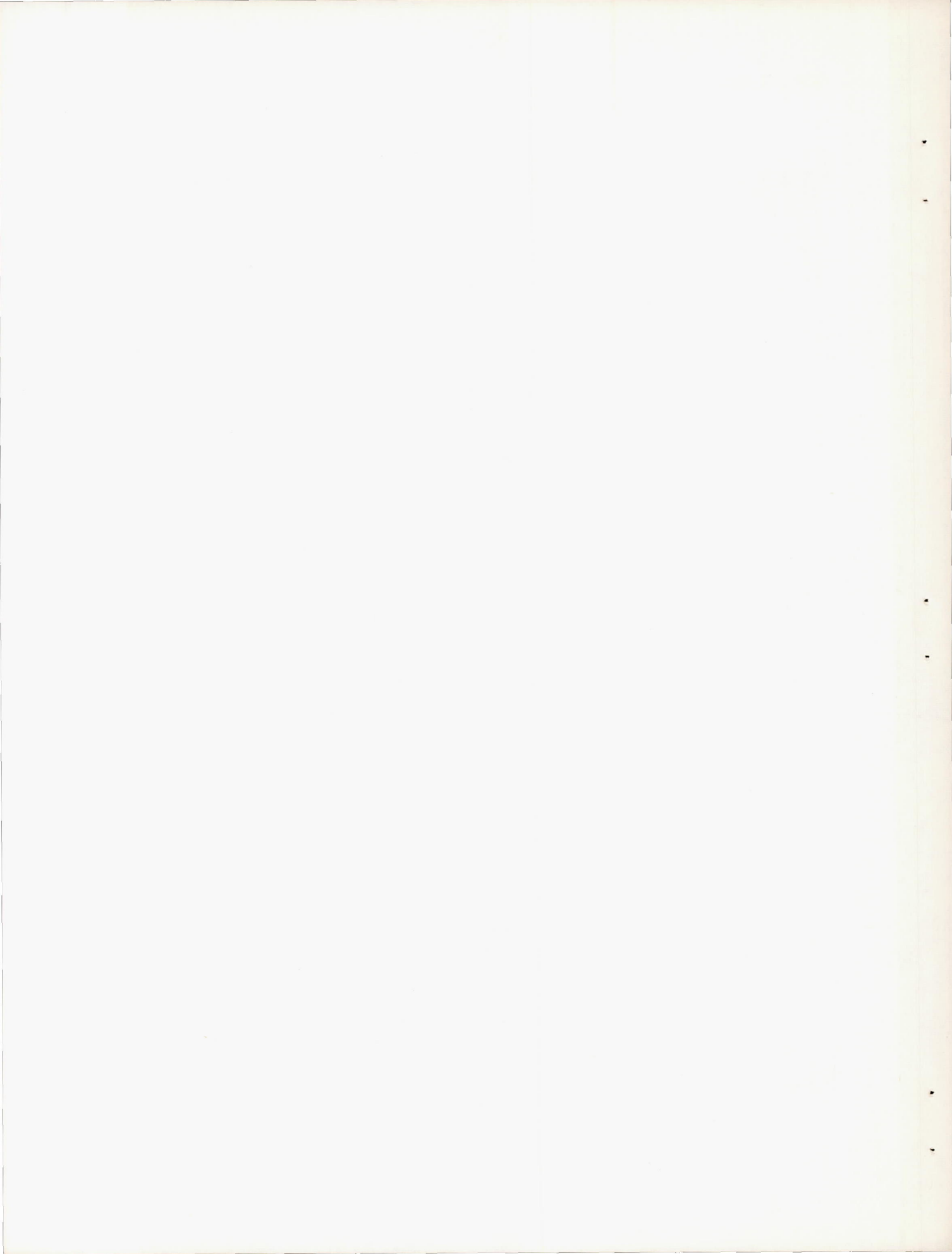
Figure 3.- Triangular plan-form wing as mounted for investigation in the Ames 40- by 80-foot wind tunnel.

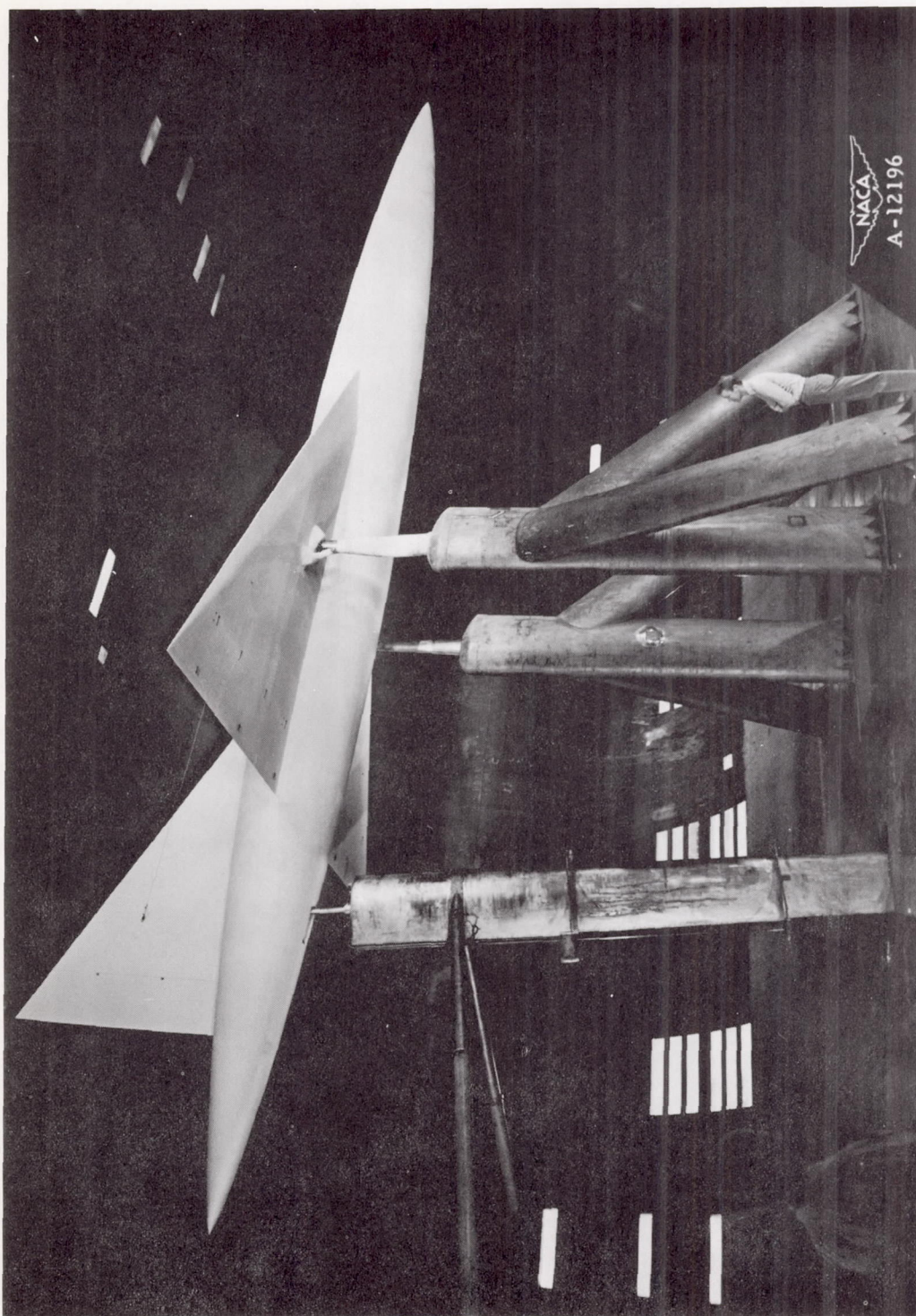




(b) Wing plus body; split flaps deflected 45.4° .

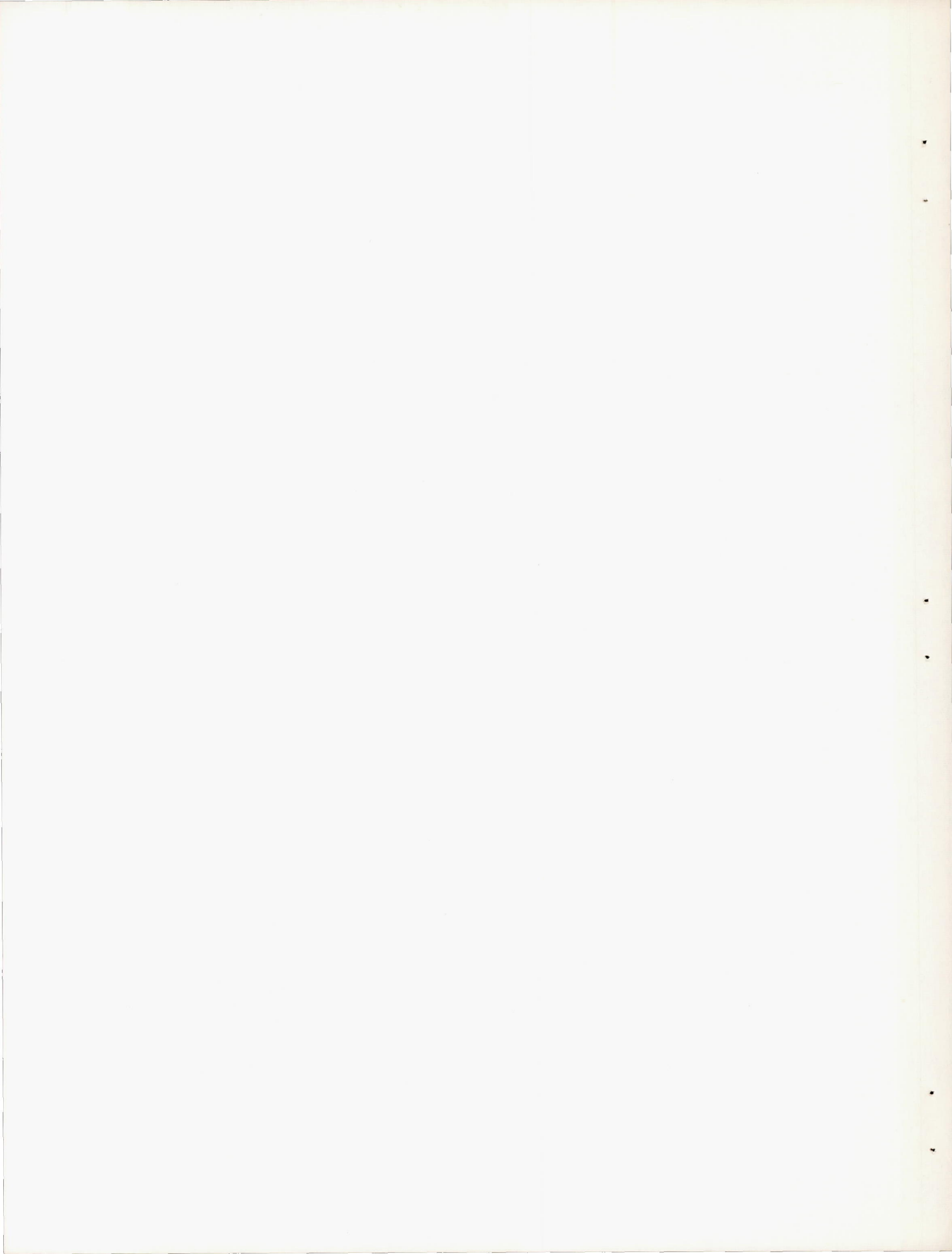
Figure 3.- Continued.

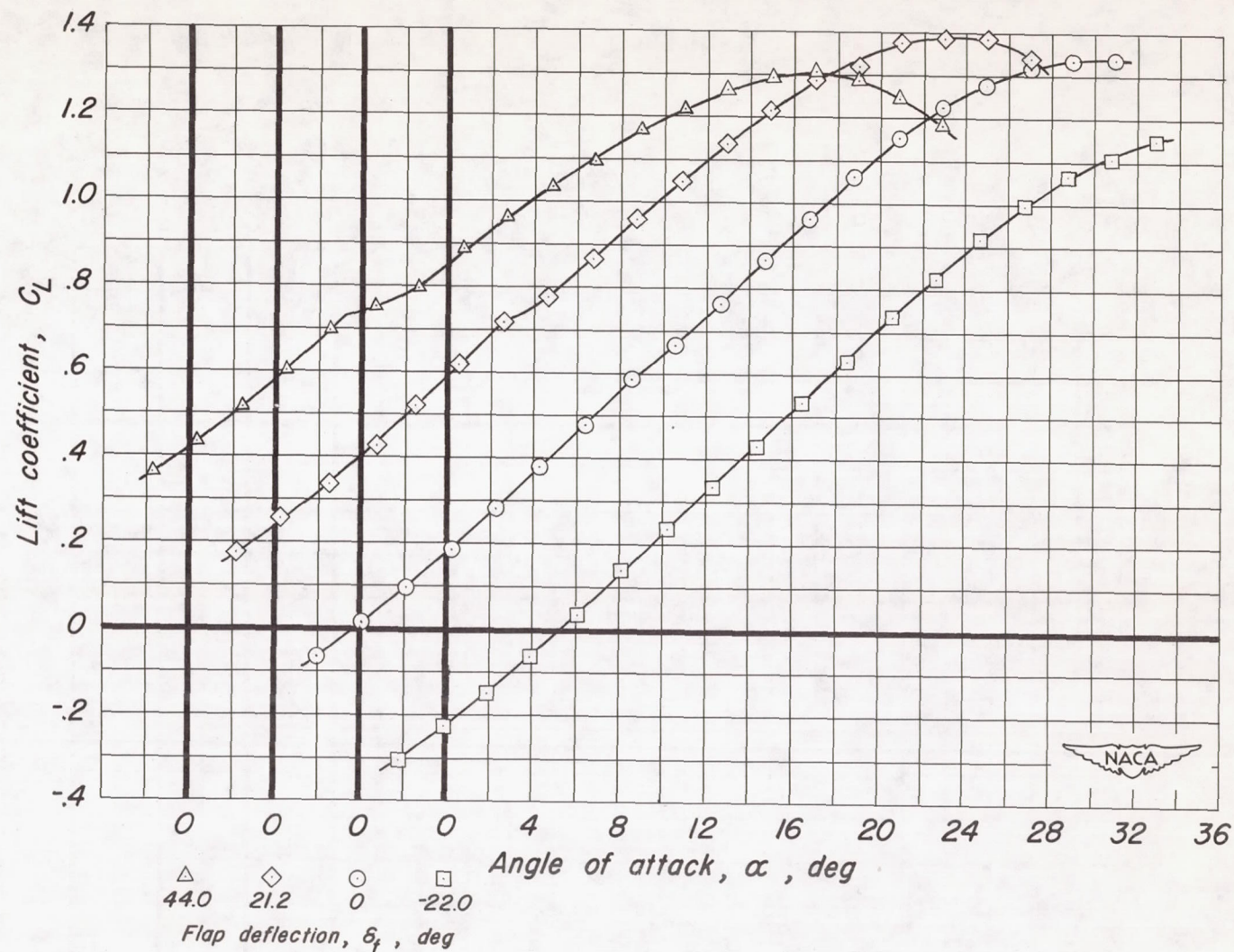


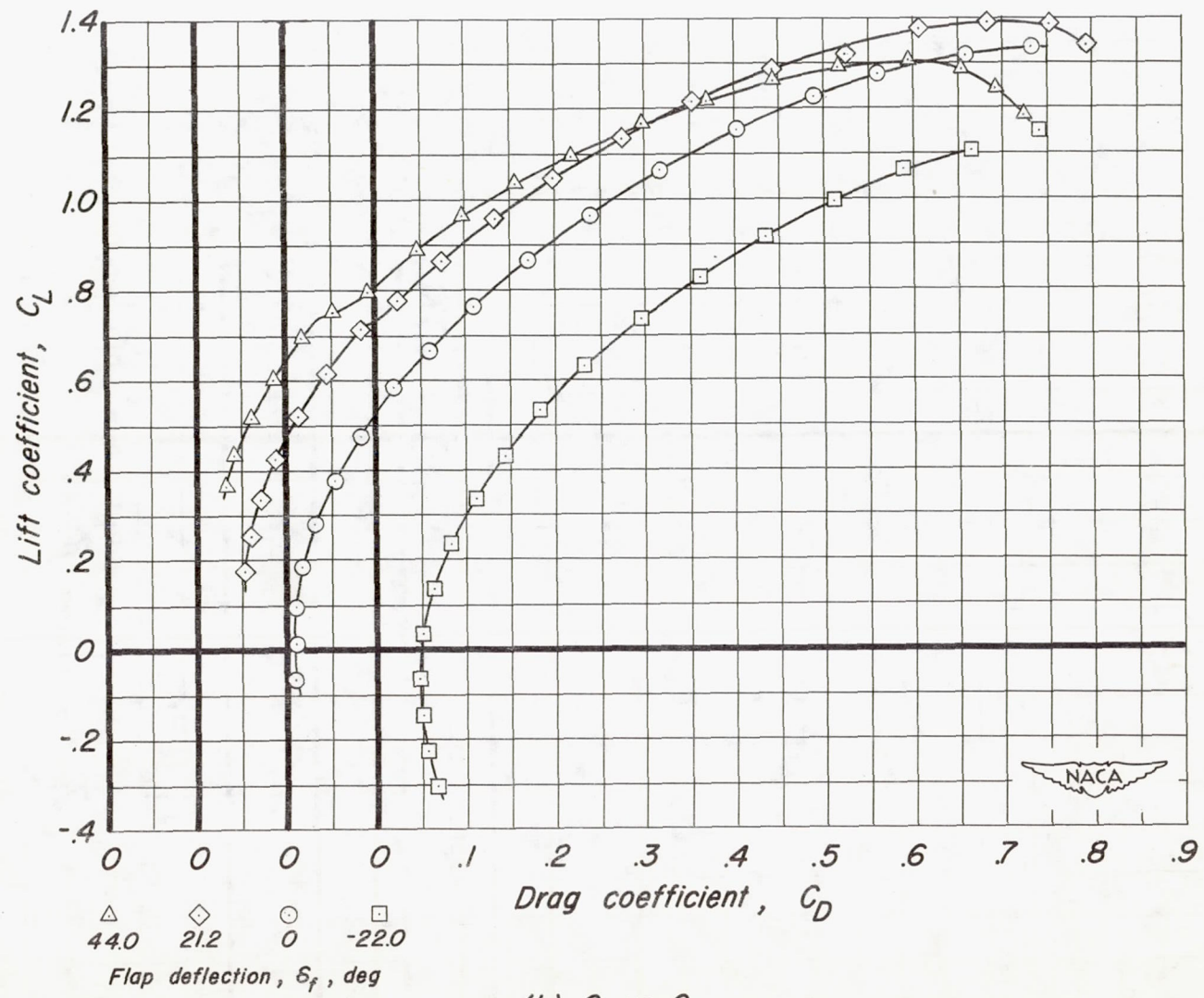


(c) Wing plus body and vertical tail.

Figure 3.- Concluded.



(a) C_L vs α .Figure 4.- Wing alone at 0.0° angle of sideslip with various flap deflections.



(b) C_L vs C_D .

Figure 4. - Continued.

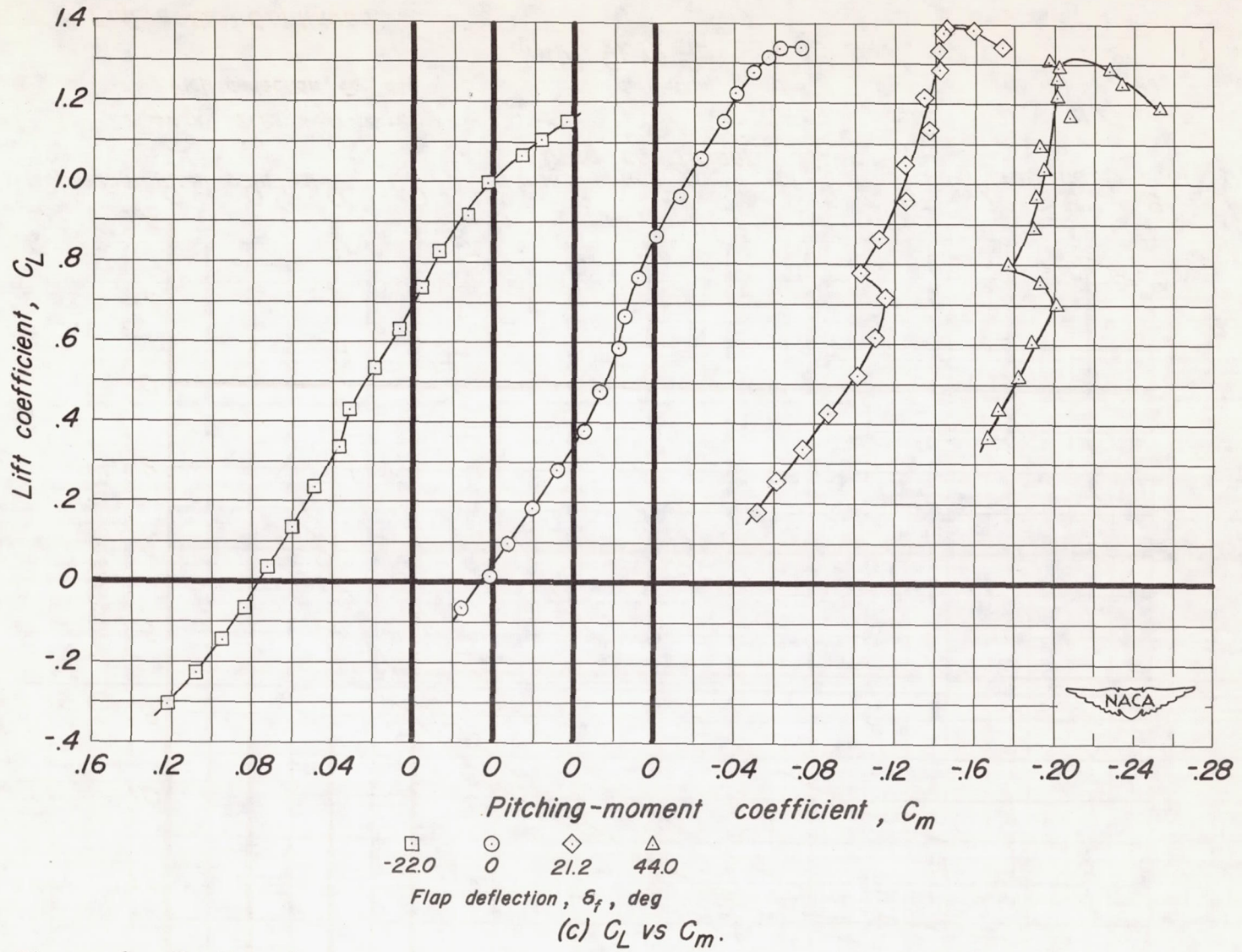


Figure 4.- Continued.

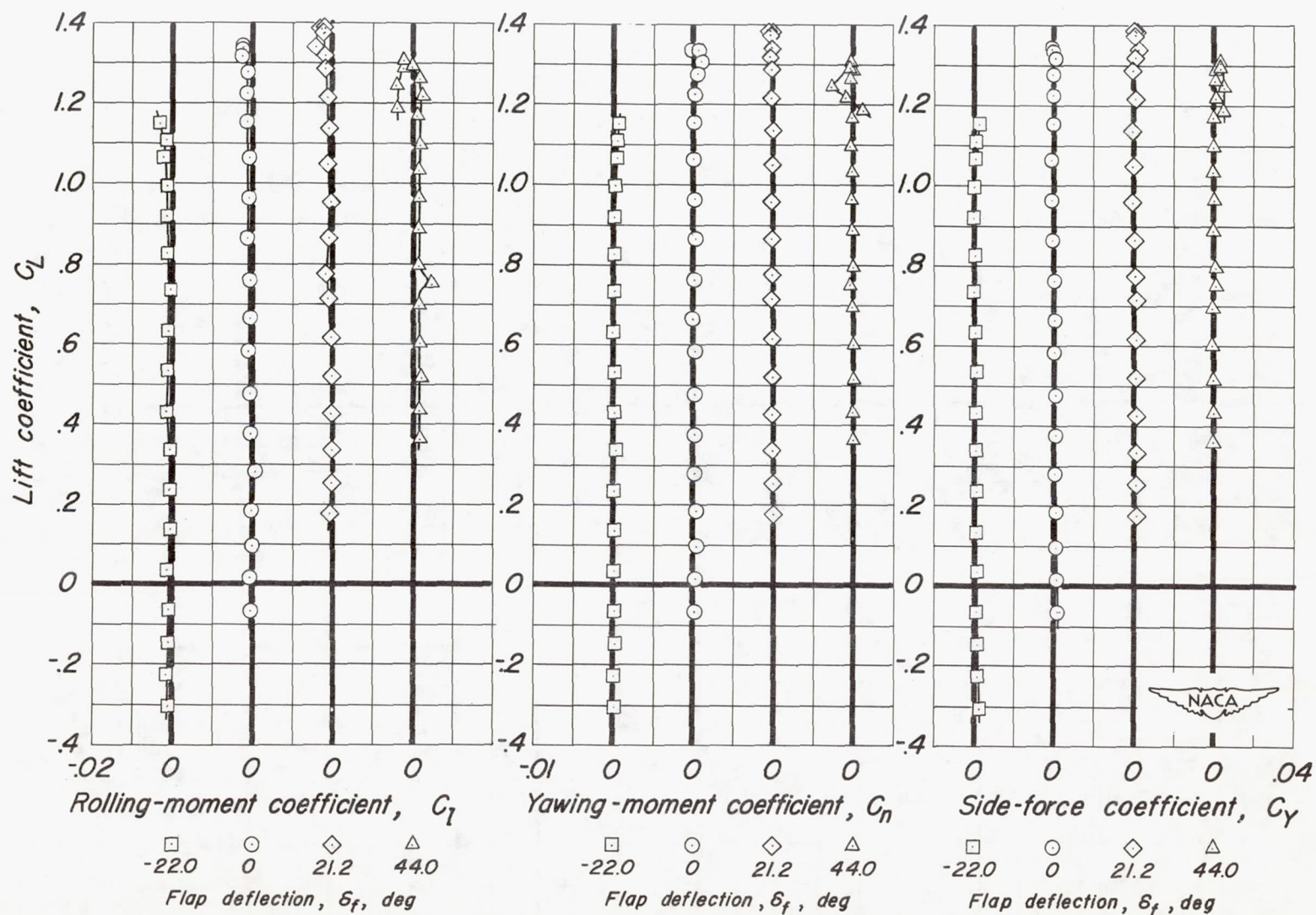
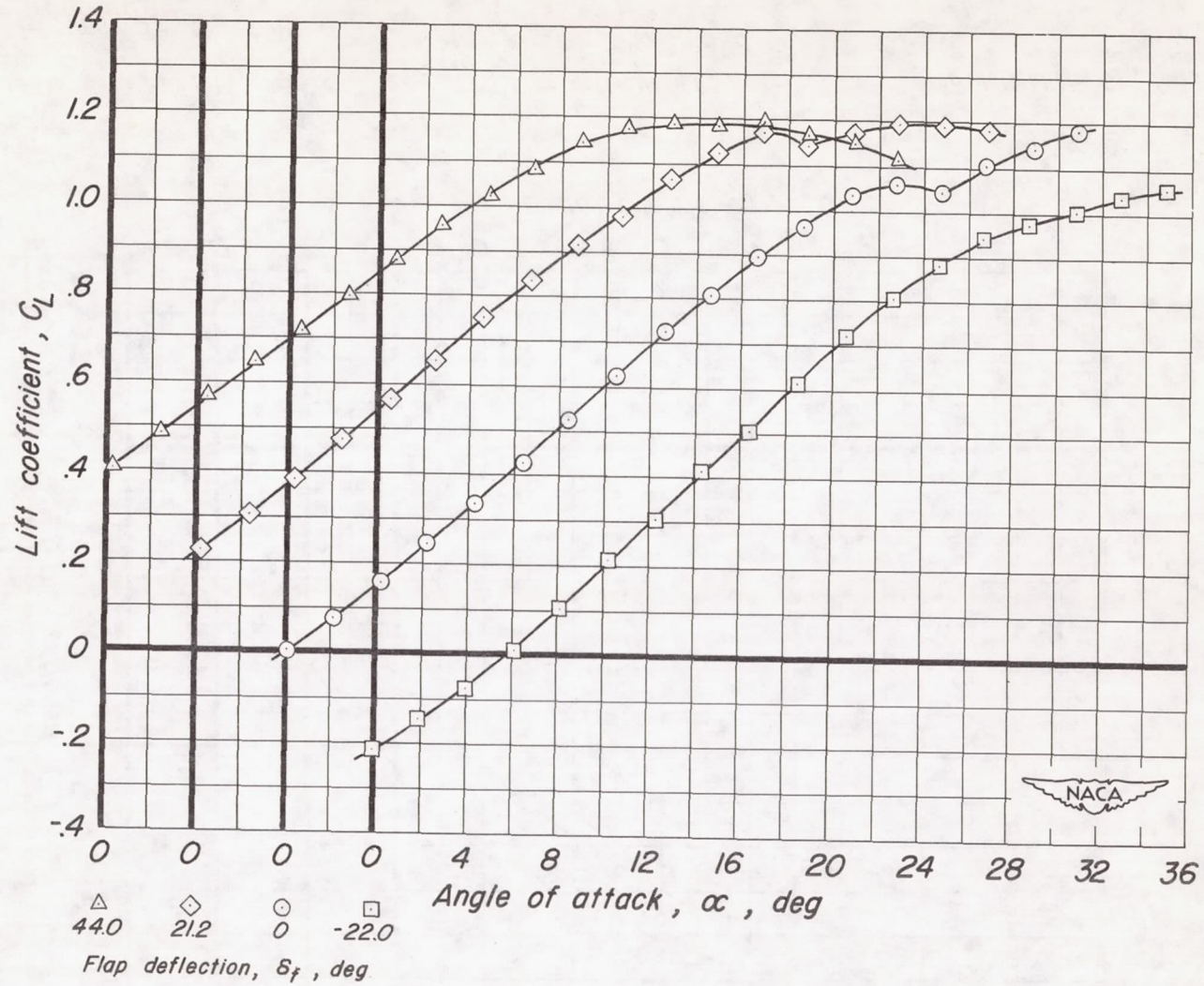


Figure 4. - Concluded.

(d) C_L vs C_l , C_n and C_y .



(a) C_L vs α .

Figure 5.- Wing alone at 12.1° angle of sideslip with various flap deflections.

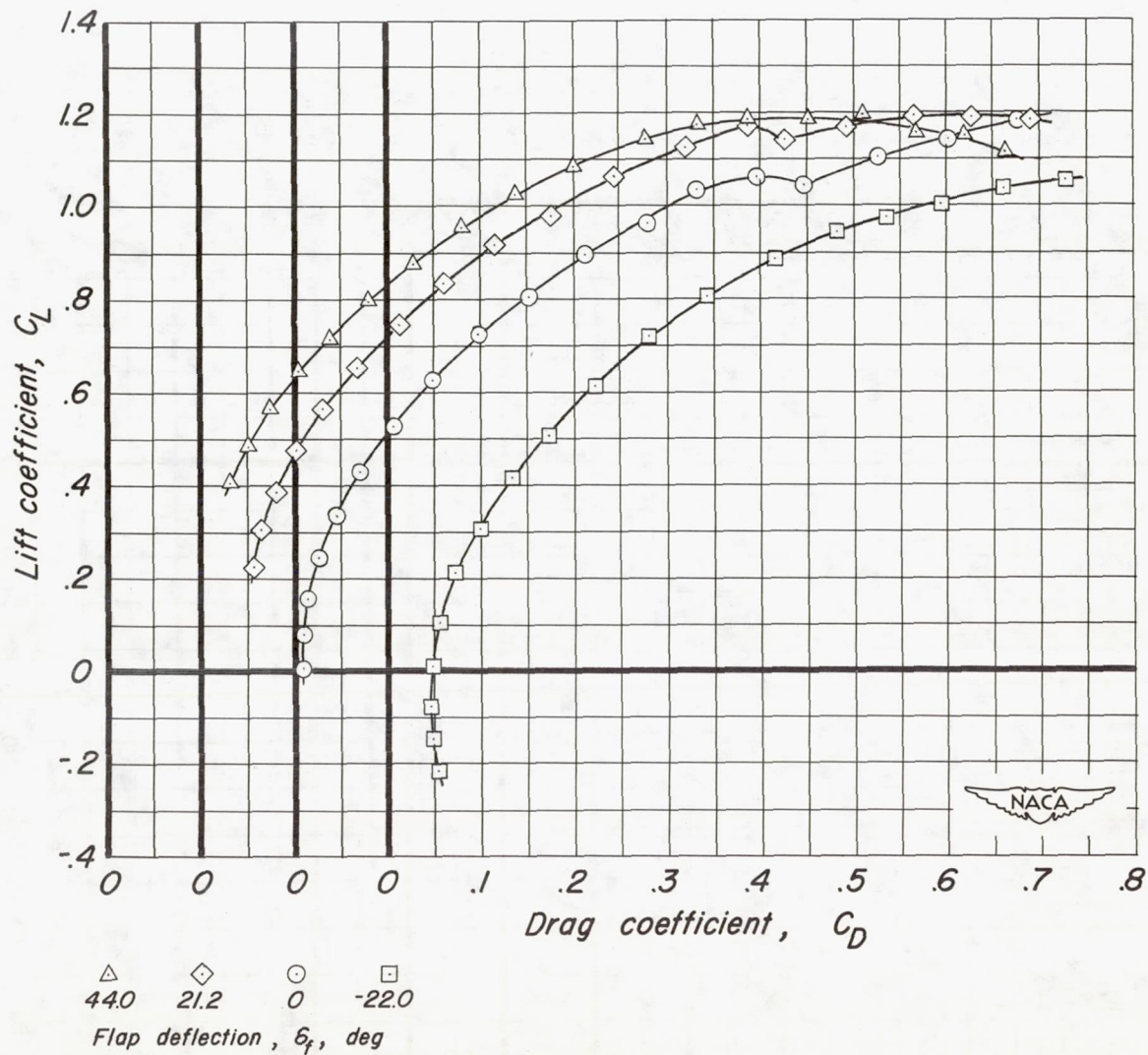


Figure 5.- Continued.

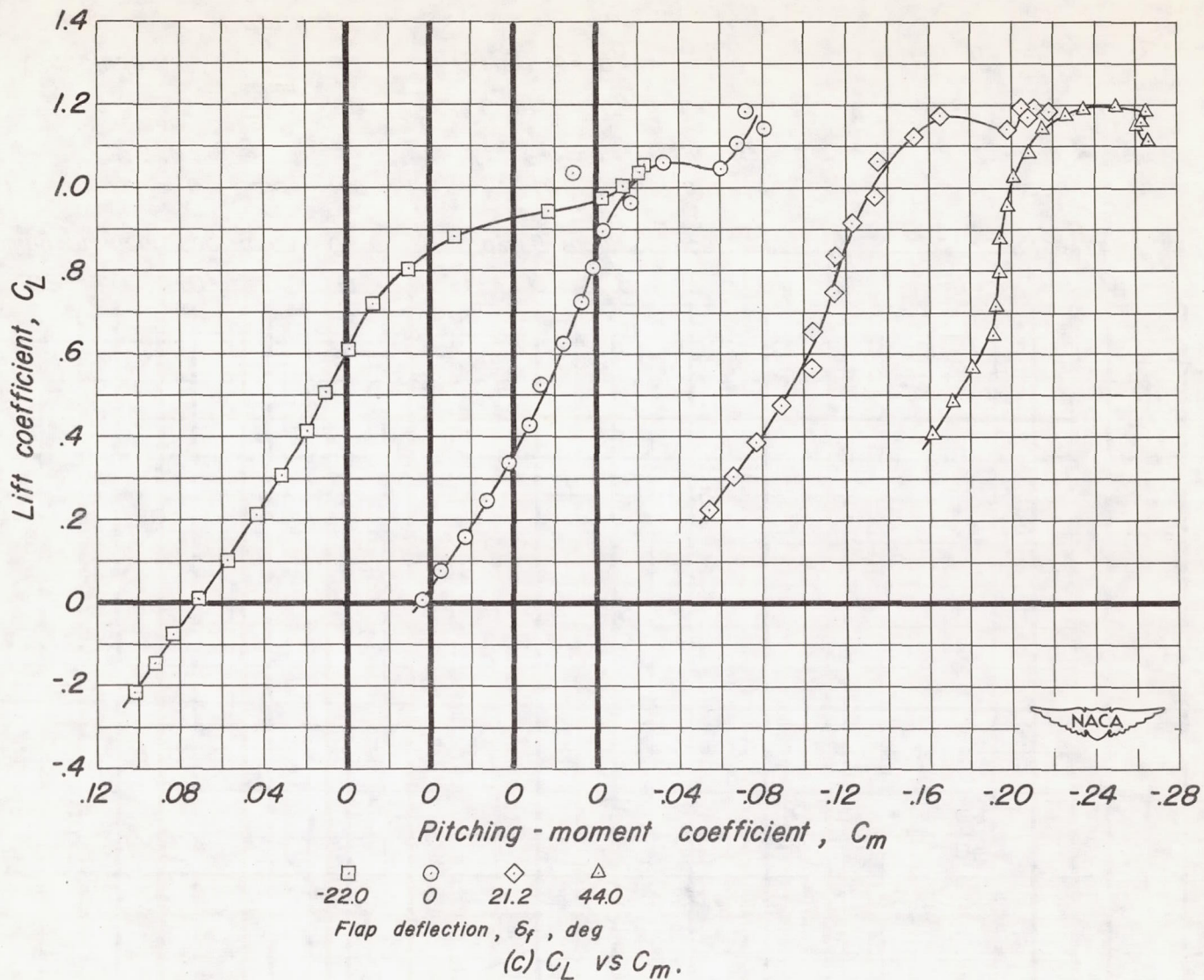


Figure 5.— Continued.

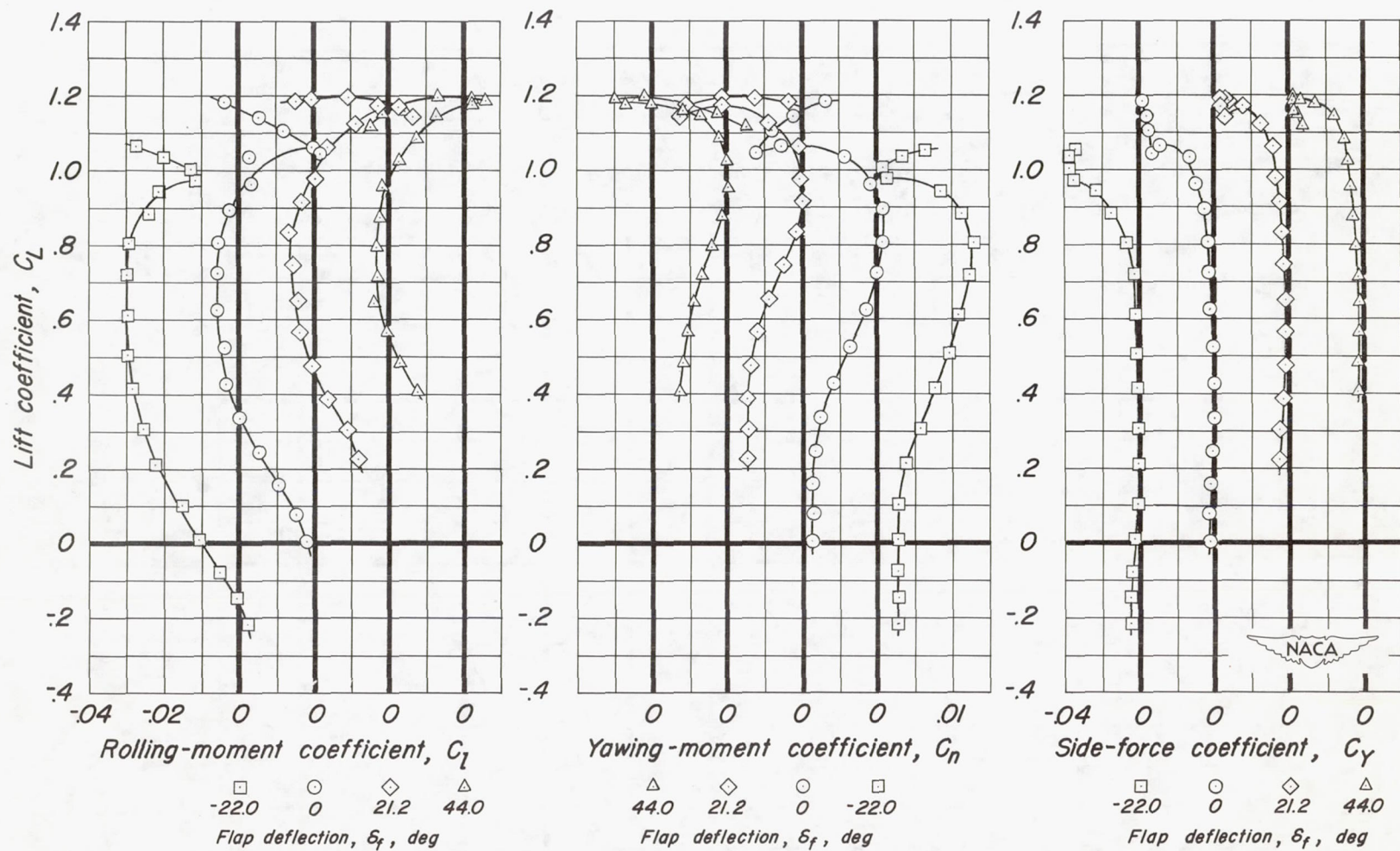
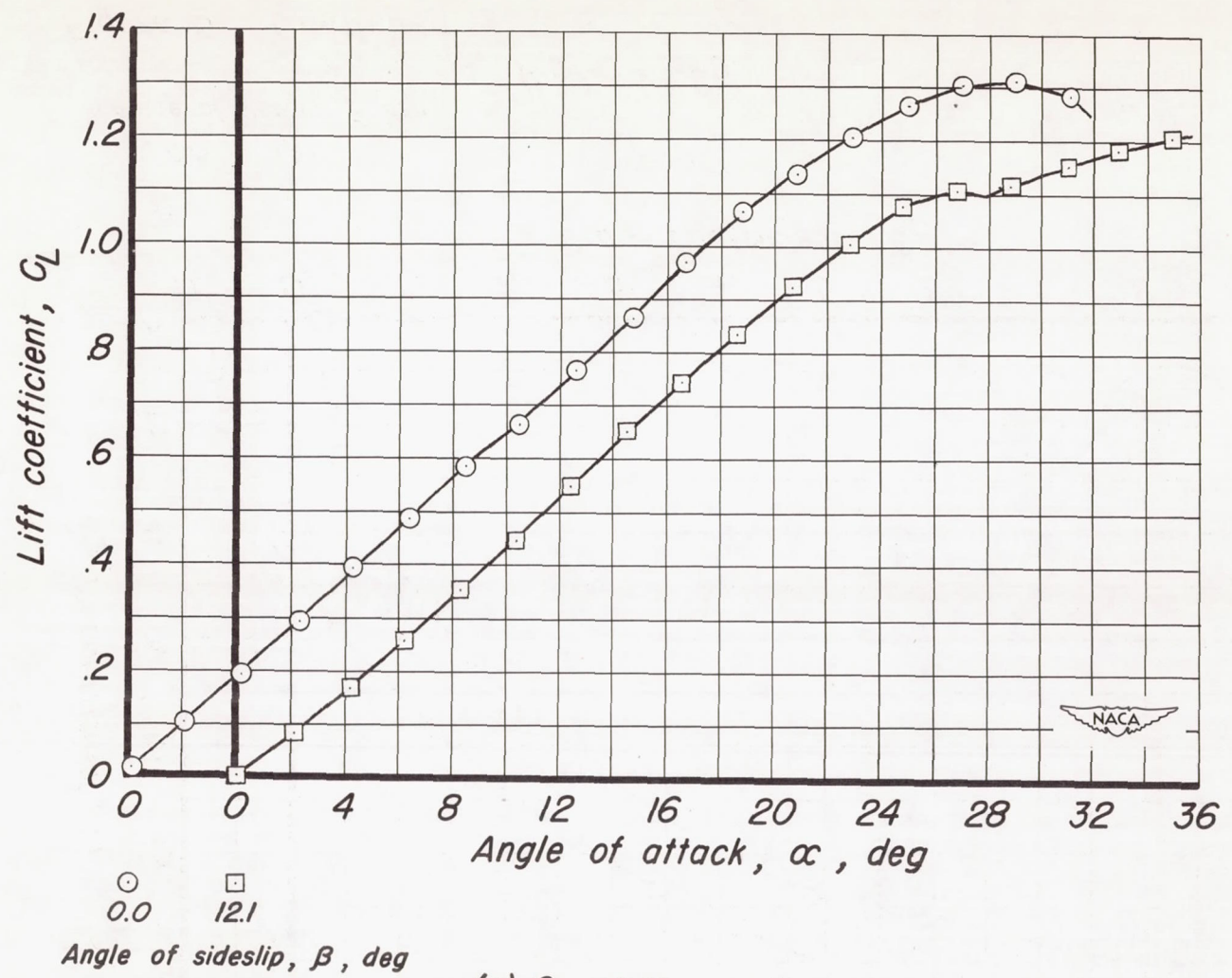
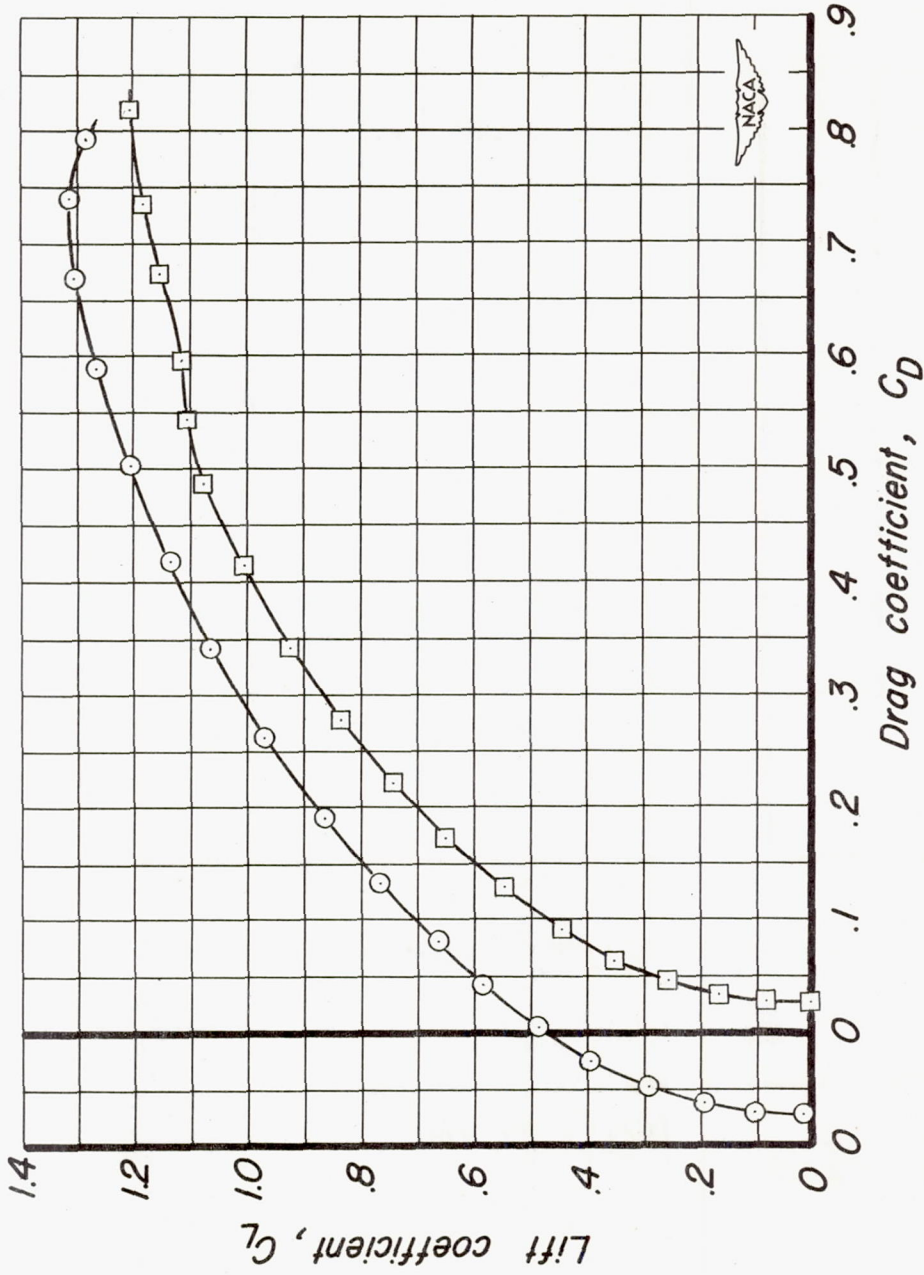
(d) C_L vs C_l , C_n and C_Y .

Figure 5.— Concluded.

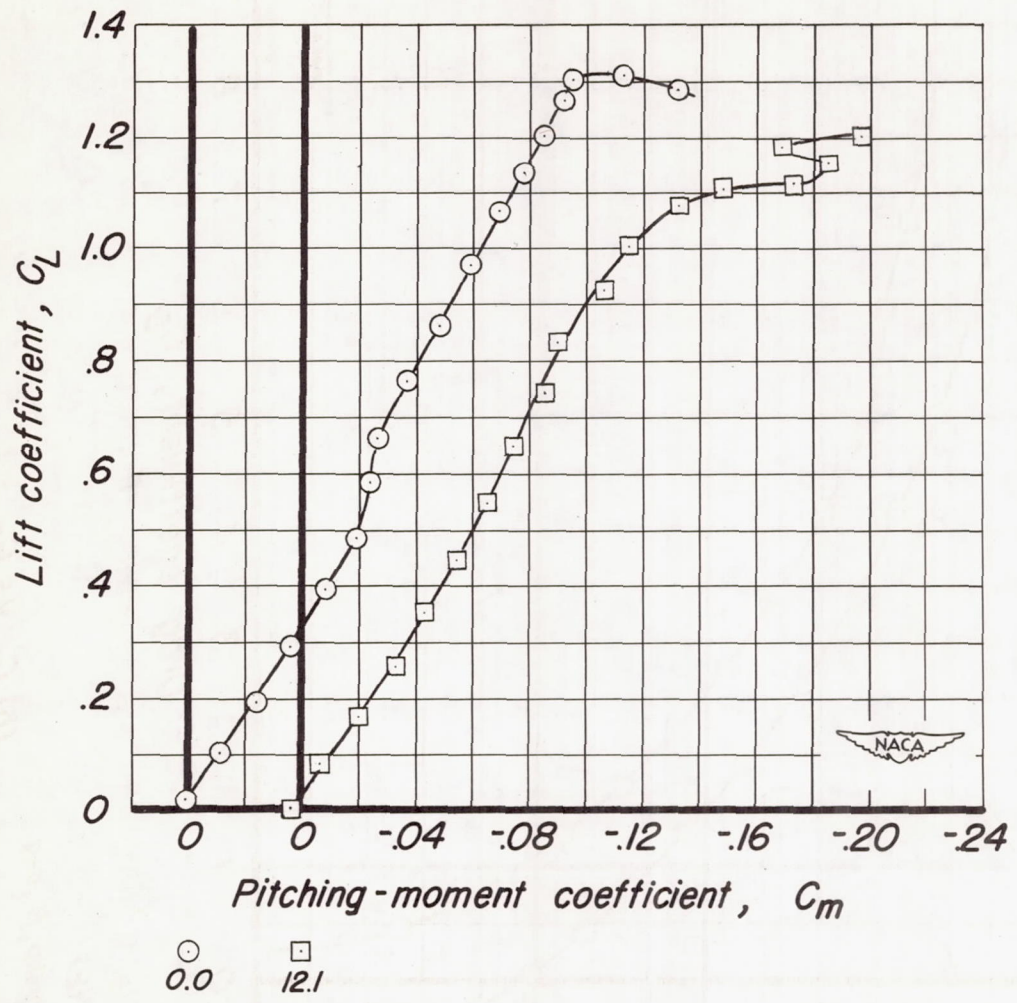


(a) C_L vs α .

Figure 6.- Wing alone at two angles of sideslip with left aileron deflected 11.7° and right aileron deflected -11.3° .



(b) C_L vs C_D .
 Figure 6. - Continued.



(c) C_L vs C_m .

Figure 6.— Continued.

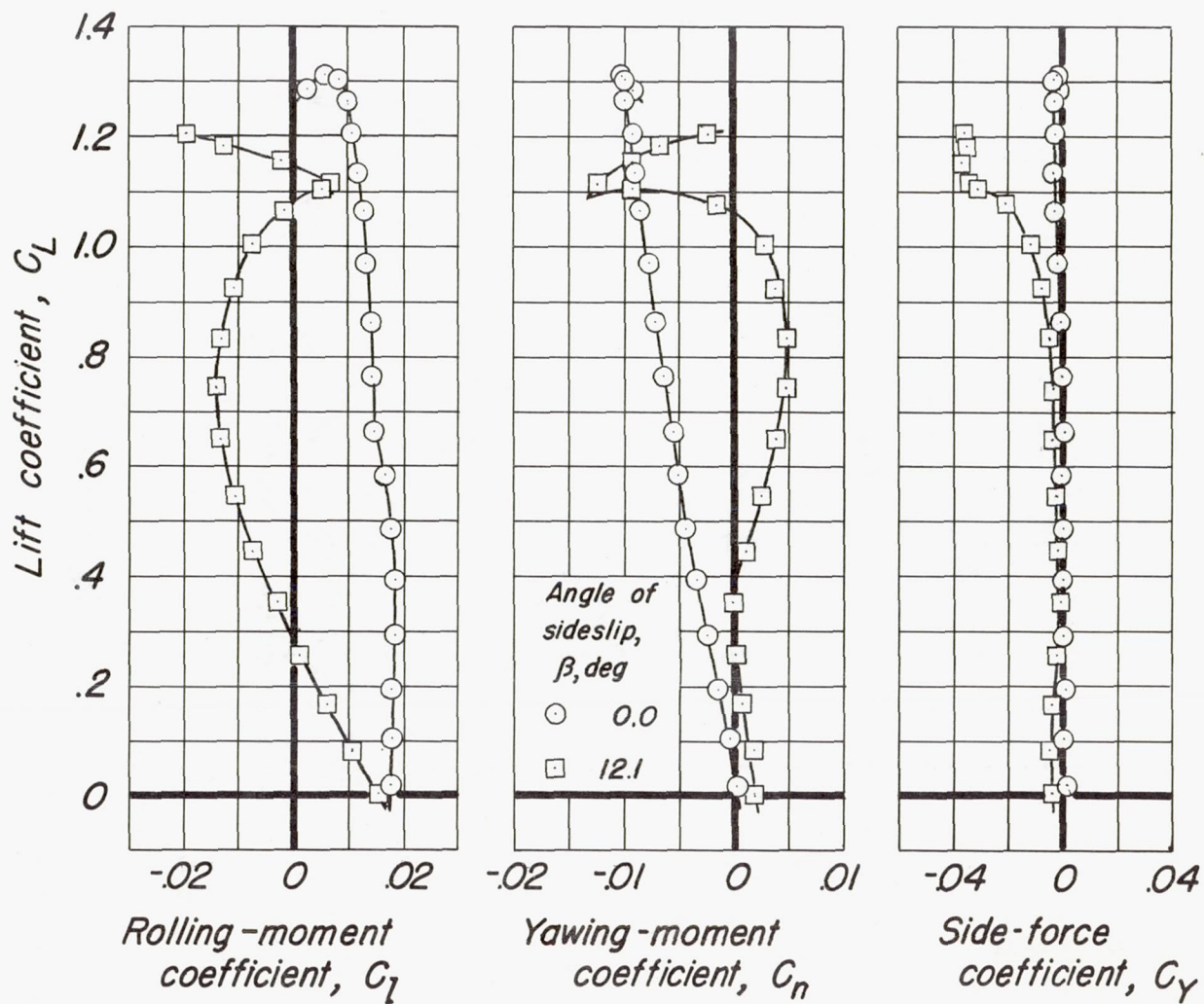
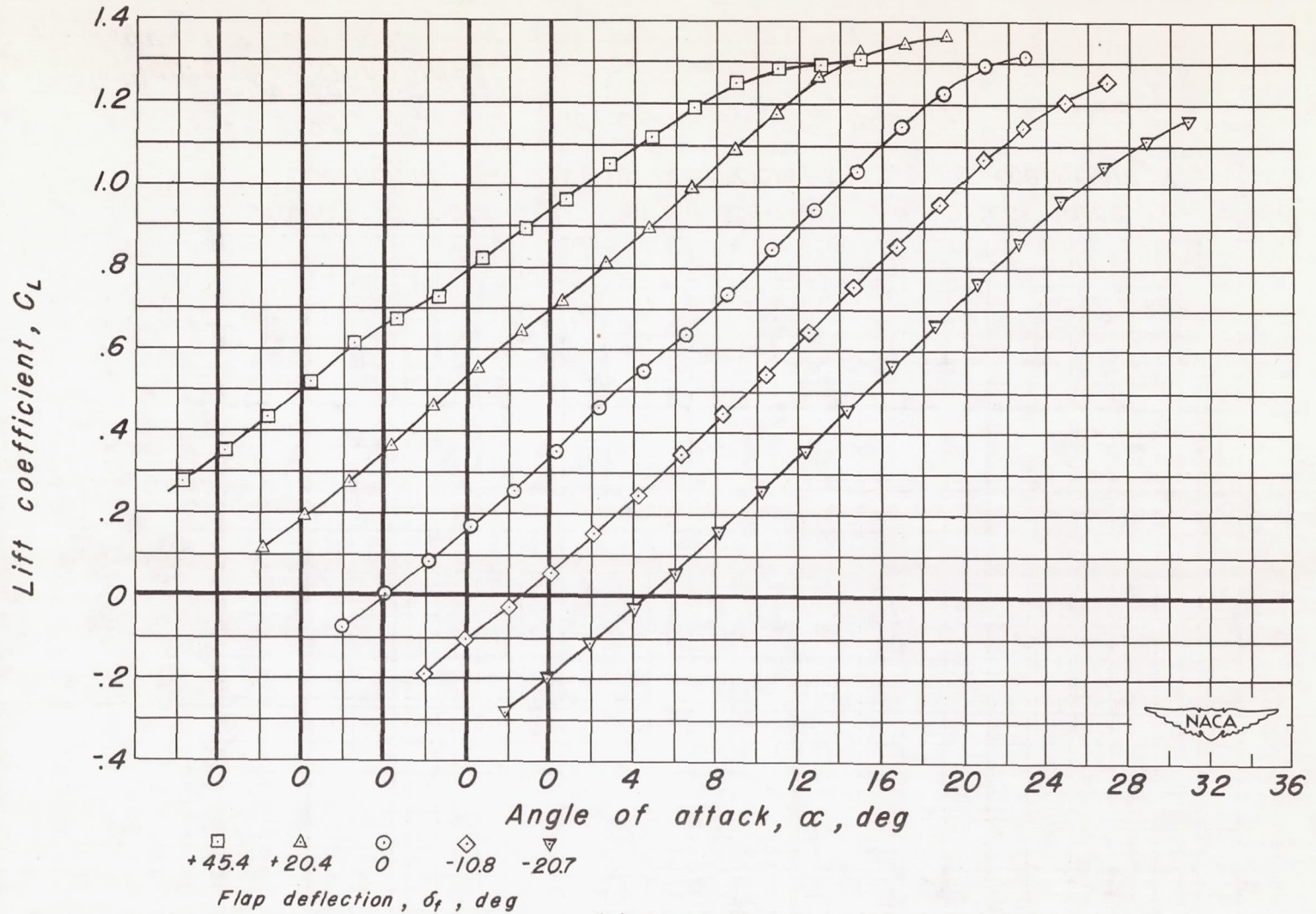
(d) C_L vs C_l , C_n and C_y .

Figure 6.— Concluded.



(a) C_L vs α .

Figure 7. - Wing plus body at 0.0° angle of sideslip with various flap deflections.

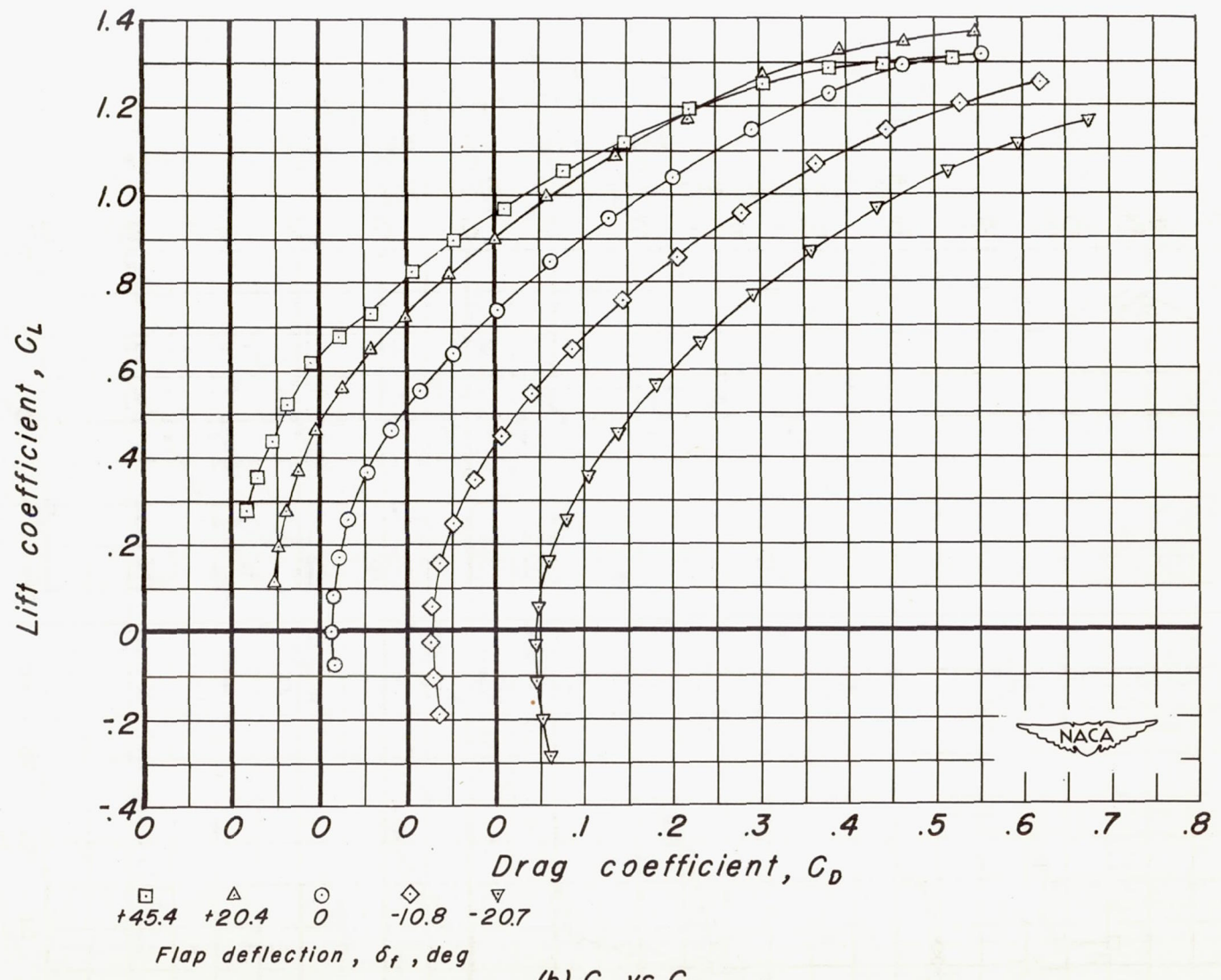


Figure 7. - Continued.

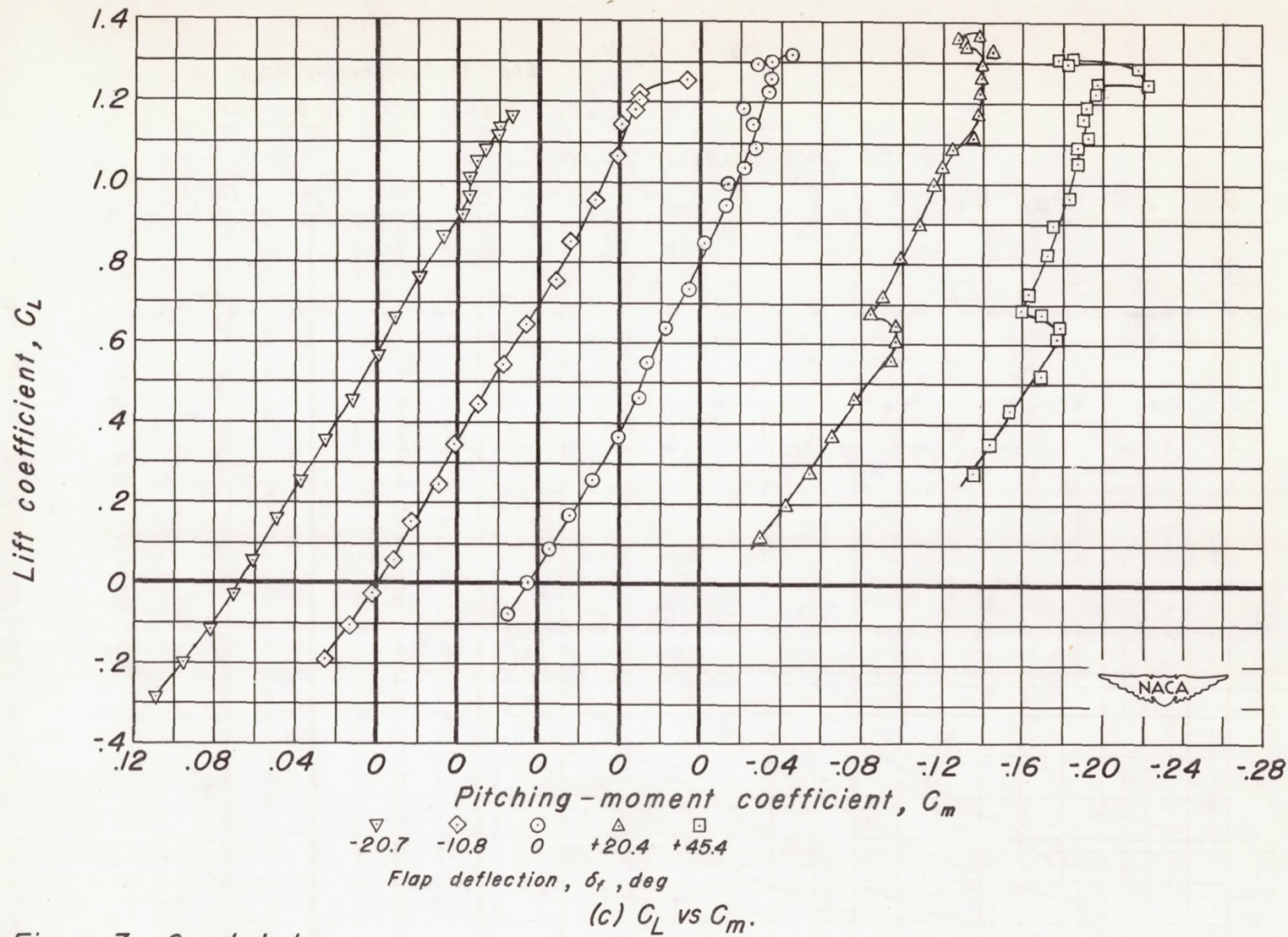


Figure 7.- Concluded.

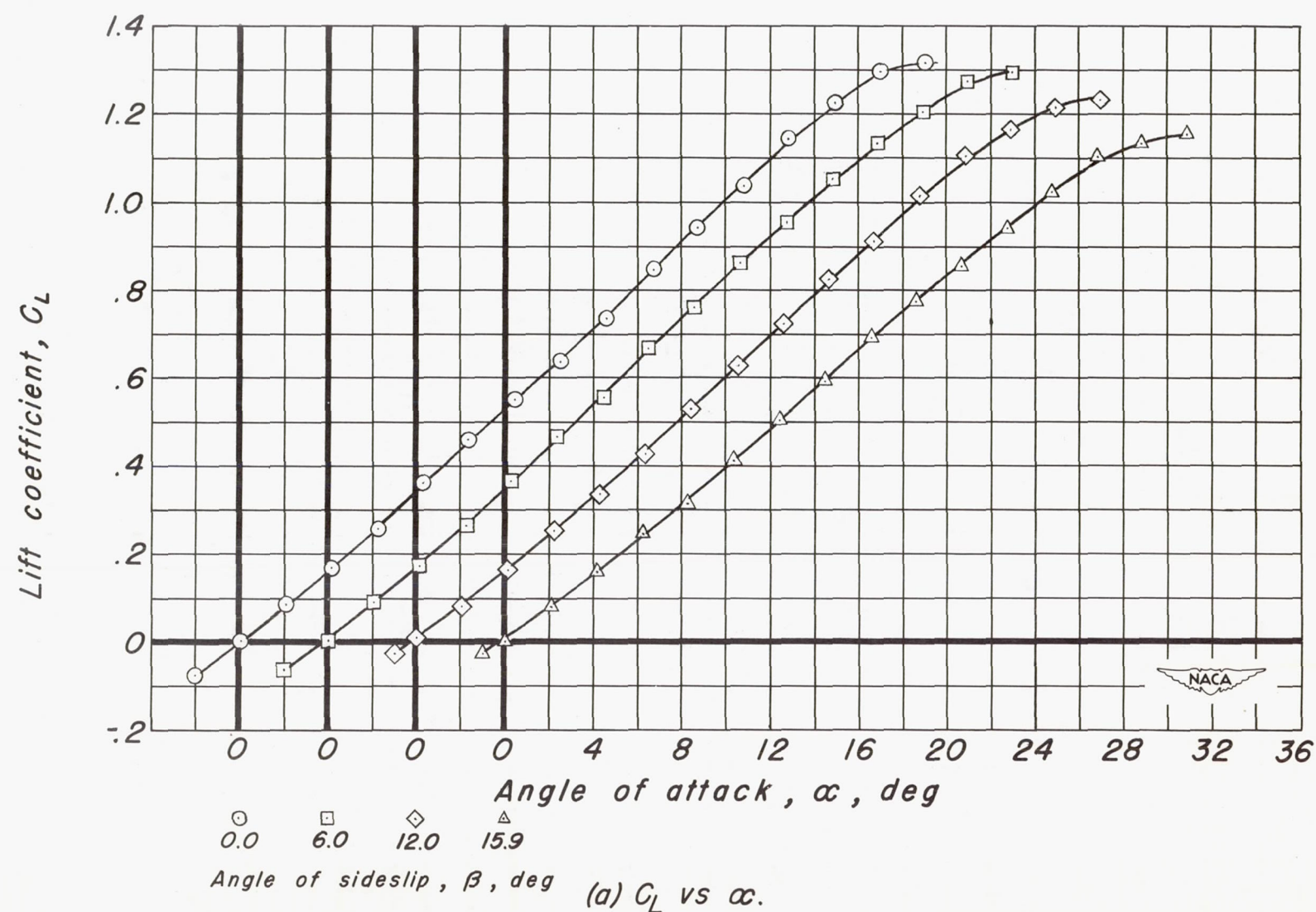
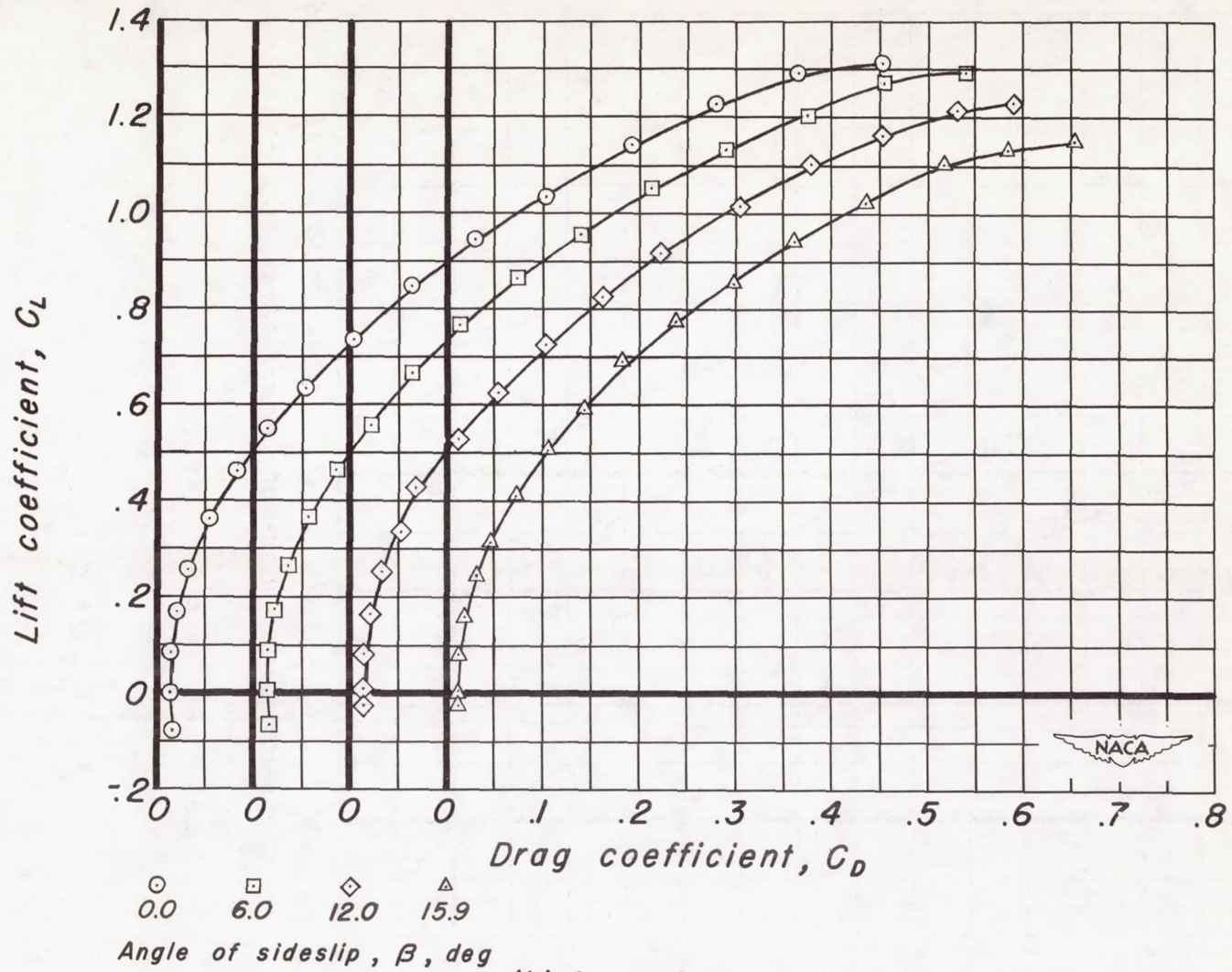
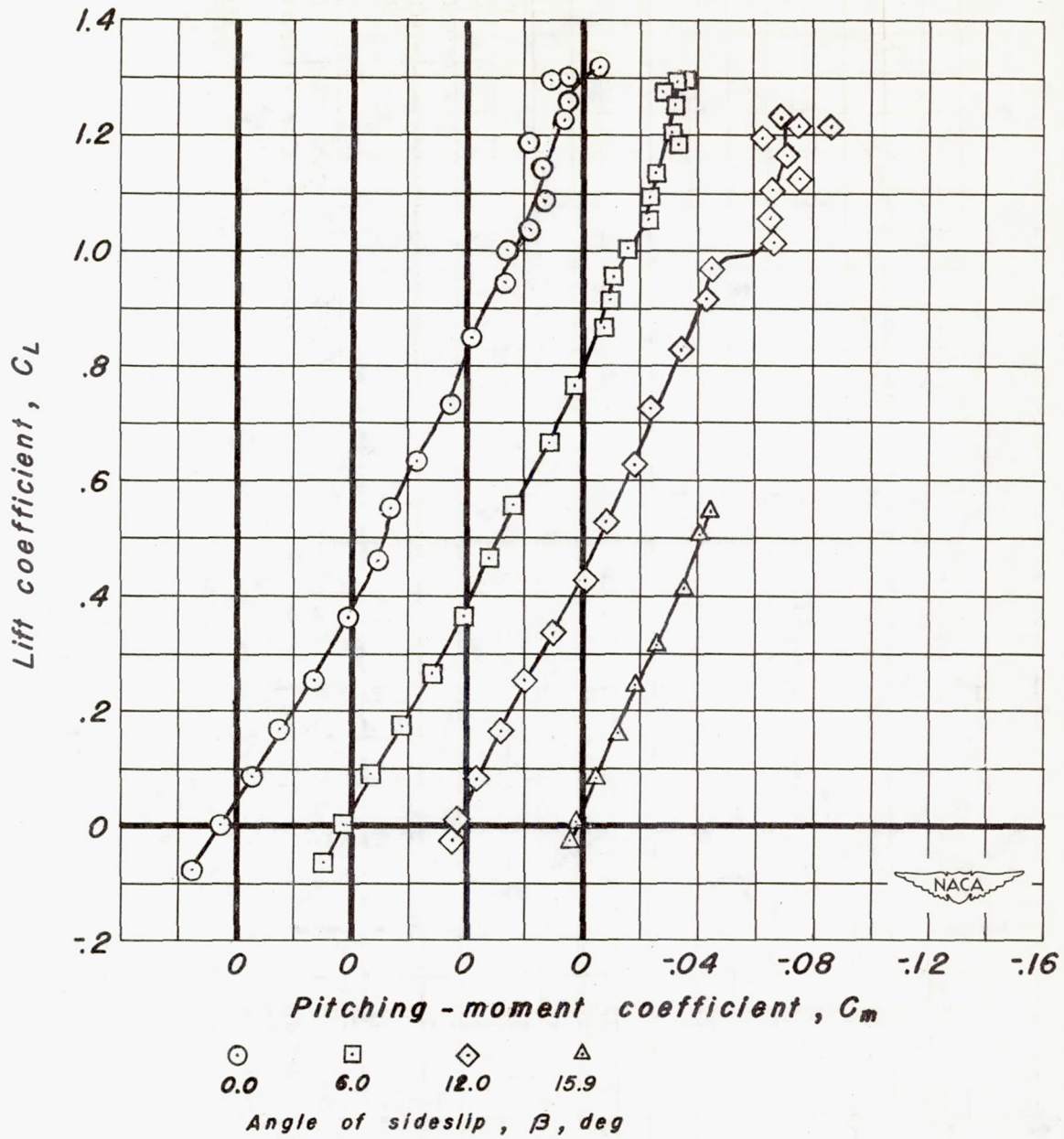


Figure 8.— Wing plus body at various angles of sideslip with flaps undeflected.



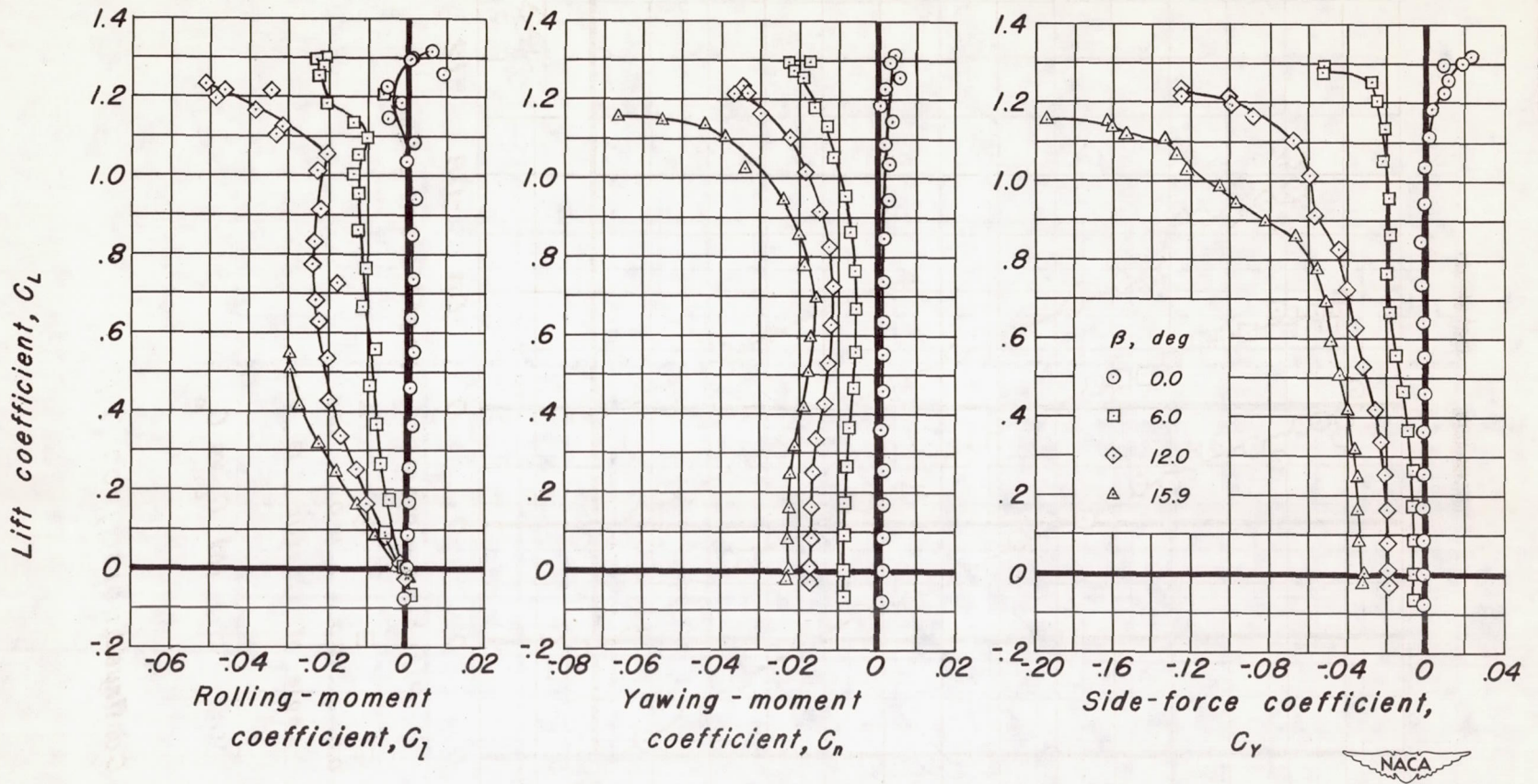
(b) C_L vs C_D .

Figure 8. - Continued.



(c) C_L vs C_m .

Figure 8.— Continued.



(d) C_L vs C_l , C_n and C_y .

Figure 8.— Concluded.

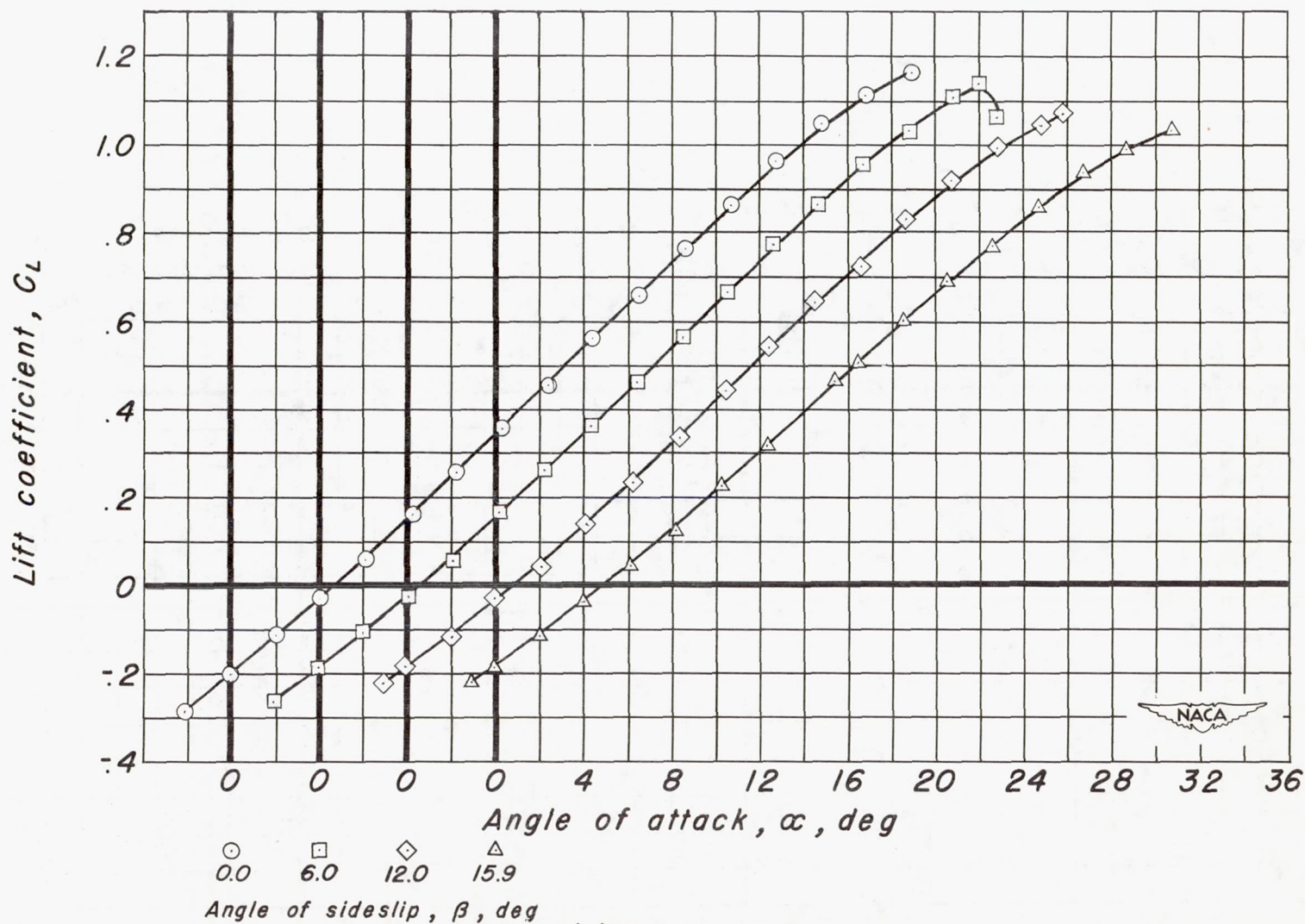


Figure 9.- Wing plus body at various angles of sideslip with flaps deflected -20.7° .

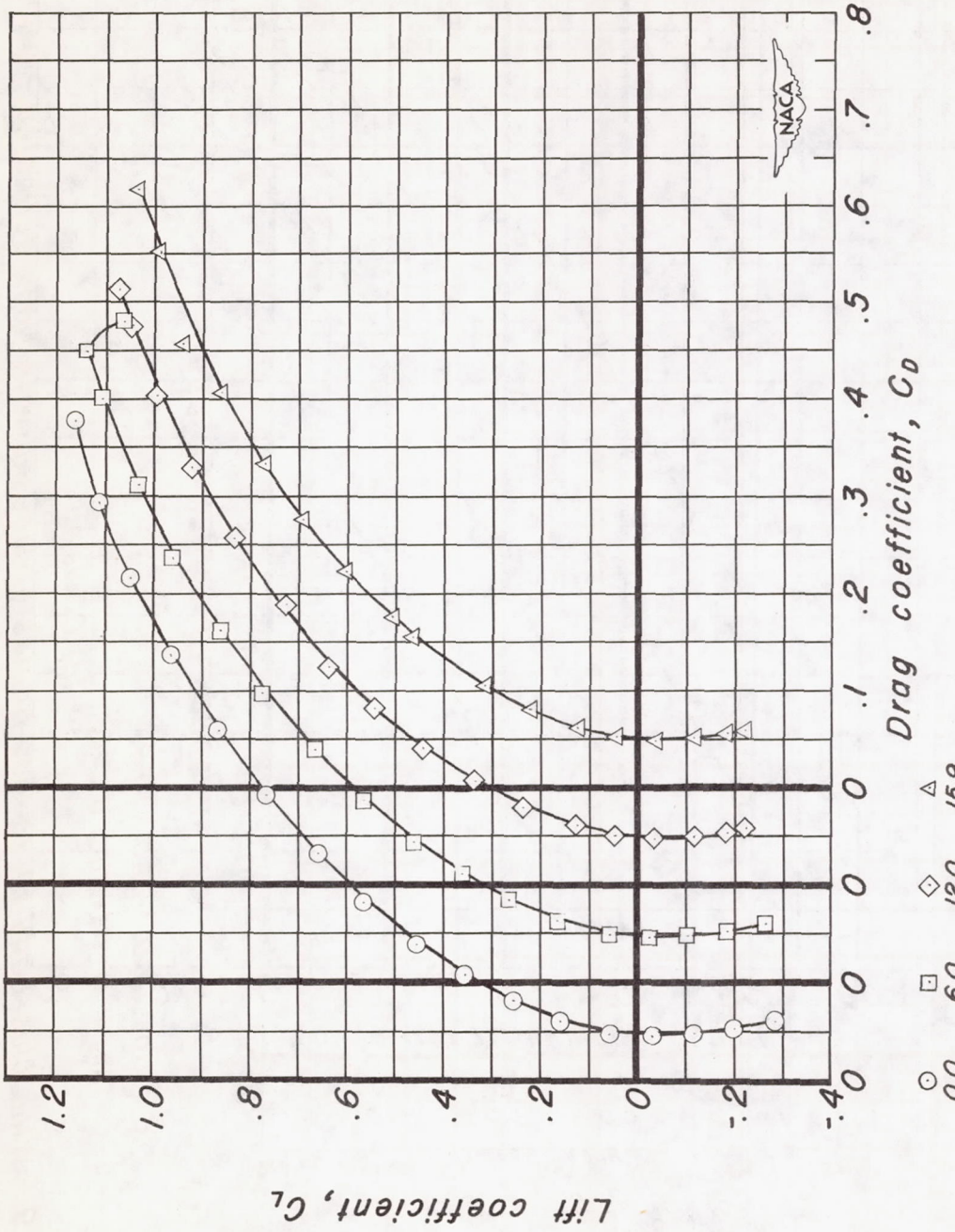


Figure 9.- Continued.
(b) C_L vs C_D .

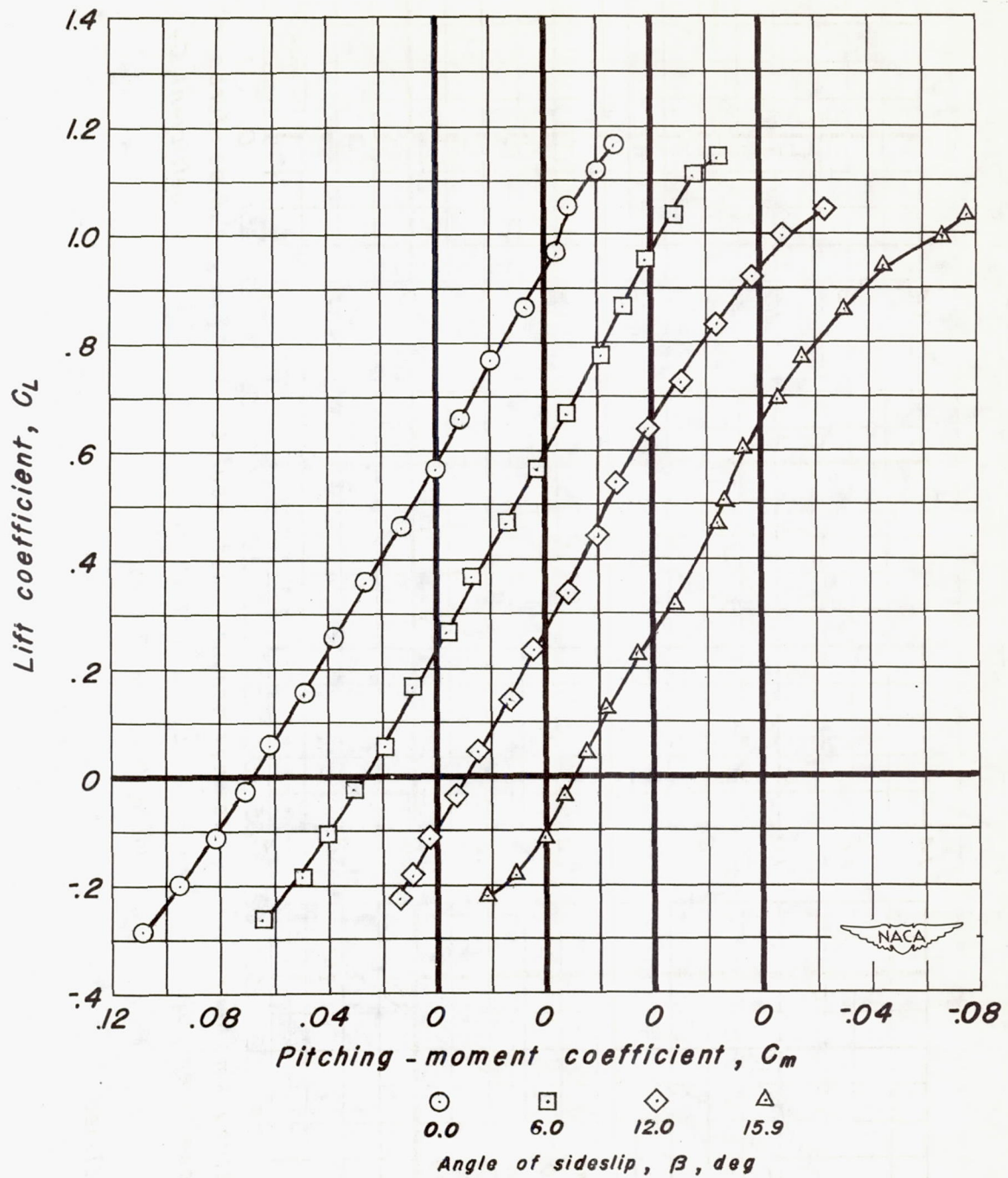
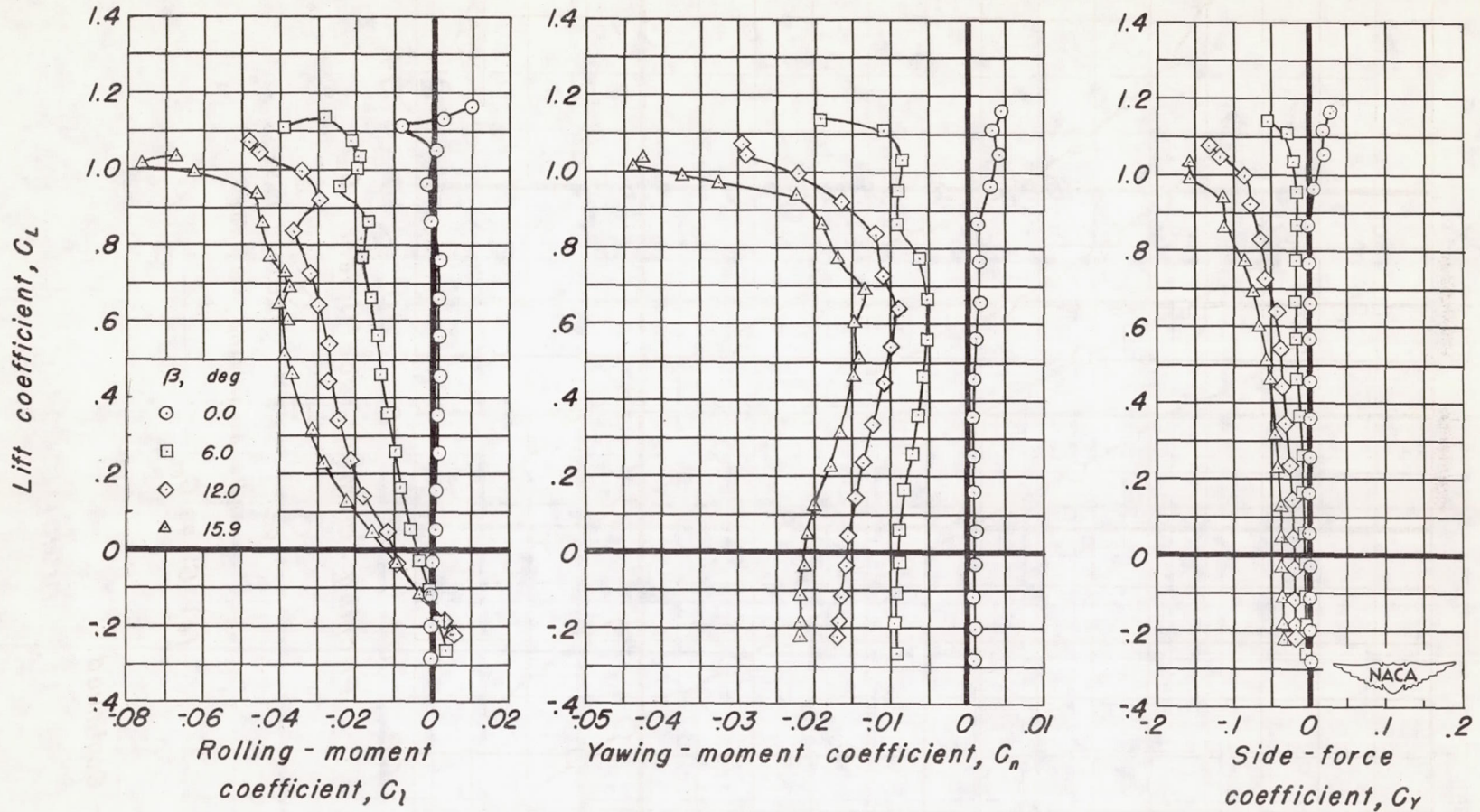
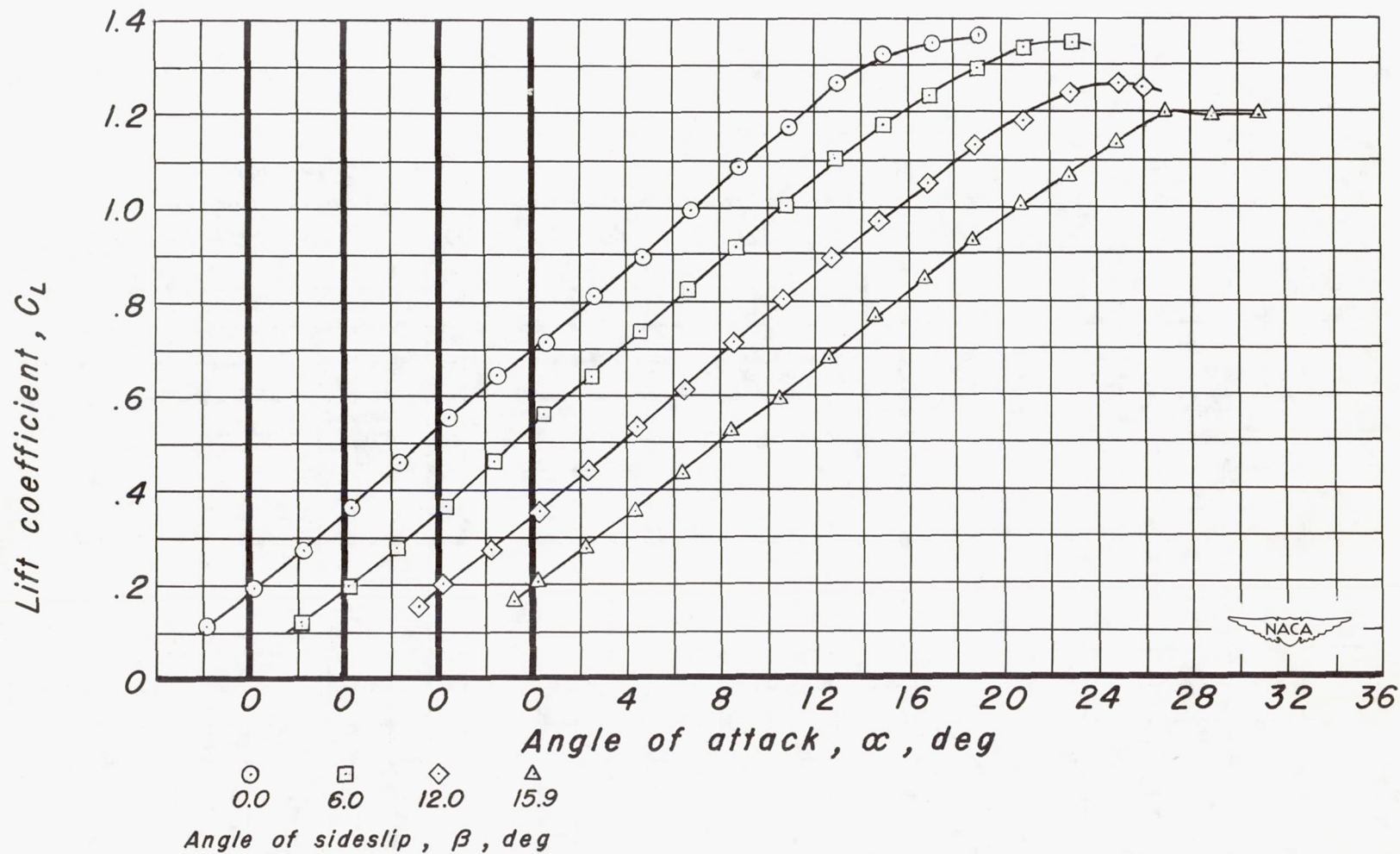
(c) C_L vs C_m .

Figure 9.— Continued.



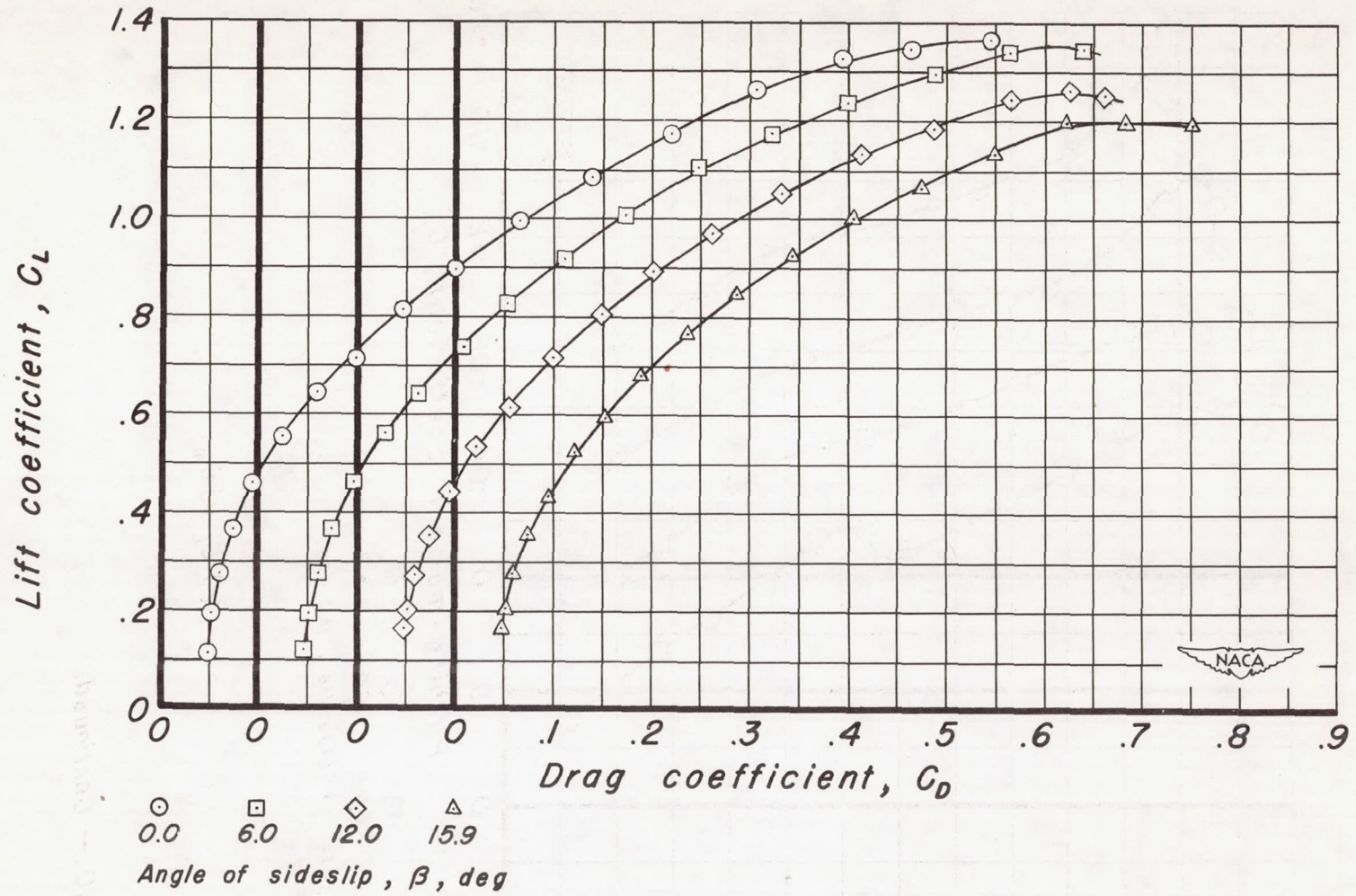
(d) C_L vs C_l , C_n and C_y .

Figure 9.— Concluded.



(a) C_L vs α .

Figure 10. - Wing plus body at various angles of sideslip with flaps deflected 20.4° .



(b) C_L vs C_D .

Figure 10.— Continued.

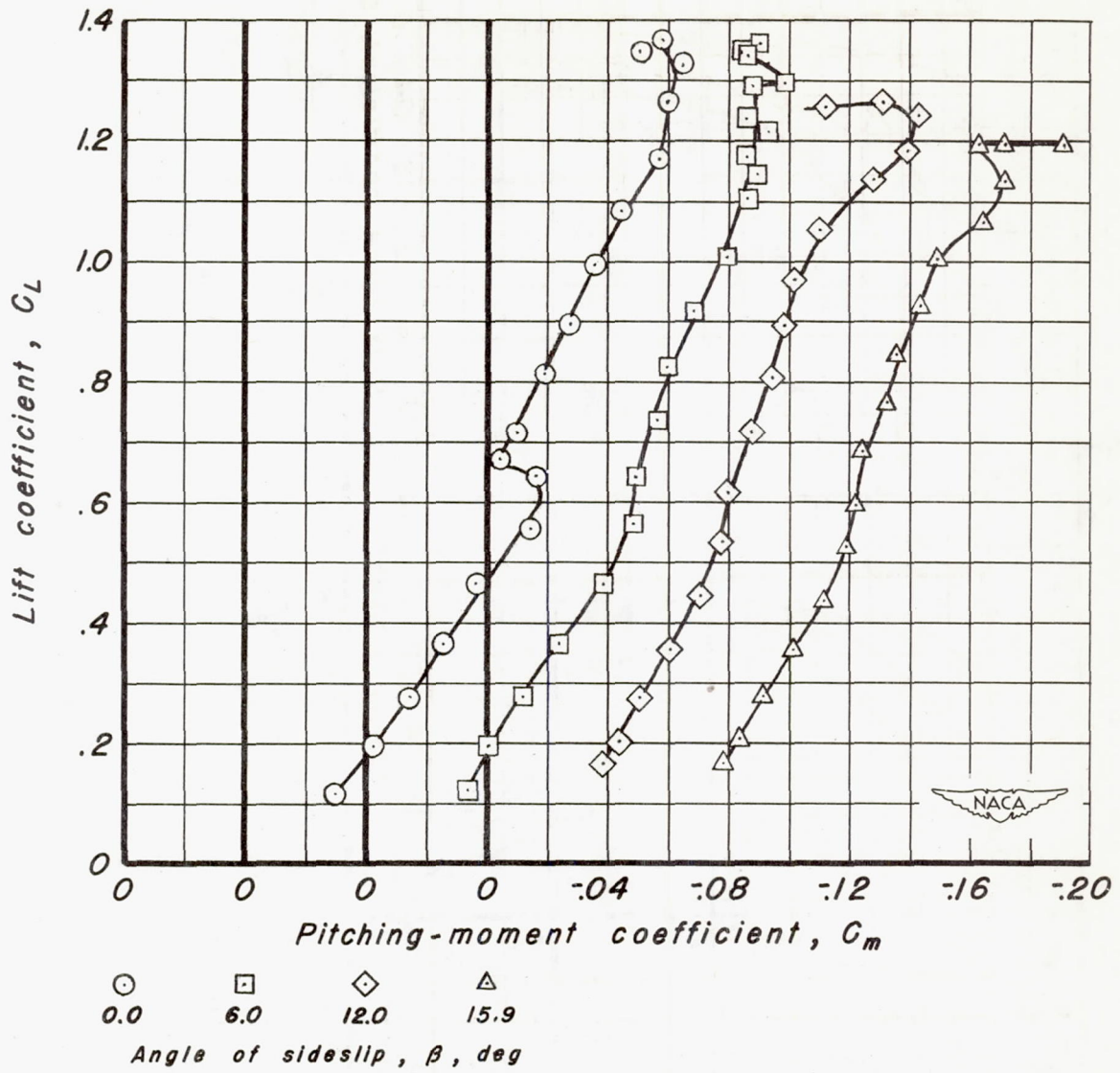
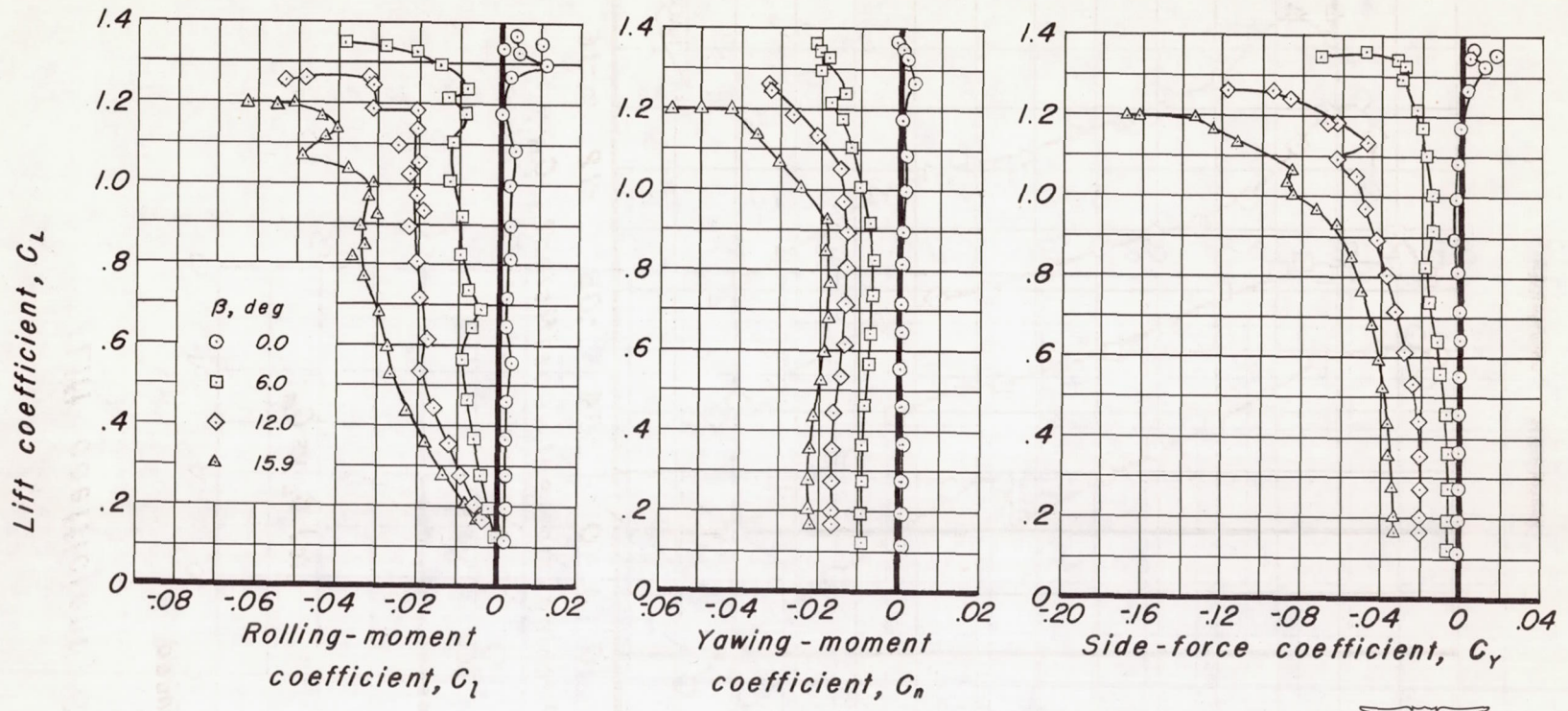
(c) C_L vs C_m .

Figure 10.— Continued.



(d) C_L vs C_1 , C_n and C_y .

Figure 10.— Concluded.



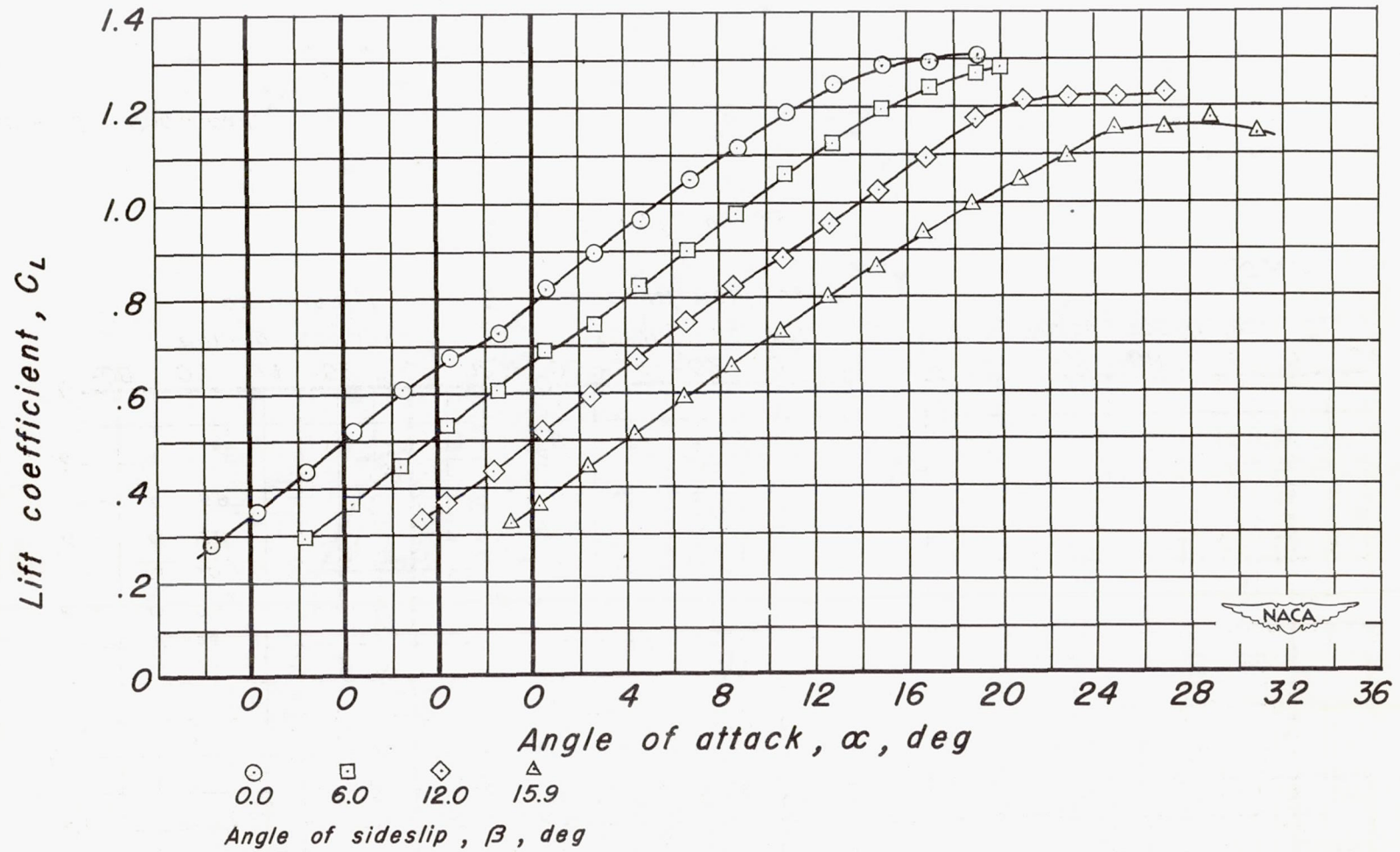
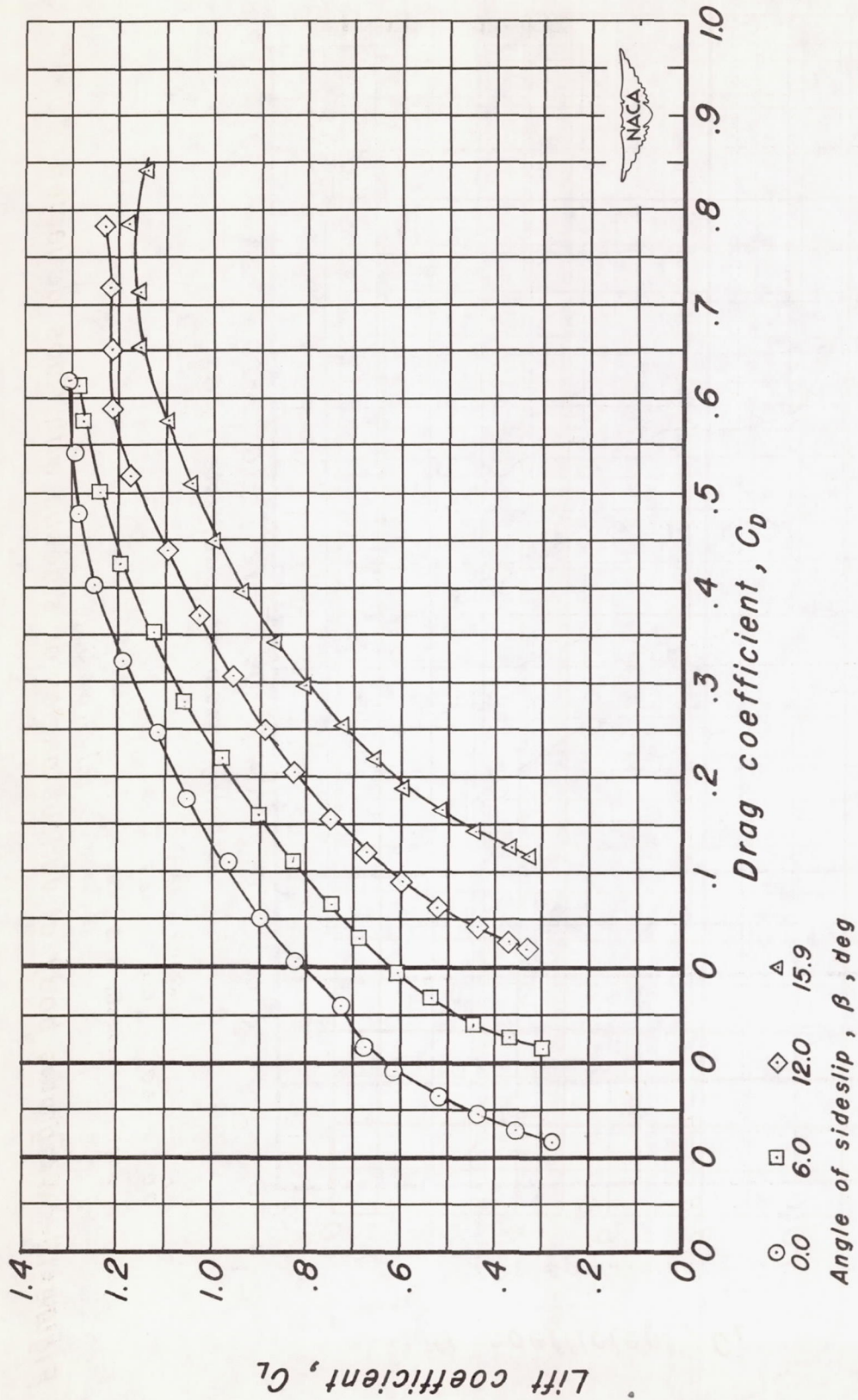


Figure 11.— Wing plus body at various angles of sideslip with flaps deflected 45.4° .



(b) C_L vs C_D .

Figure 11. - Continued.

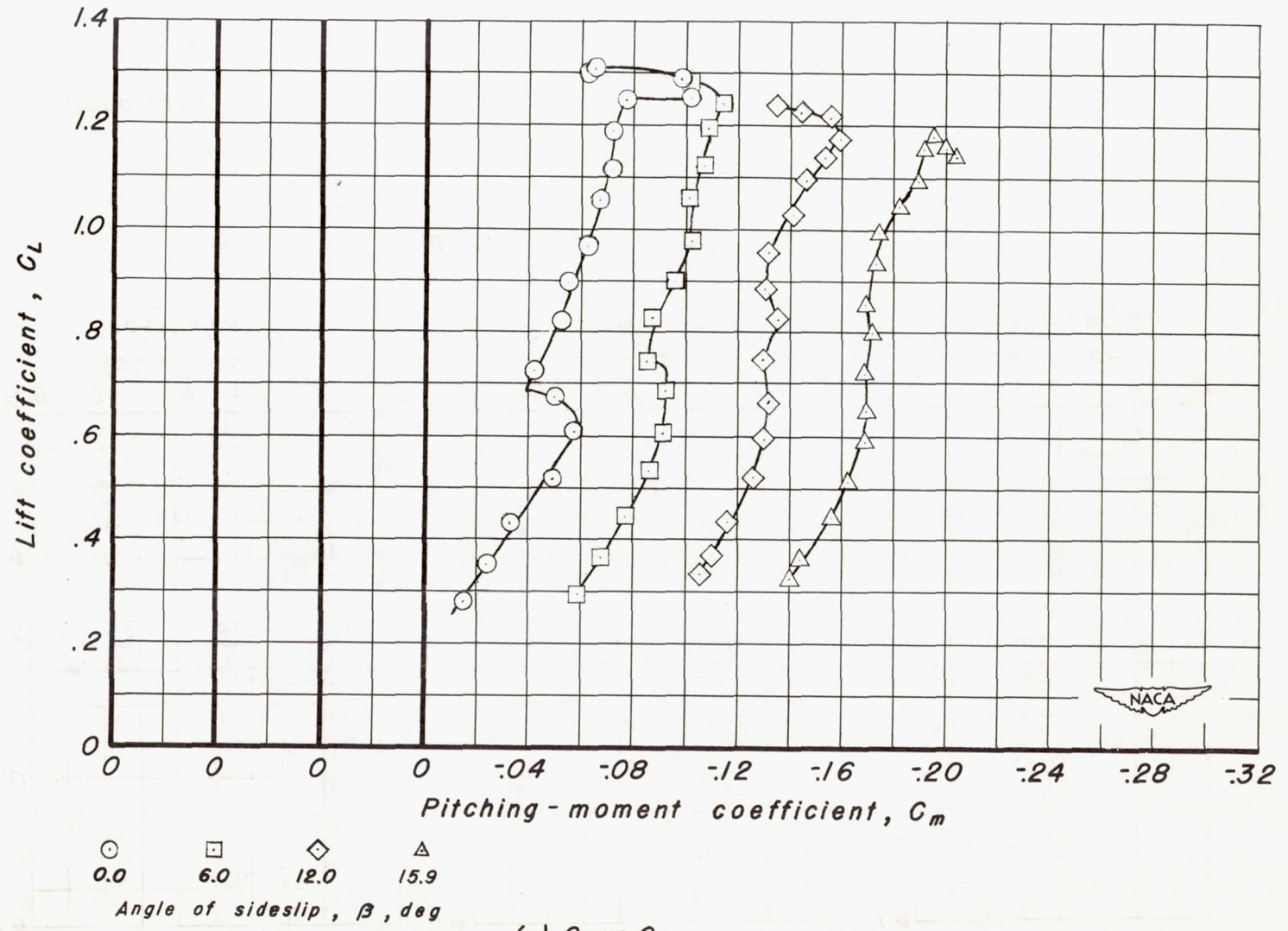
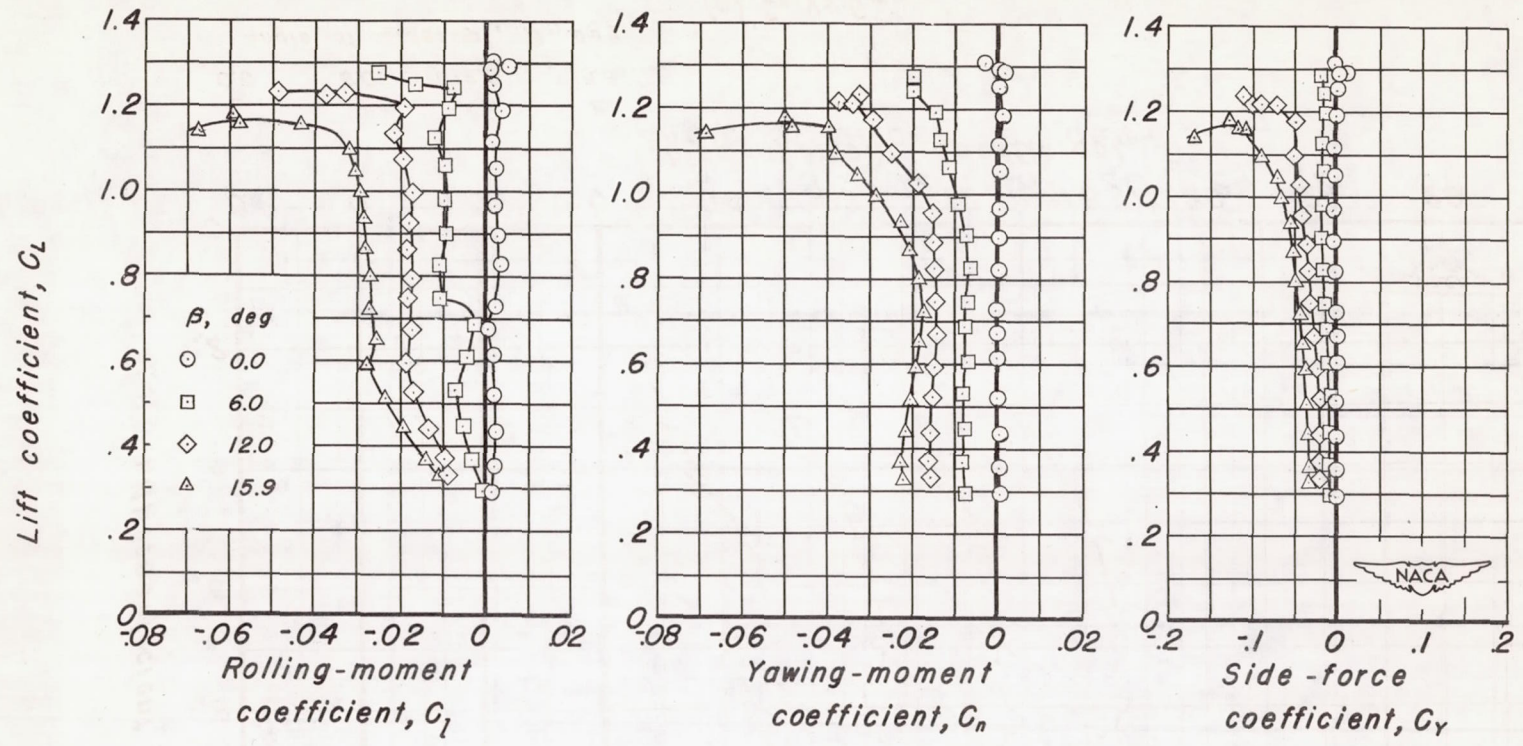


Figure 11. — Continued.

(c) C_L vs C_m .



(d) C_L vs C_{Lr} , C_{Ln} and C_{Ly} .

Figure 11.— Concluded.

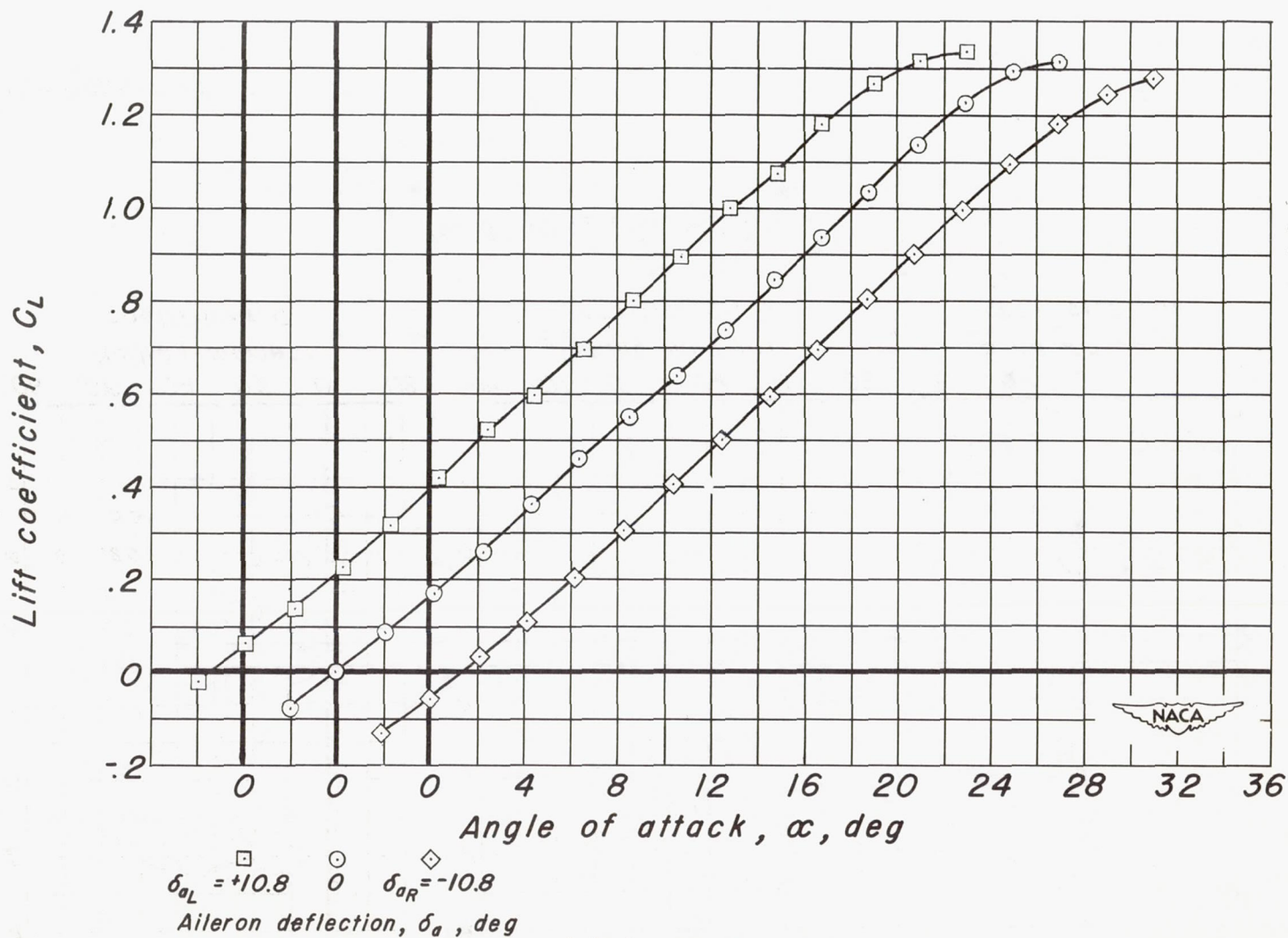


Figure 12.—Wing plus body at 0.0° angle of sideslip with one aileron deflected.

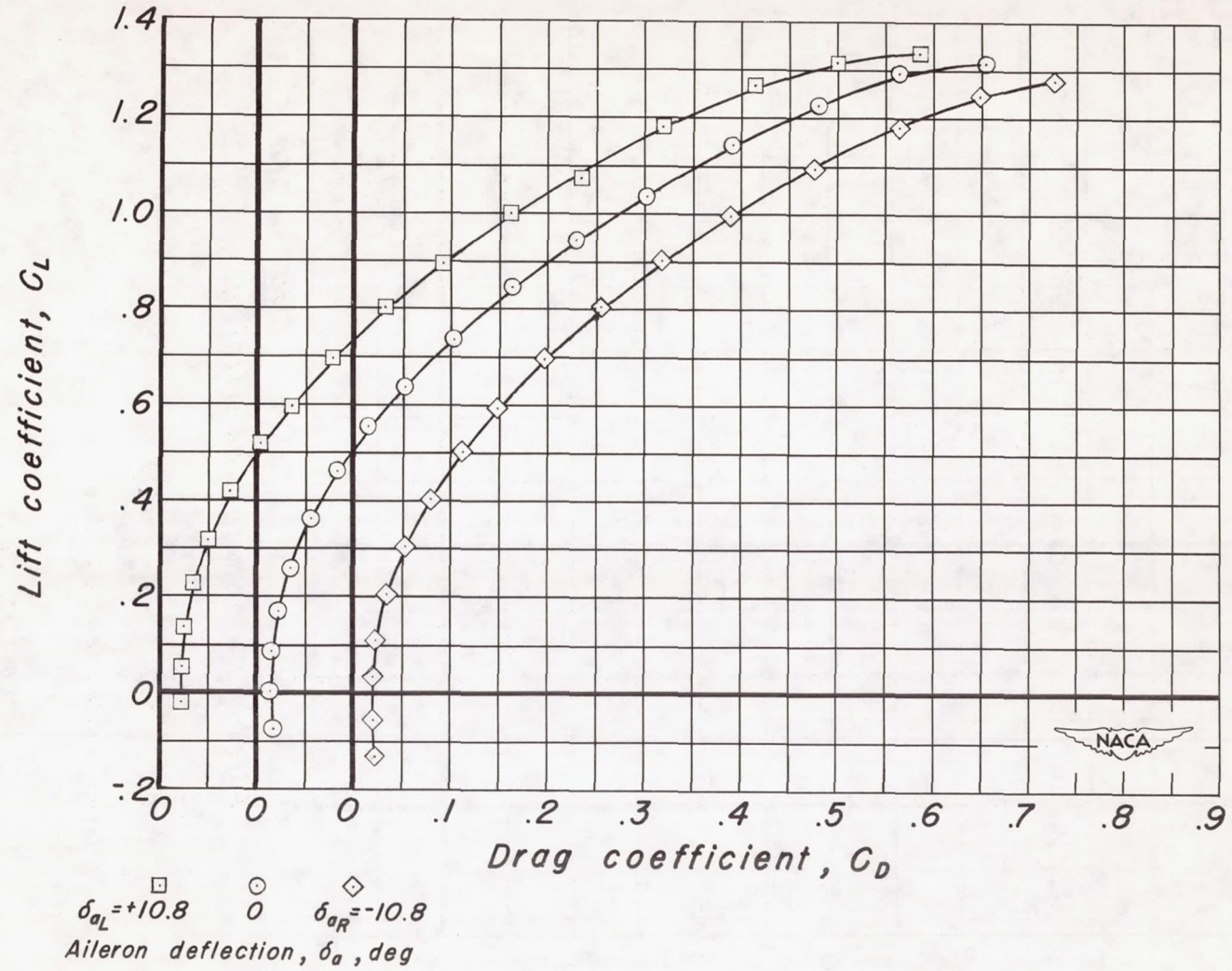


Figure 12.— Continued. (b) C_L vs C_D .

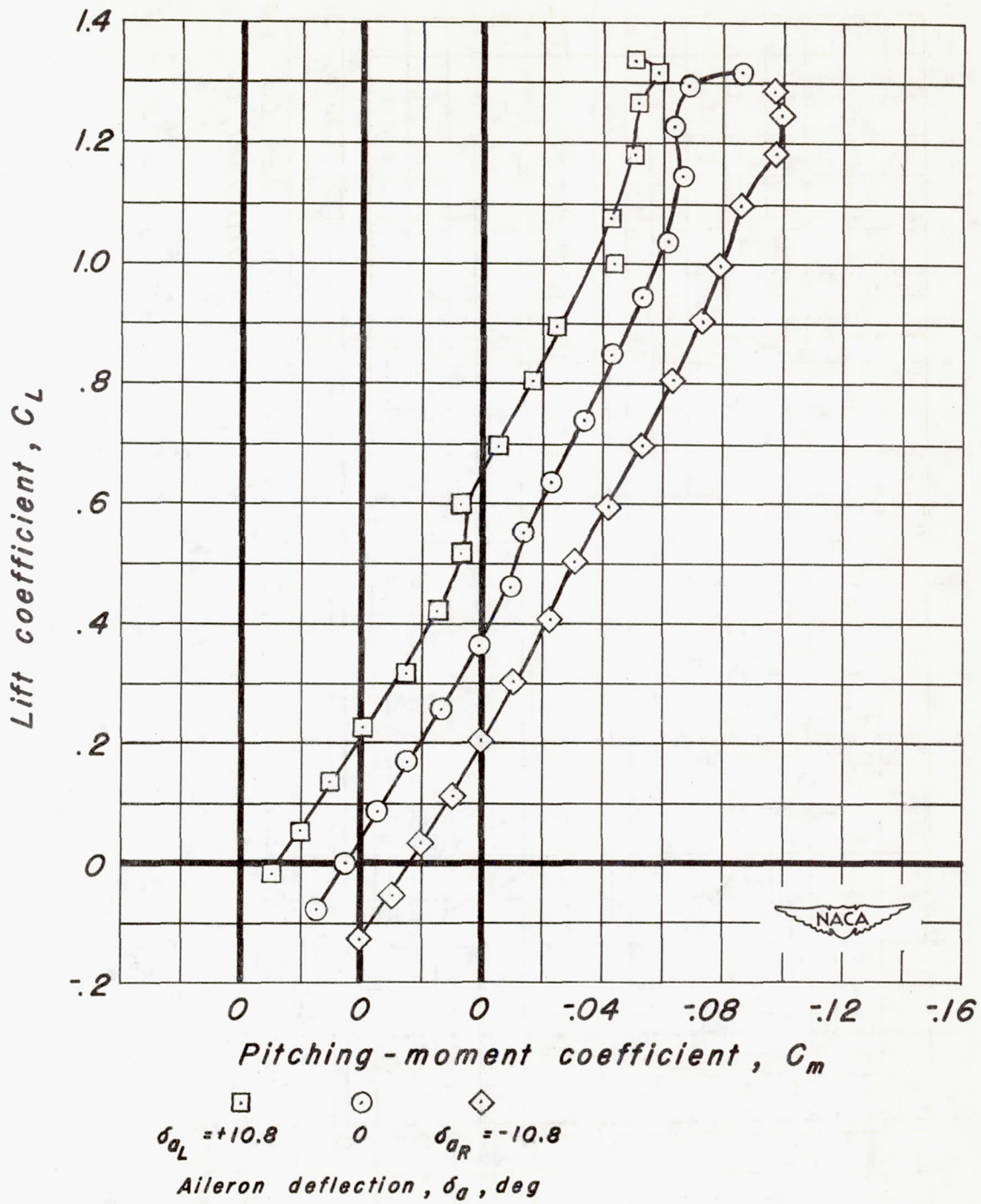
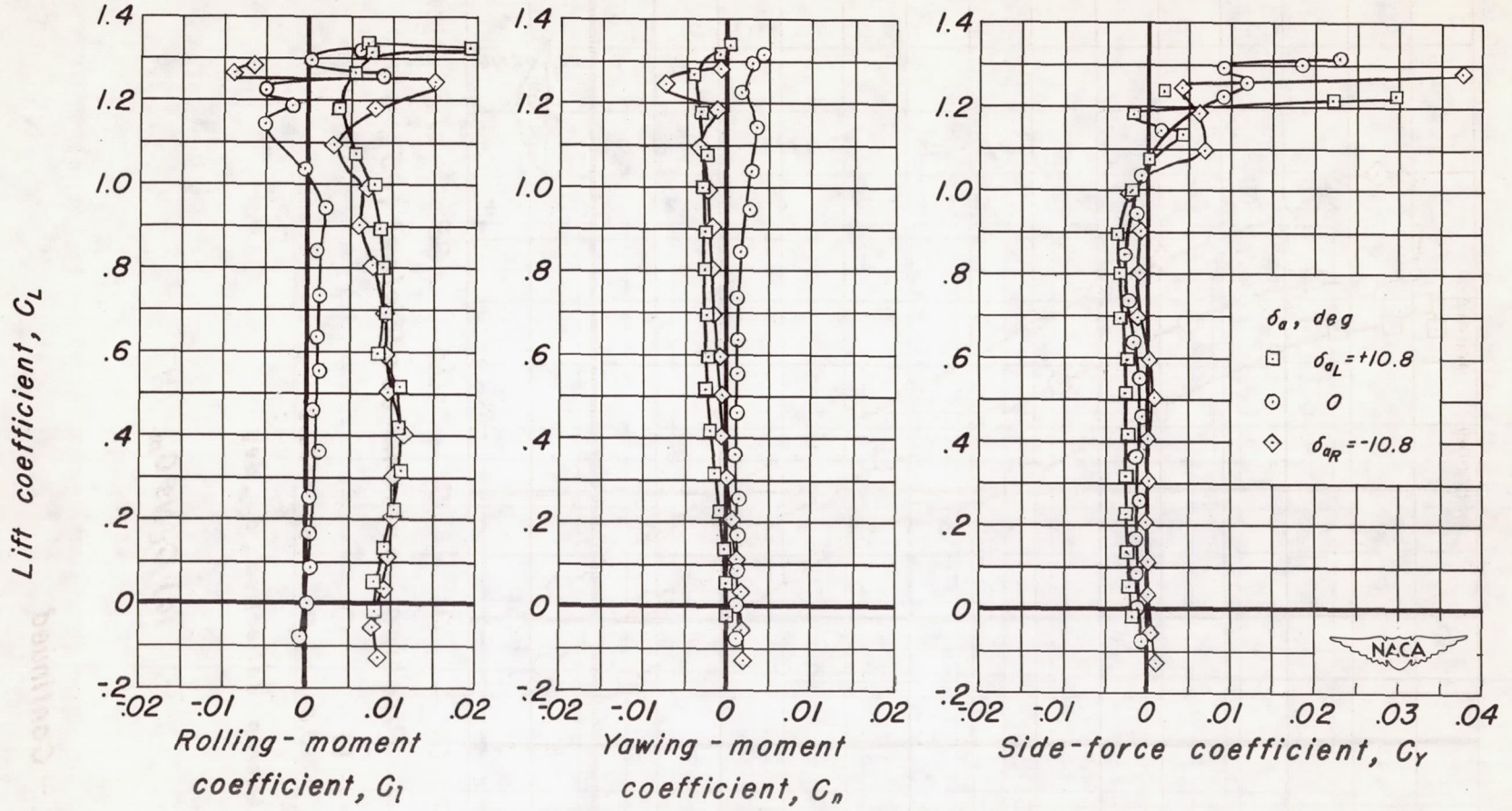
(c) C_L vs C_m .

Figure 12.—Continued.



(d) C_L vs C_{l1} , C_n and C_y .

Figure 12.- Concluded.

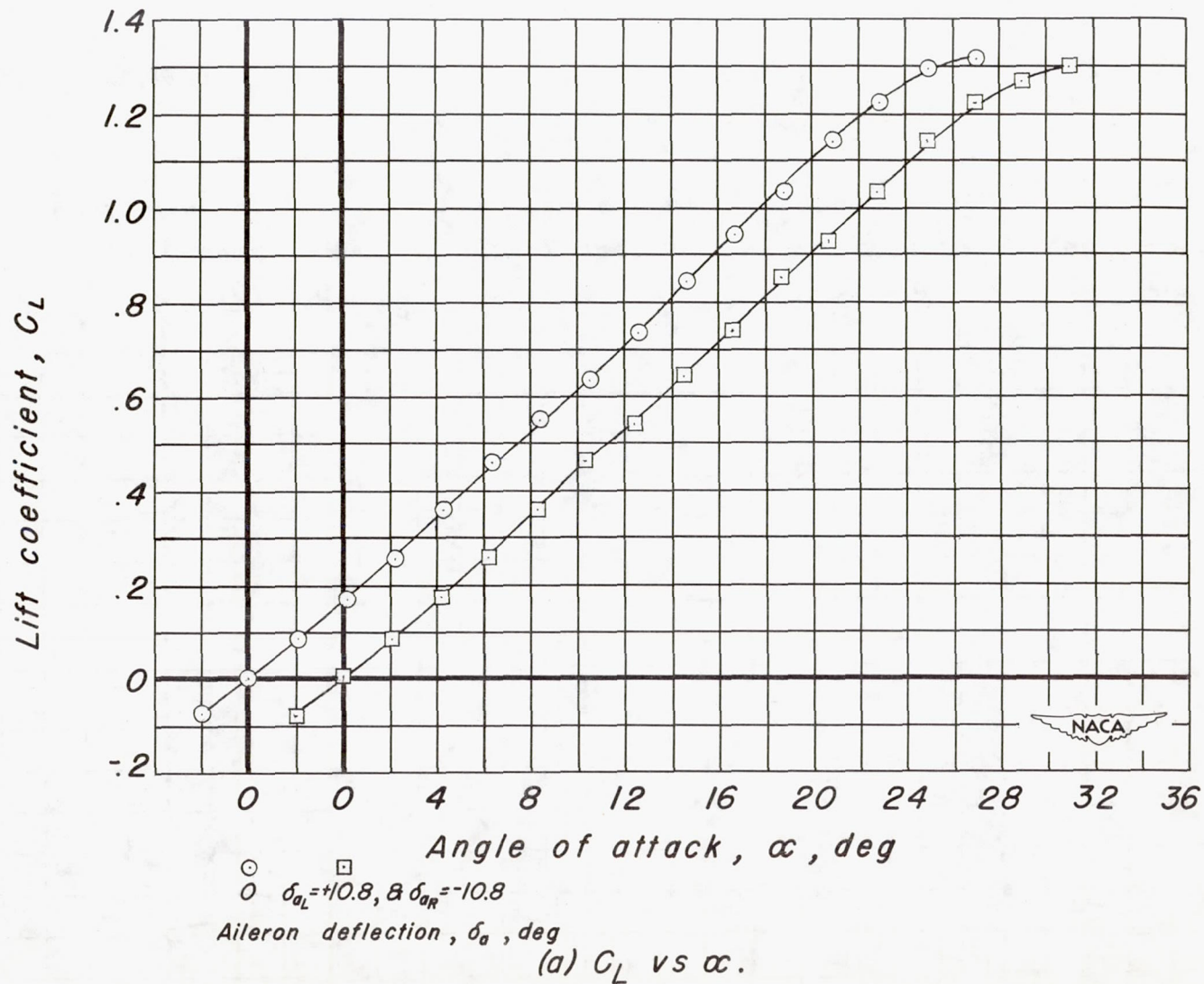


Figure 13.—Wing plus body at 0.0° angle of sideslip with both ailerons deflected.

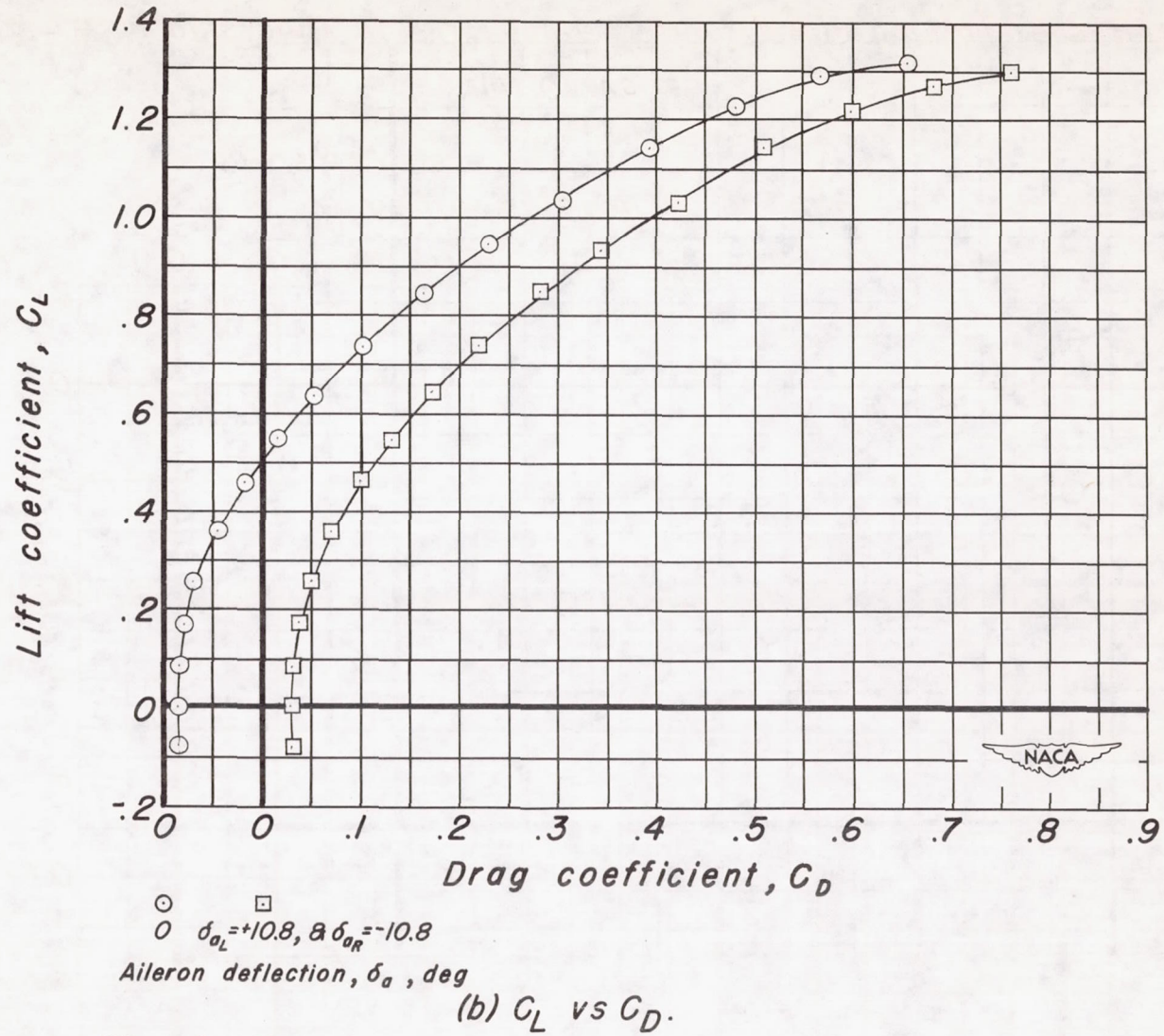
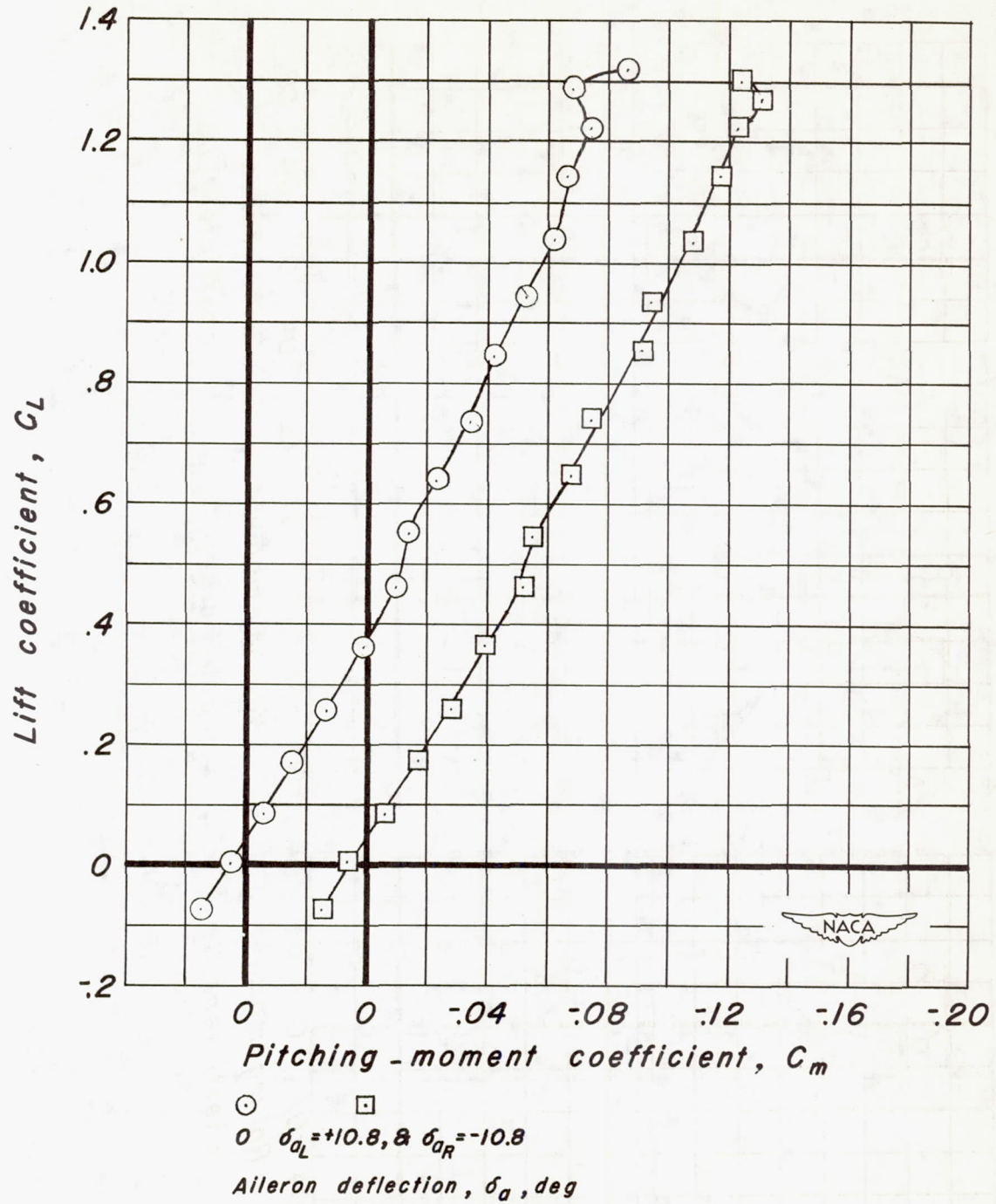
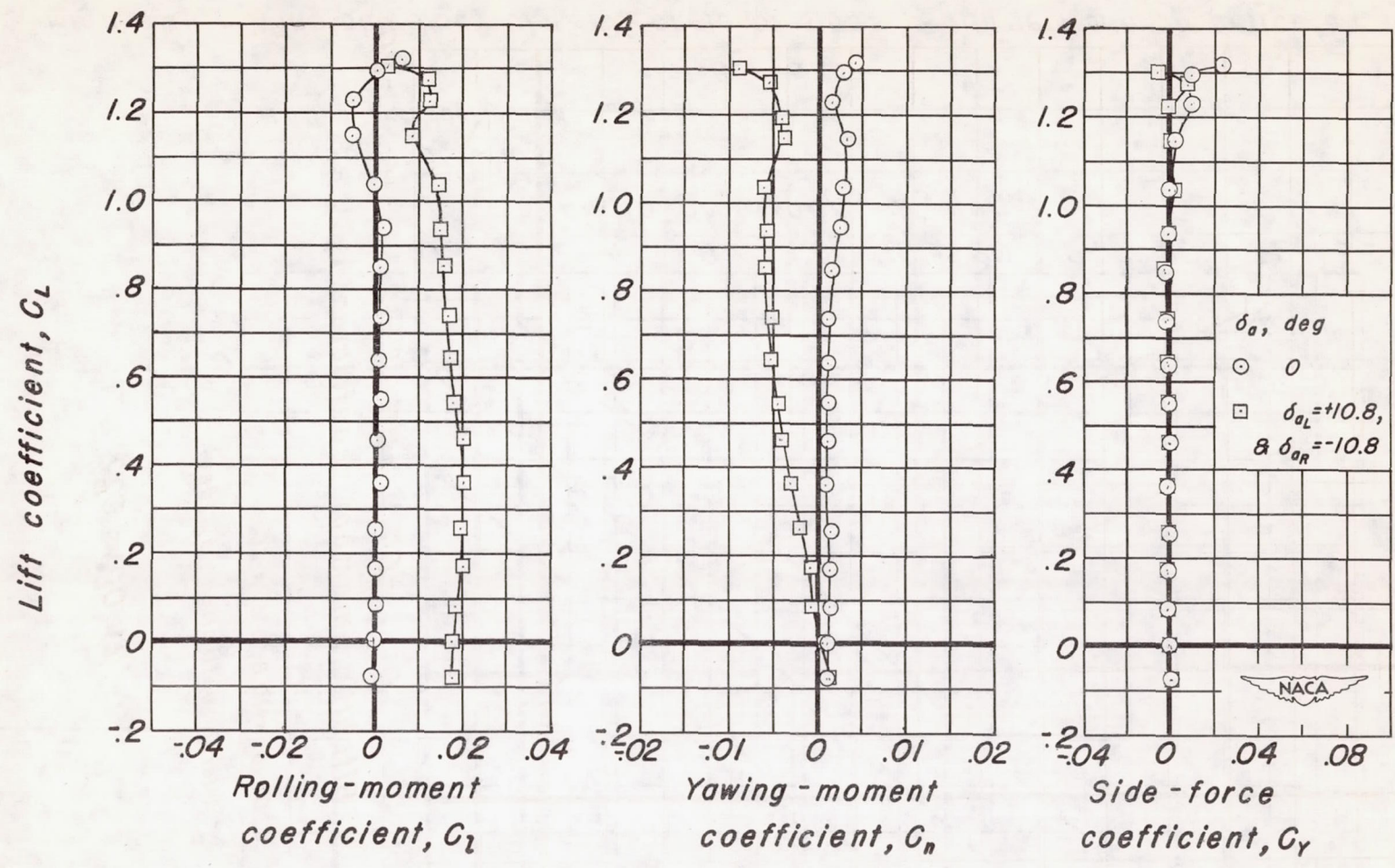


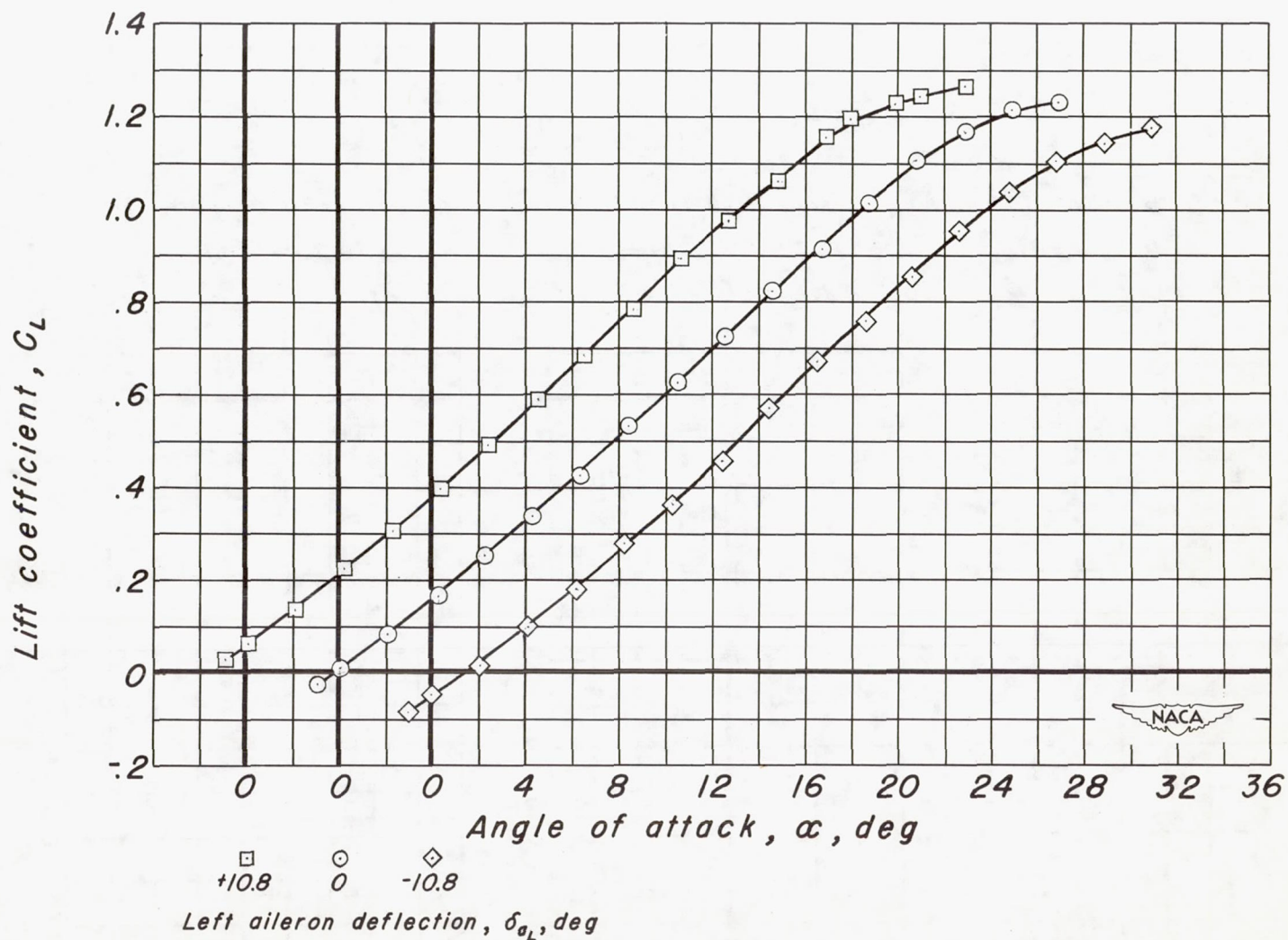
Figure 13.— Continued.





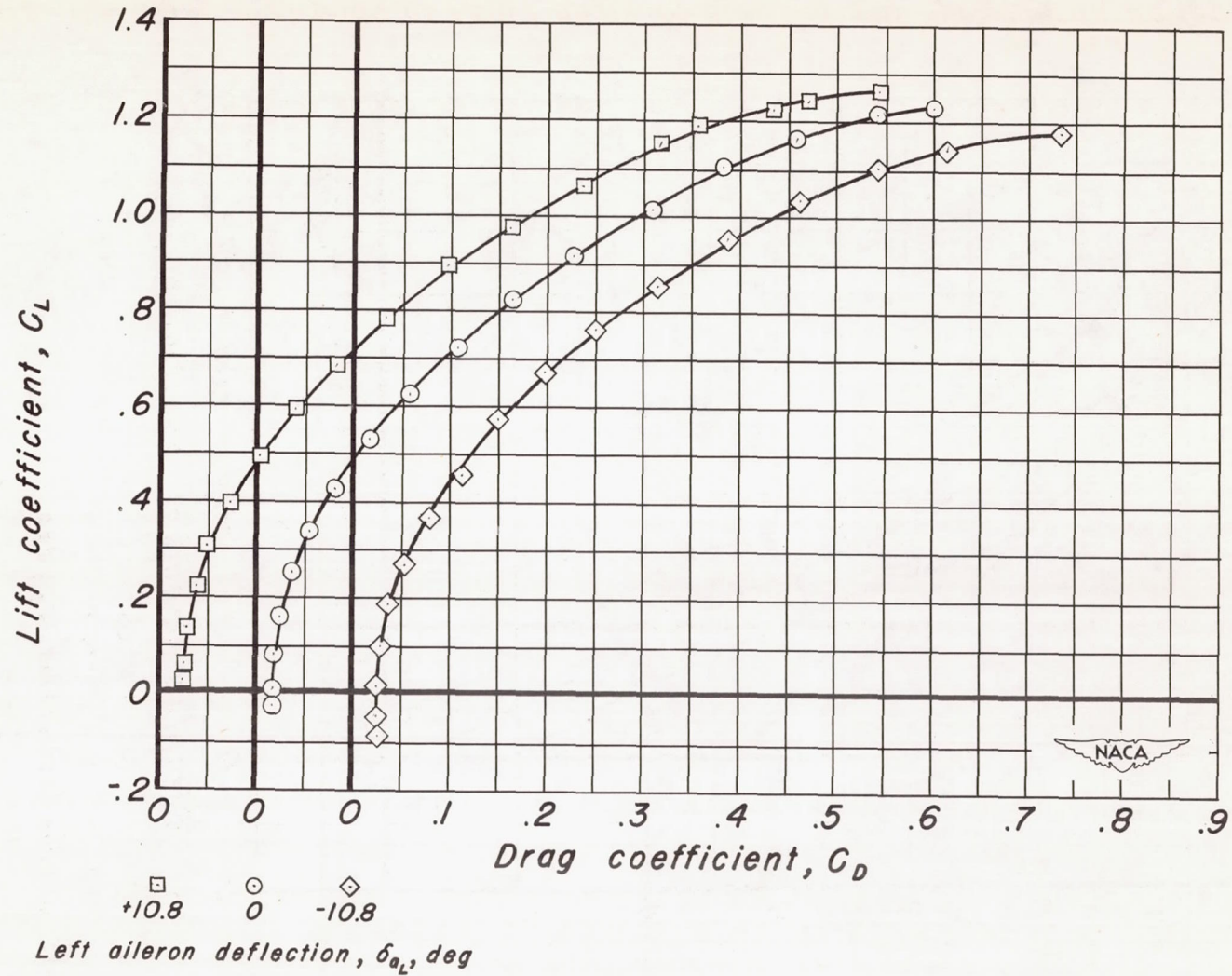
(d) C_L vs C_R , C_N and C_Y .

Figure 13.- Concluded.



(a) C_L vs α .

Figure 14.- Wing plus body at 12.0° angle of sideslip with left aileron deflected.



(b) C_L vs C_D .

Figure 14.-Continued.

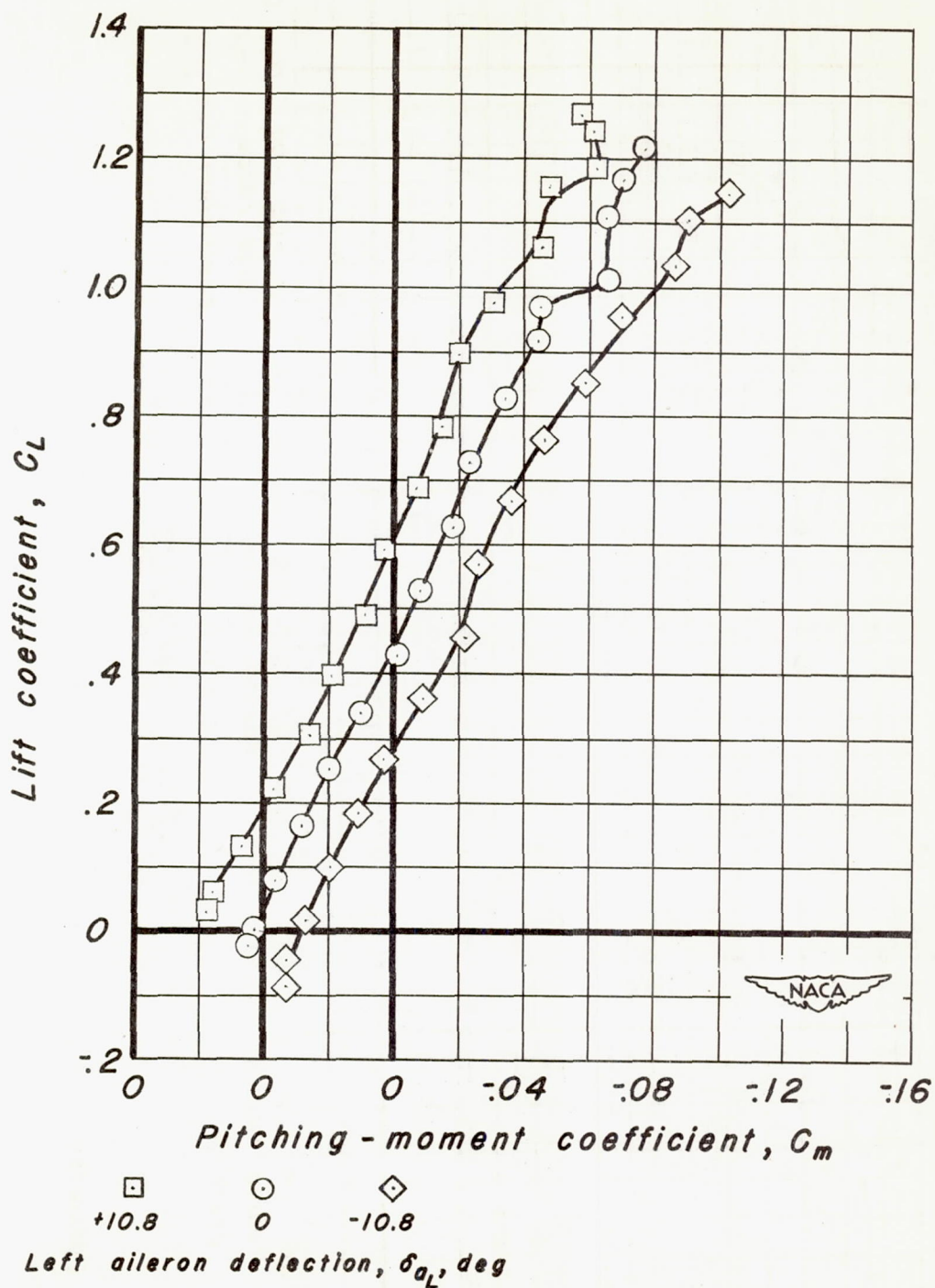
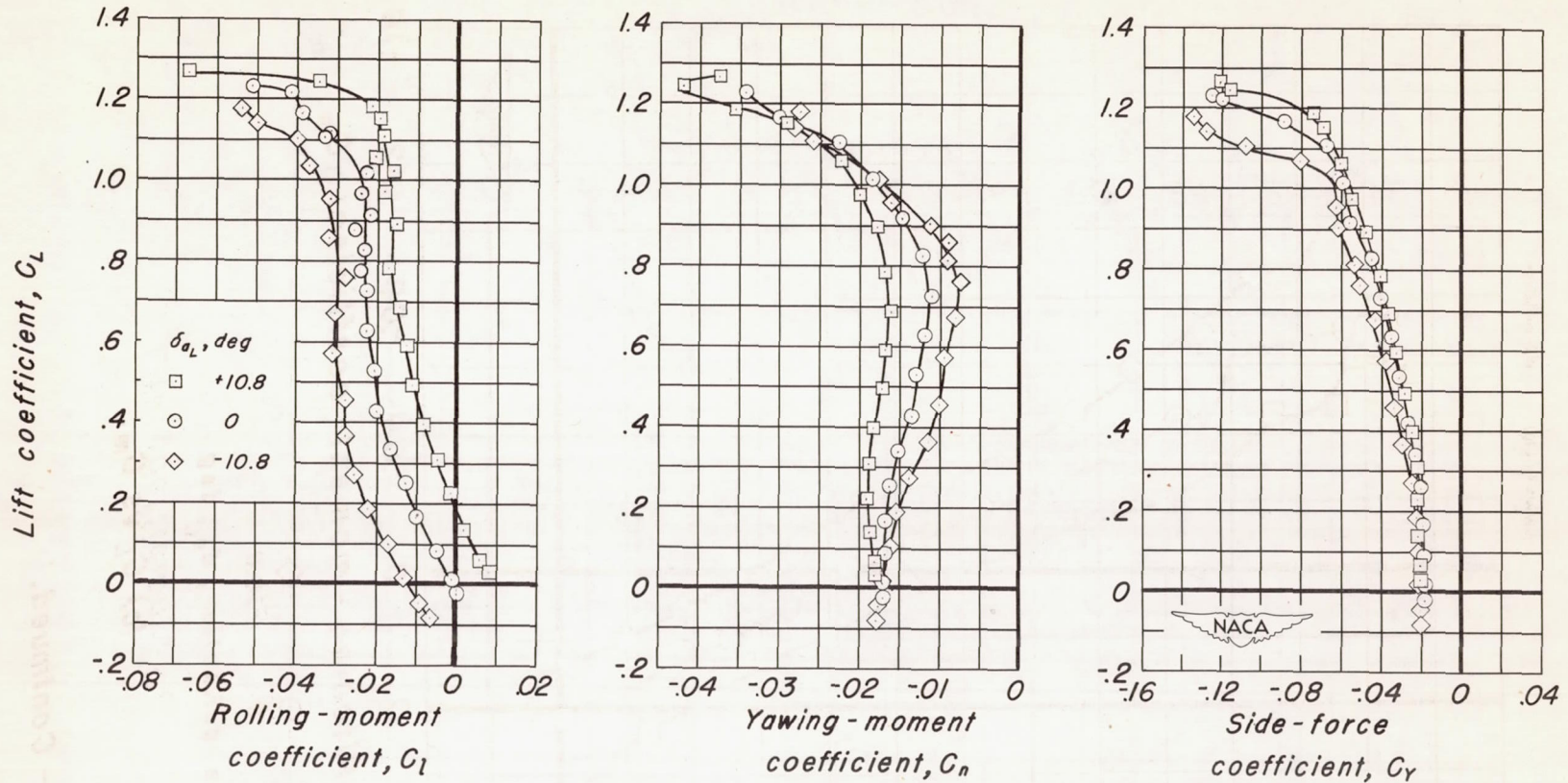
(c) C_L vs C_m .

Figure 14.— Continued.



(d) C_L vs C_l , C_n and C_y .

Figure 14.— Concluded.

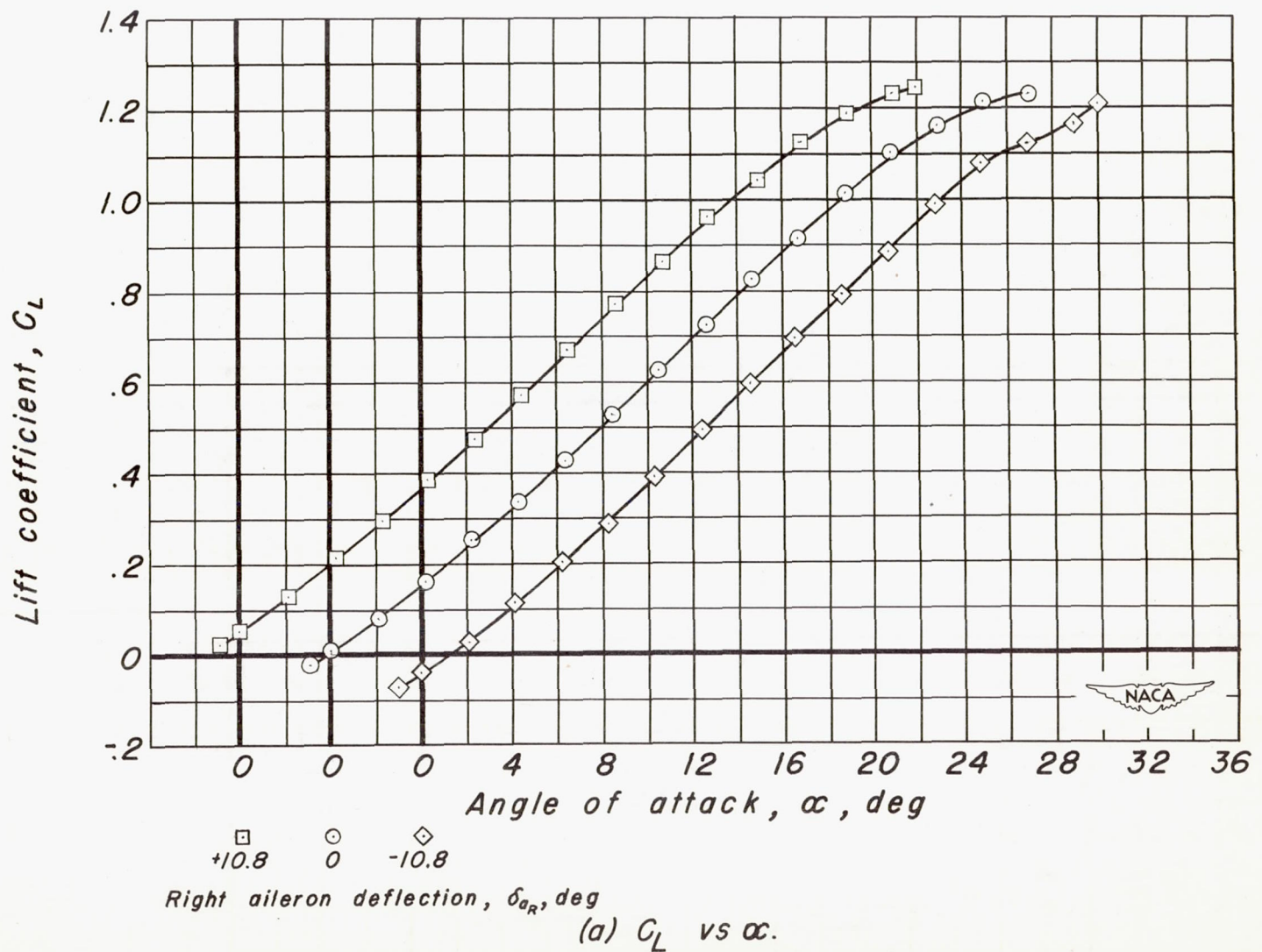
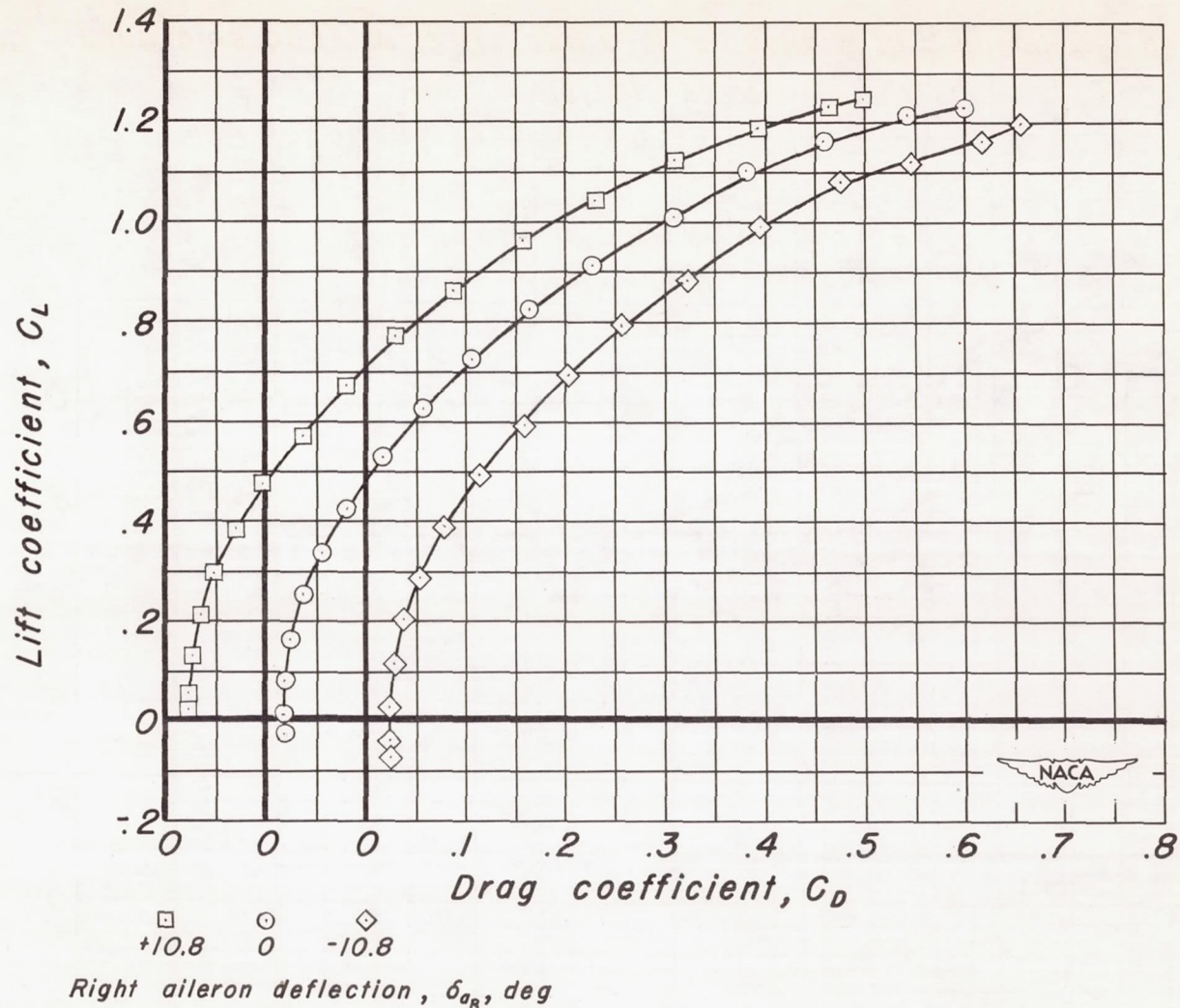
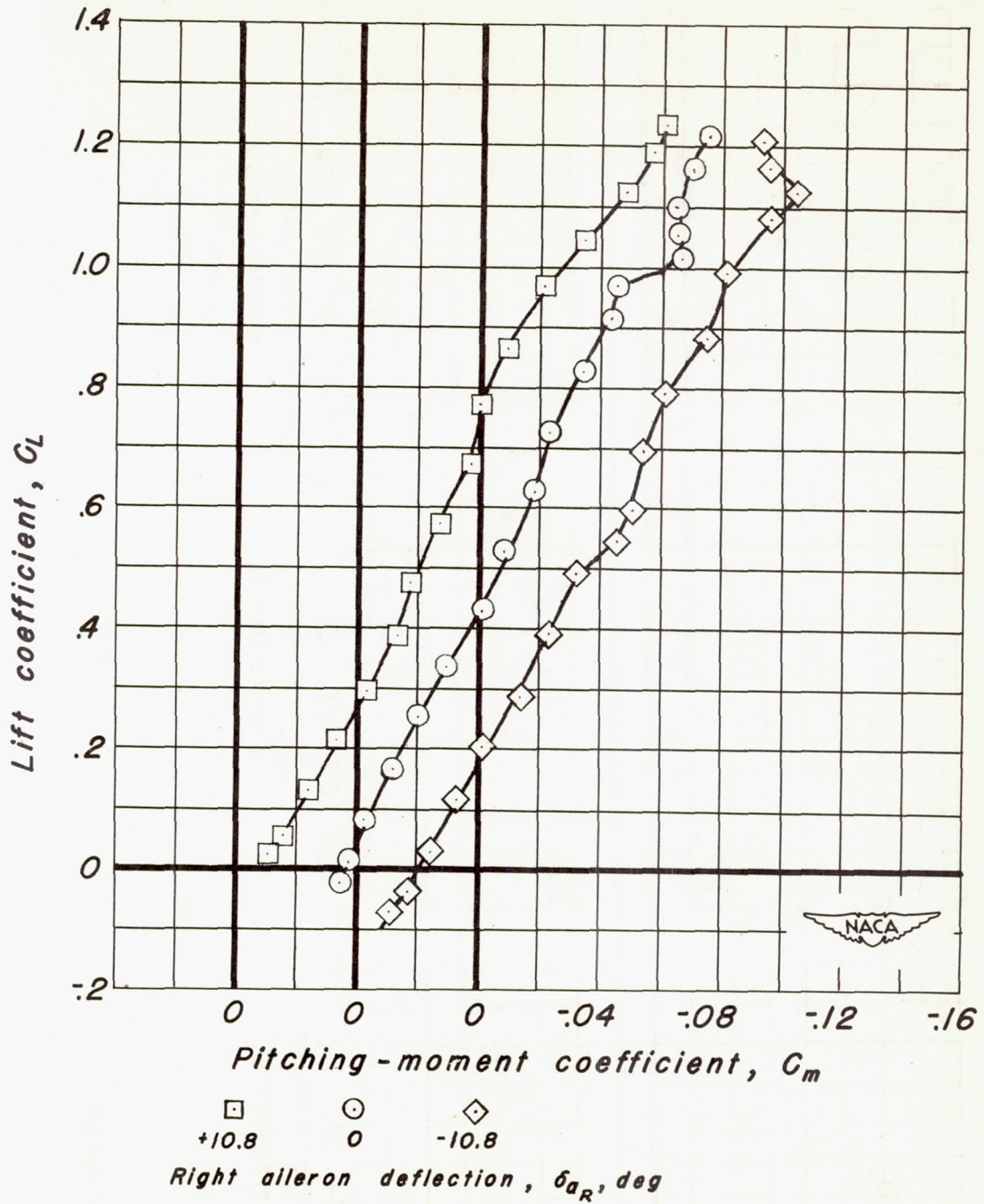


Figure 15.- Wing plus body at 12.0° angle of sideslip with right aileron deflected.

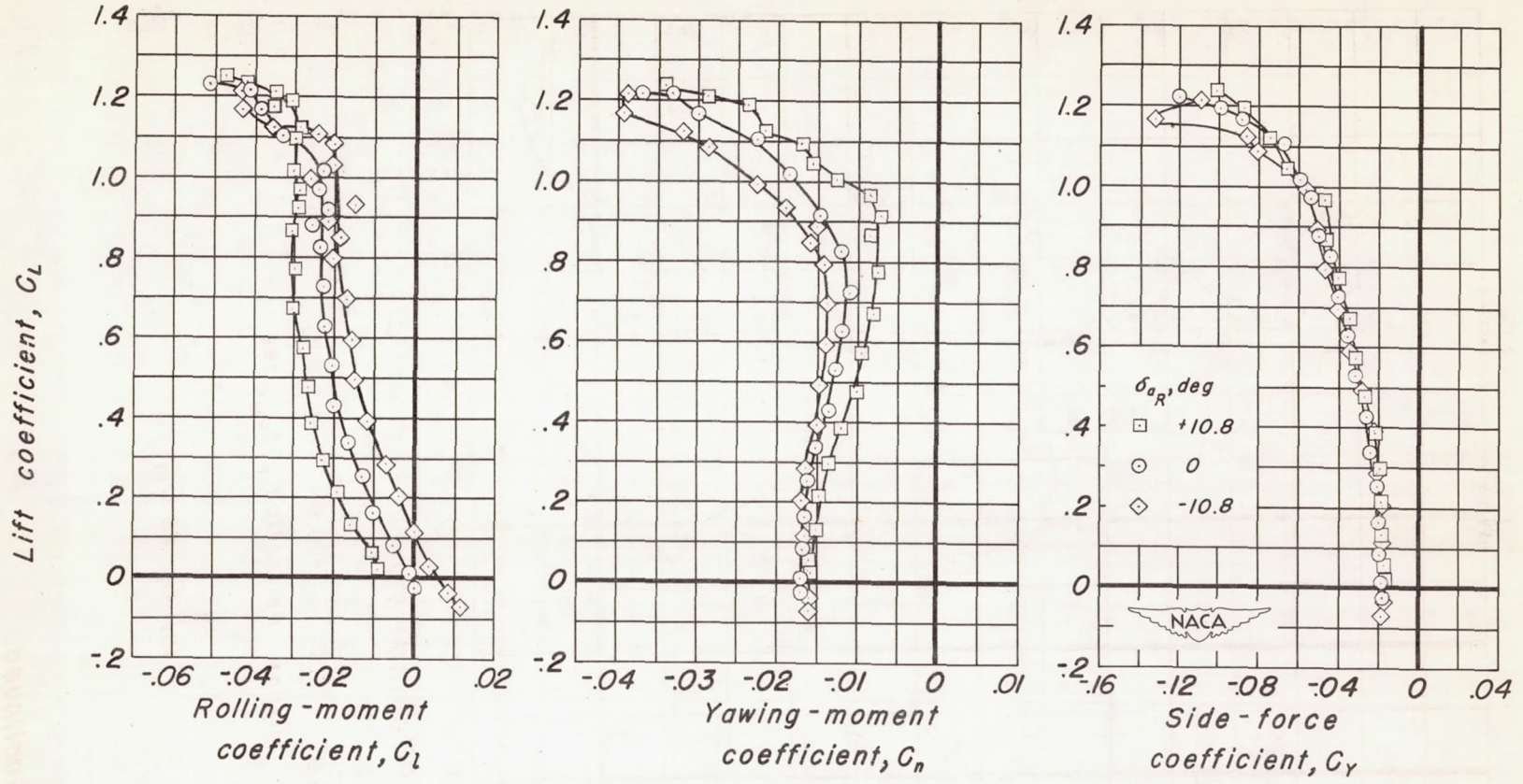


(b) C_L vs C_D .
 Figure 15.- Continued.



(c) C_L vs C_m .

Figure 15.— Continued.



(d) C_L vs C_l , C_n and C_Y .

Figure 15.— Concluded.

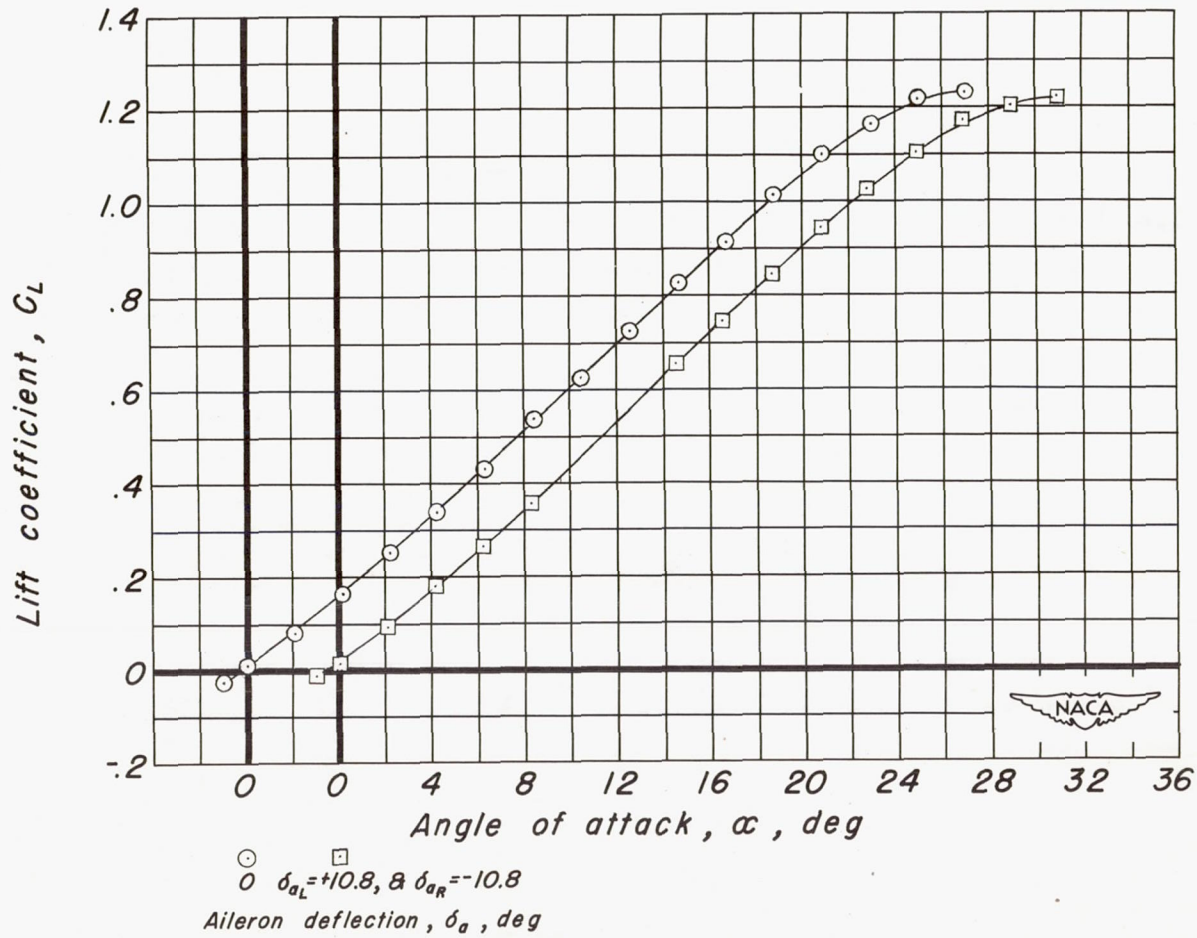


Figure 16.- Wing plus body at 12.0° angle of sideslip with both ailerons deflected.

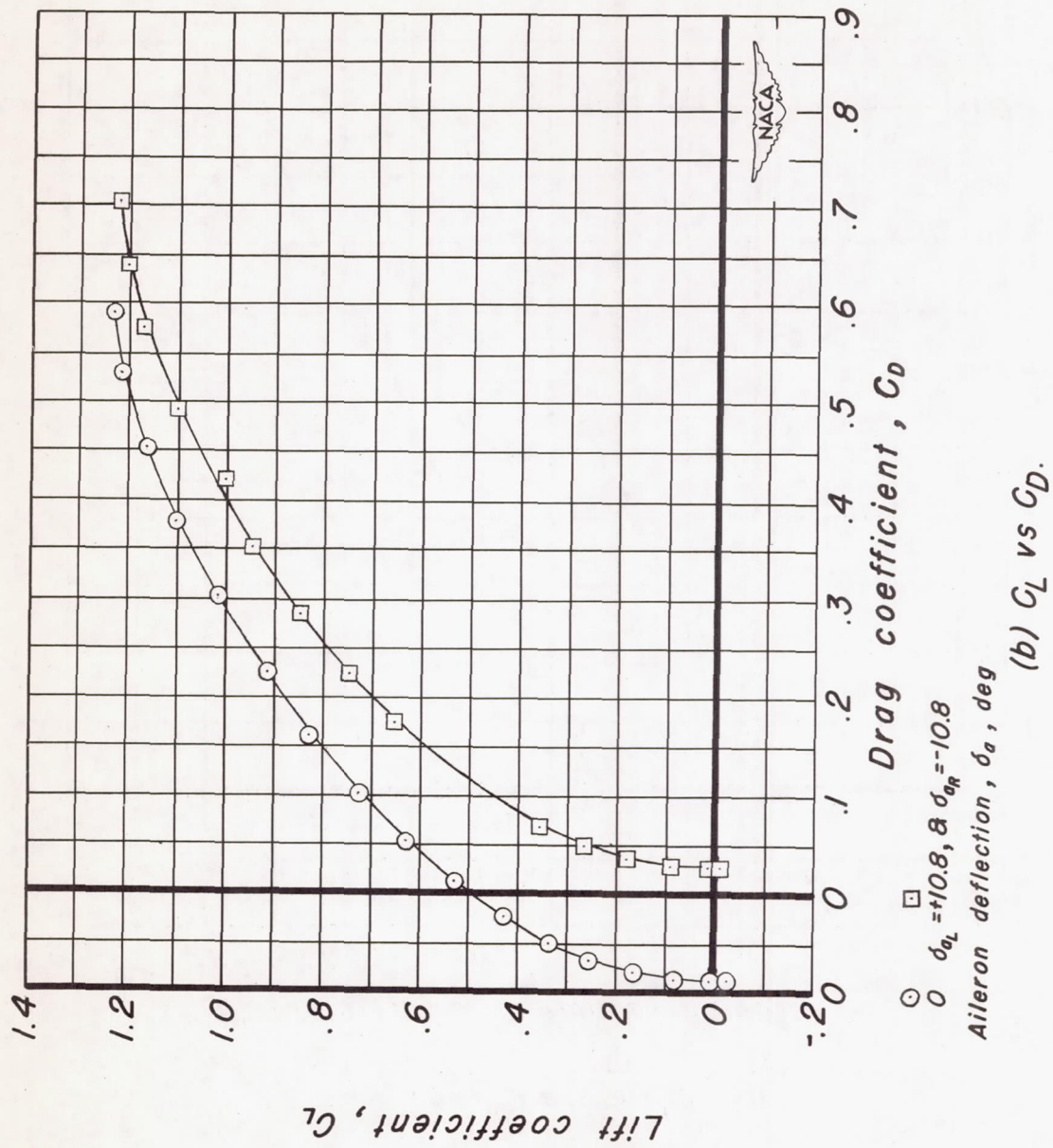
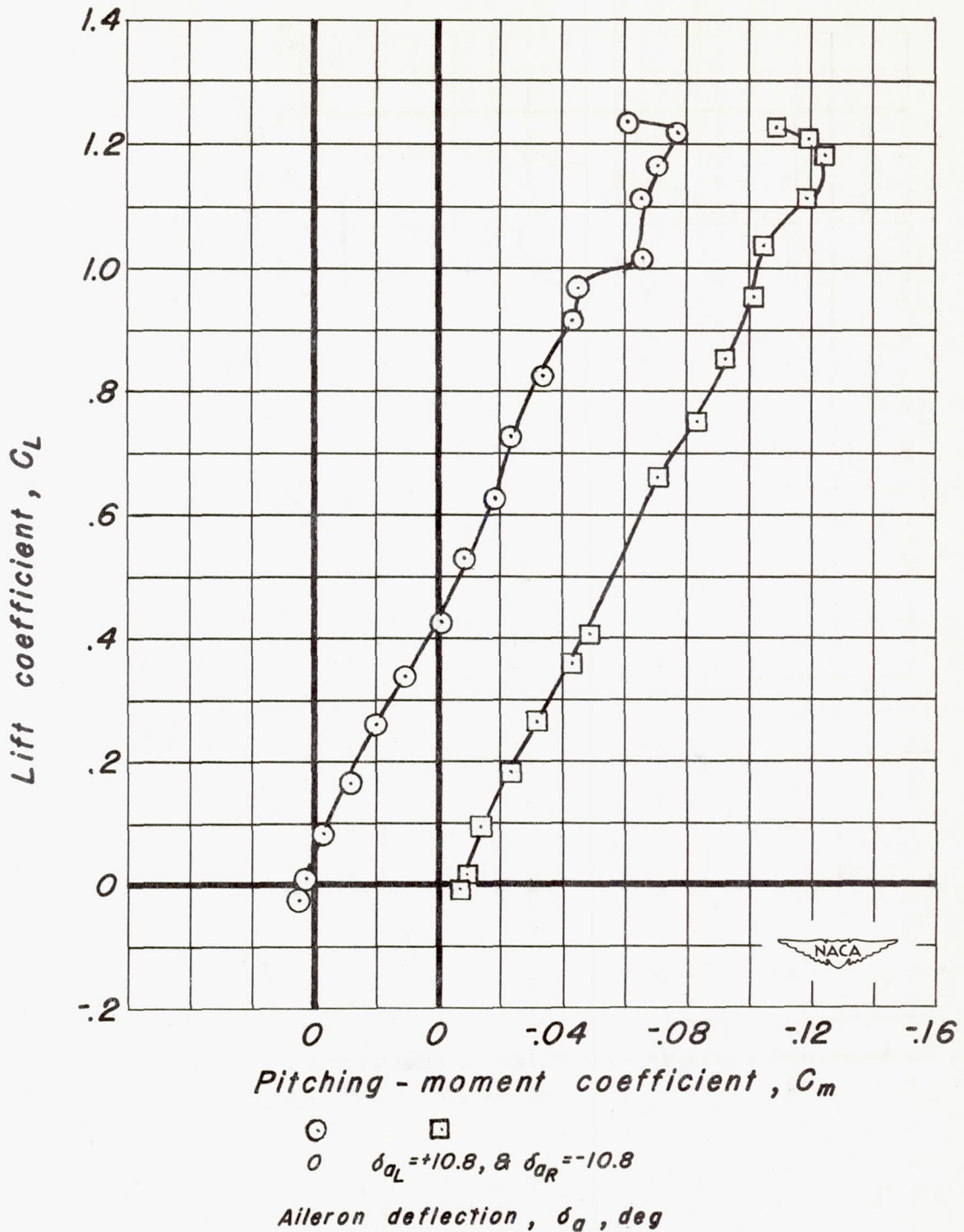
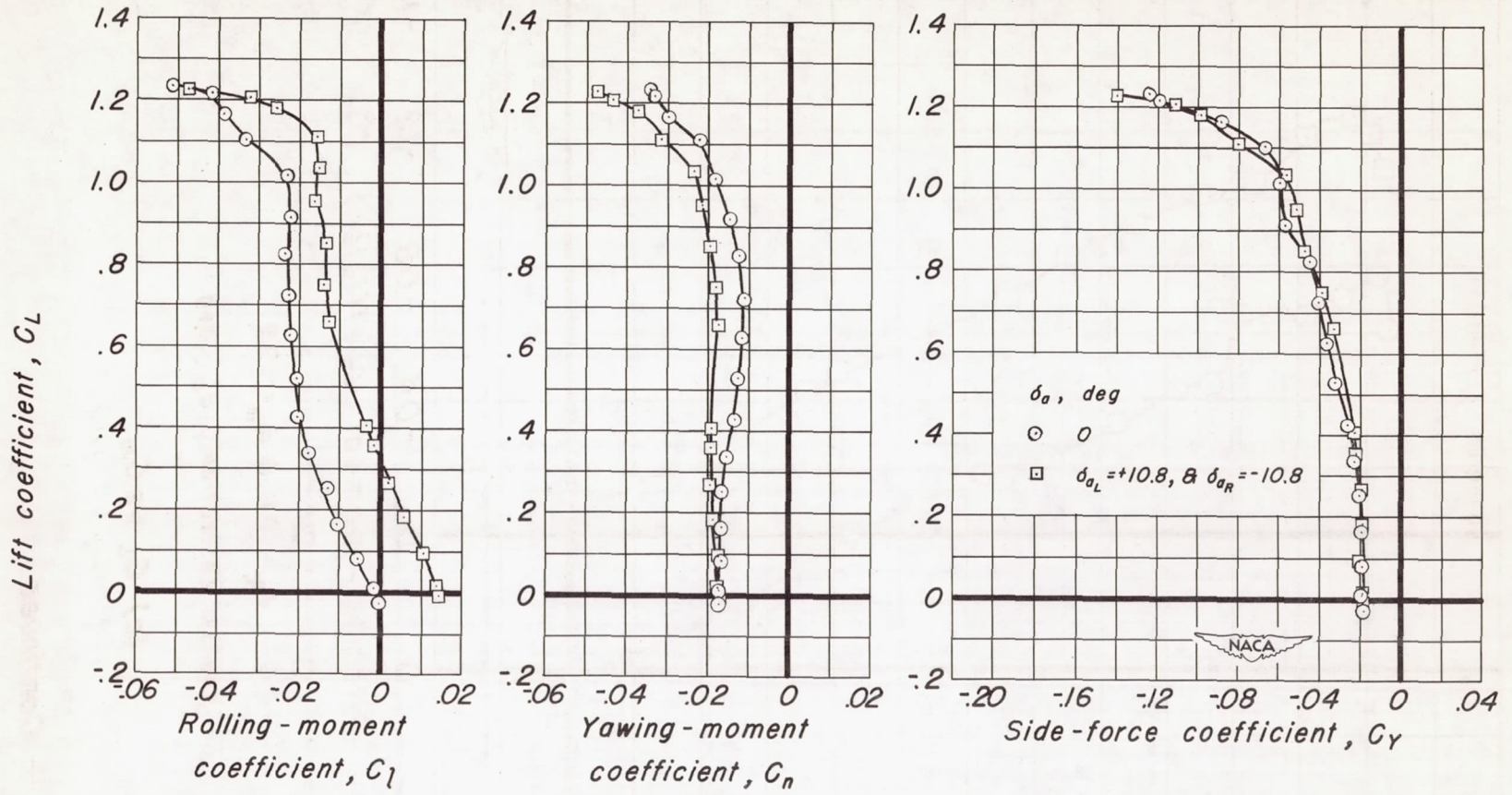


Figure 16.- Continued.



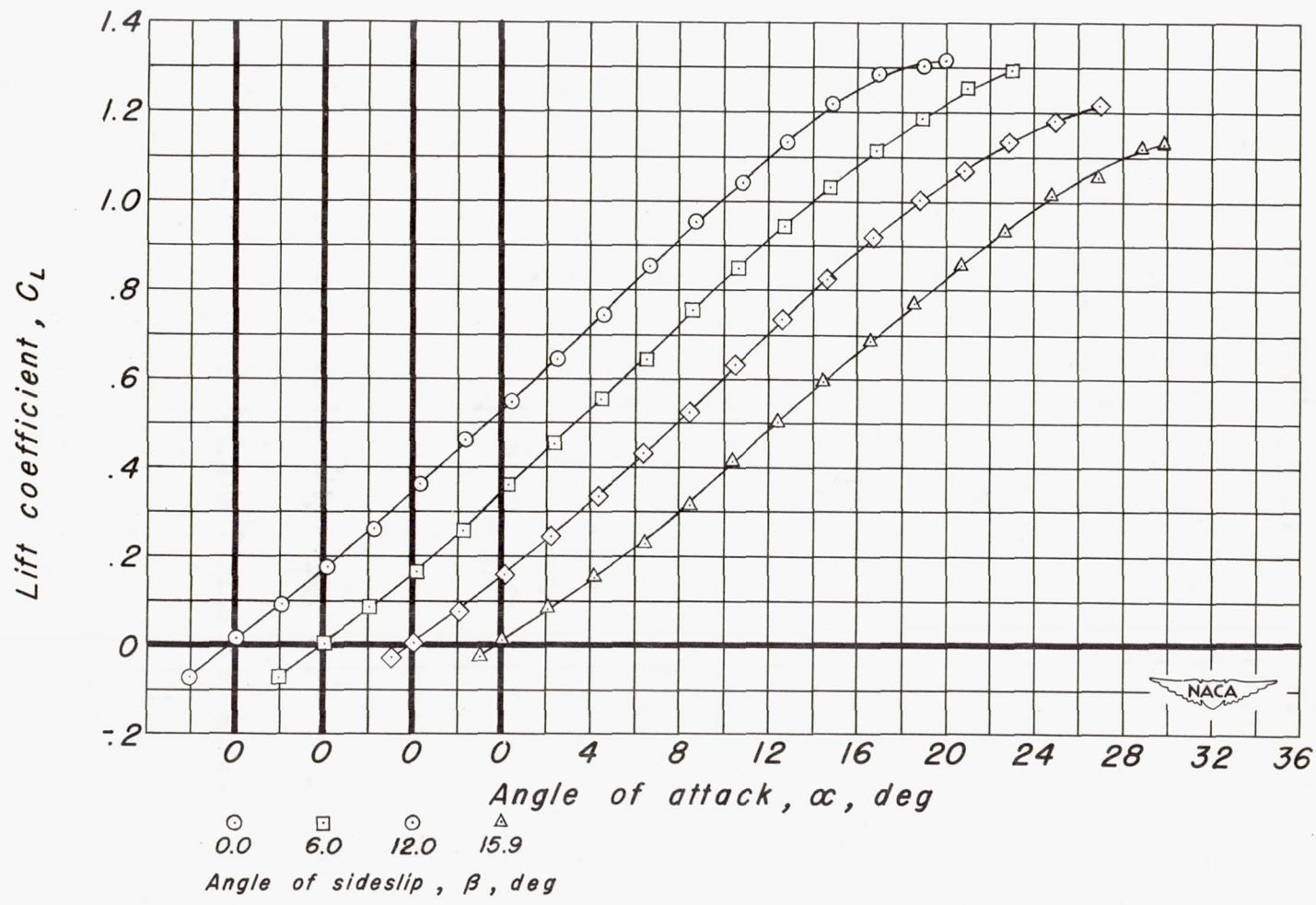
(c) C_L vs C_m .

Figure 16. — Continued.



(d) C_L vs C_l , C_n and C_Y .

Figure 16.— Concluded.



(a) C_L vs α .

Figure 17. - Wing plus body plus vertical tail at various angles of sideslip with controls neutral.

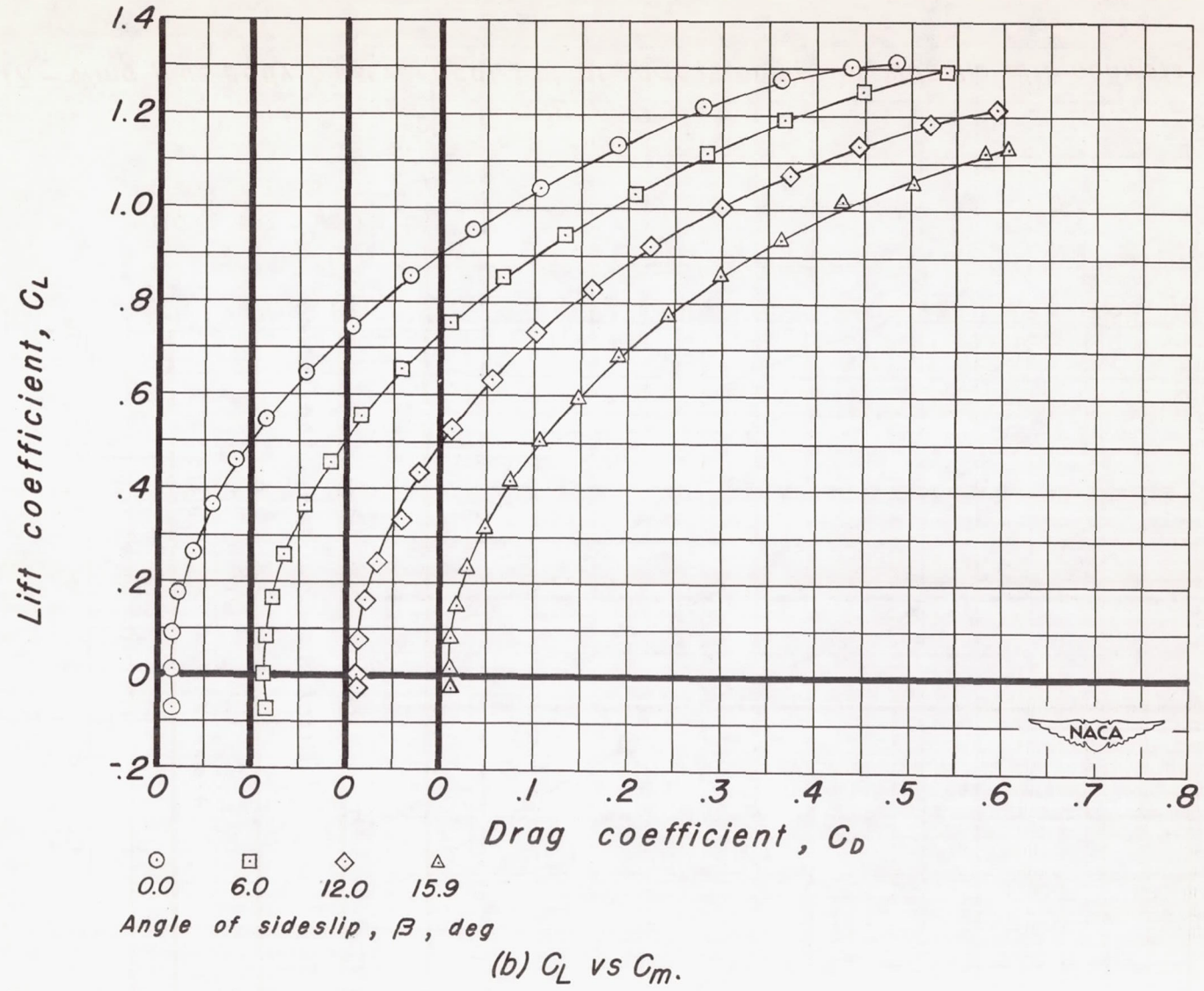
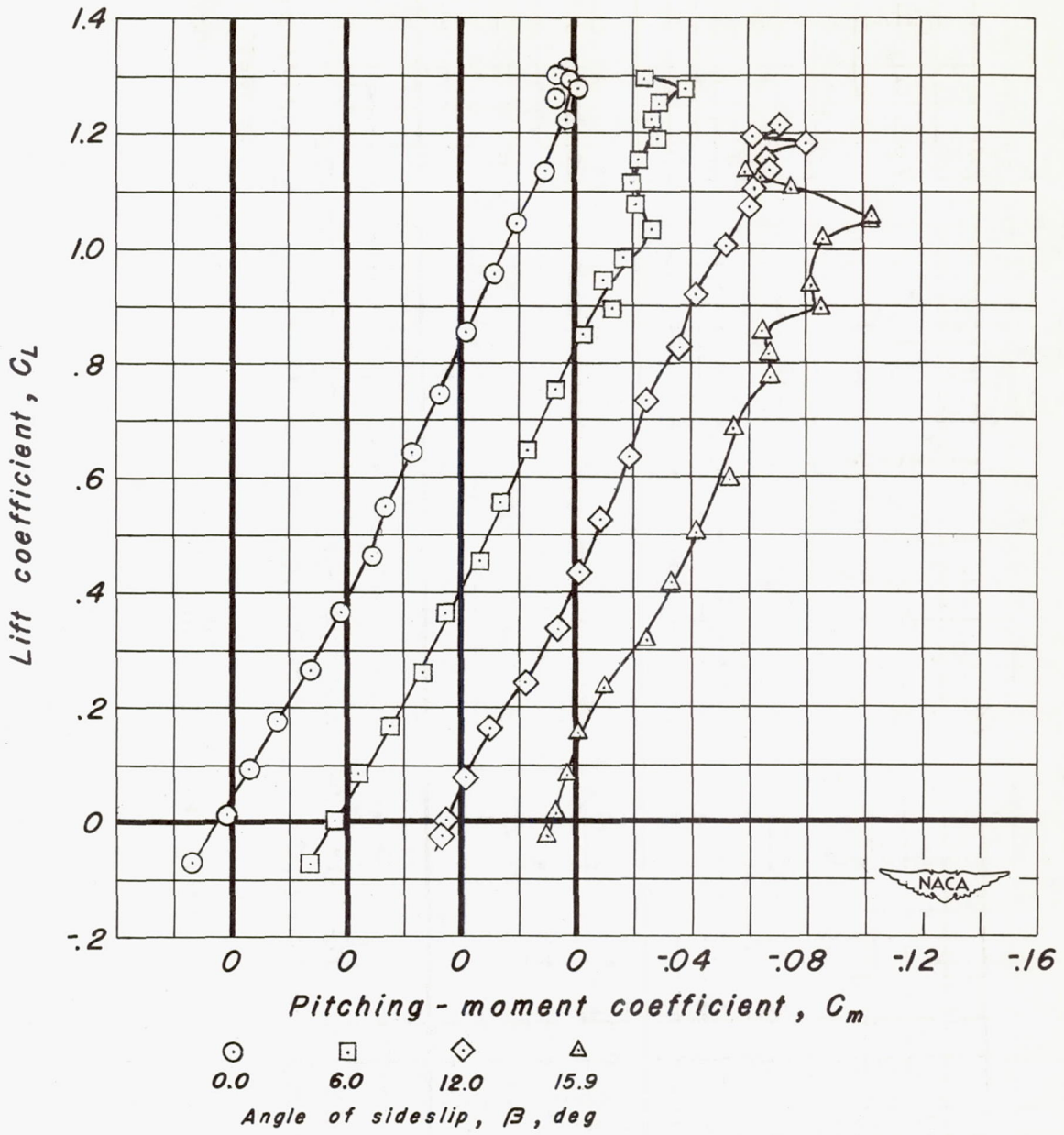
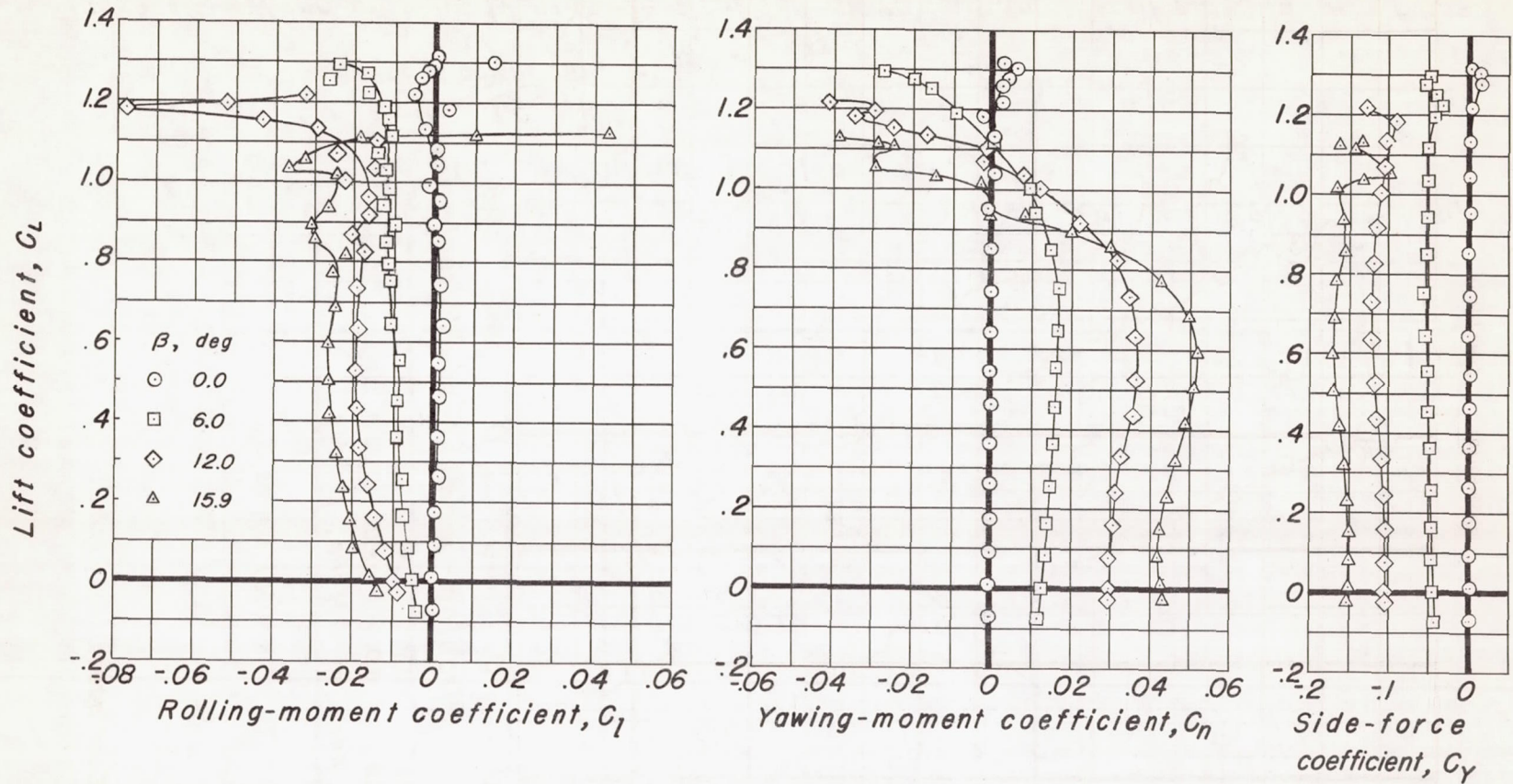


Figure 17.- Continued.



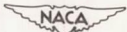
(c) C_L vs C_m .

Figure 17. — Continued.



(d) C_L vs C_{Lr} , C_N and C_Y .

Figure 17. - Concluded.



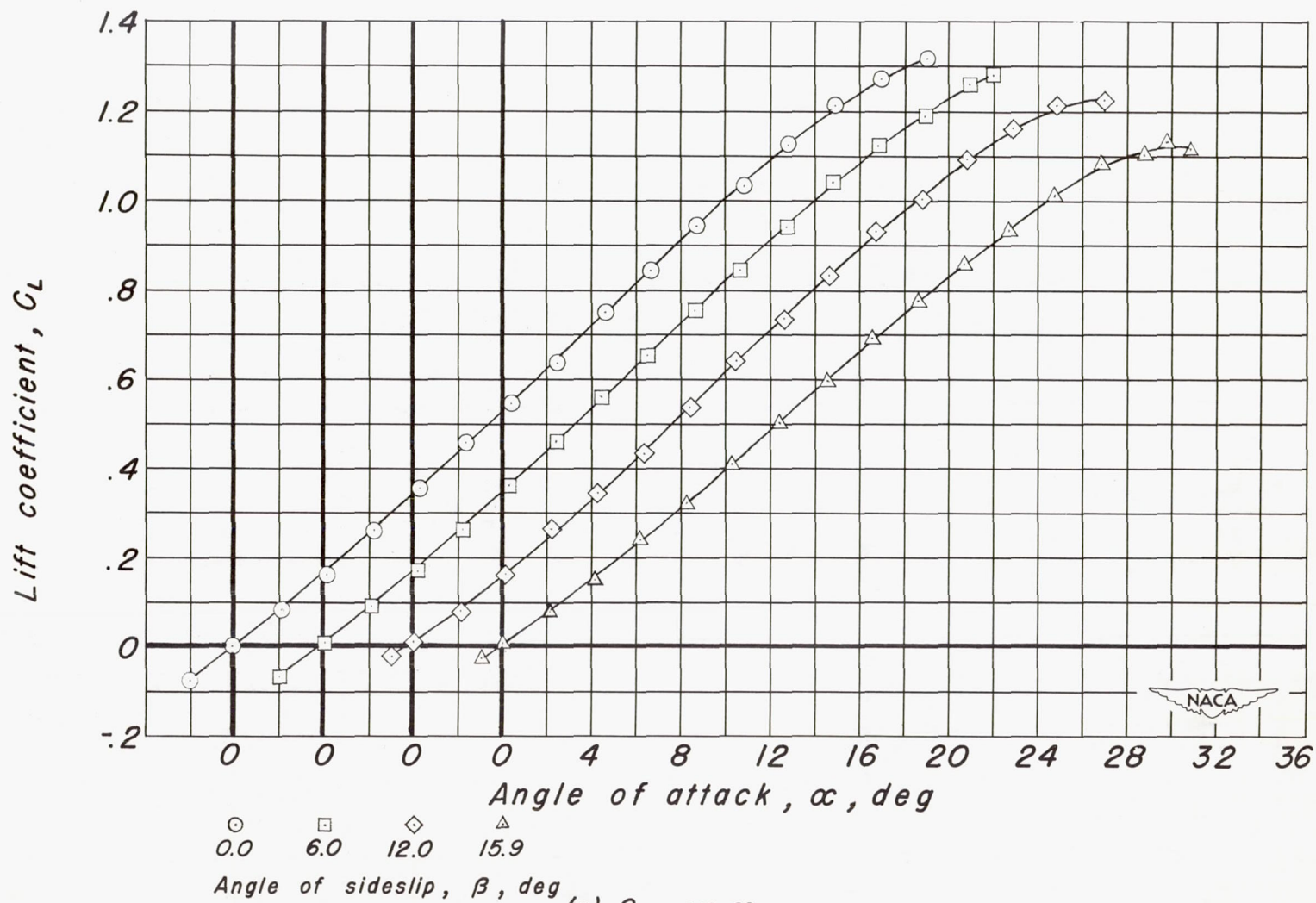
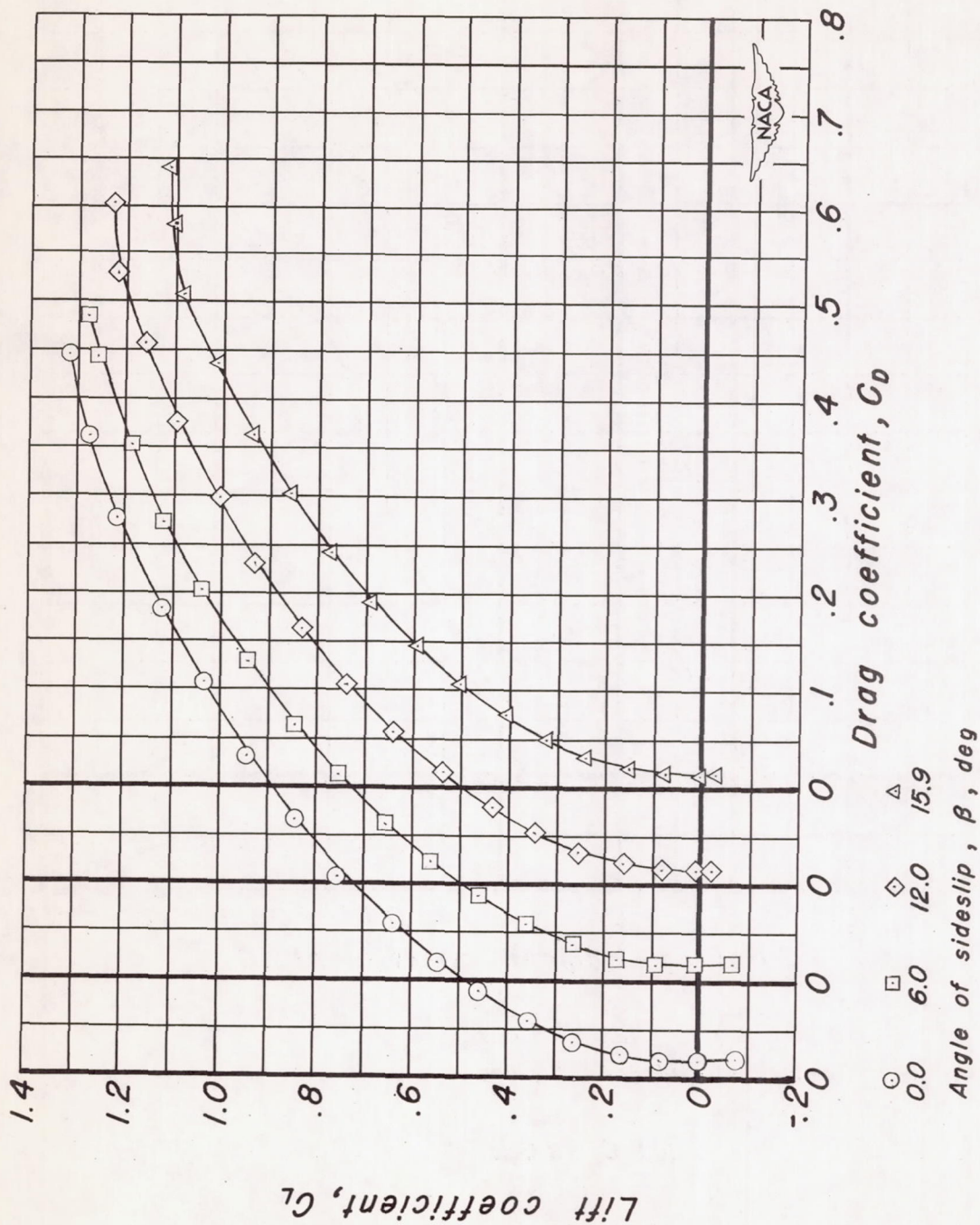


Figure 18.— Wing plus body plus vertical tail at various angles of sideslip with flaps undeflected and rudder deflected 10° .



(b) C_L vs C_D .

Figure 18.— Continued.

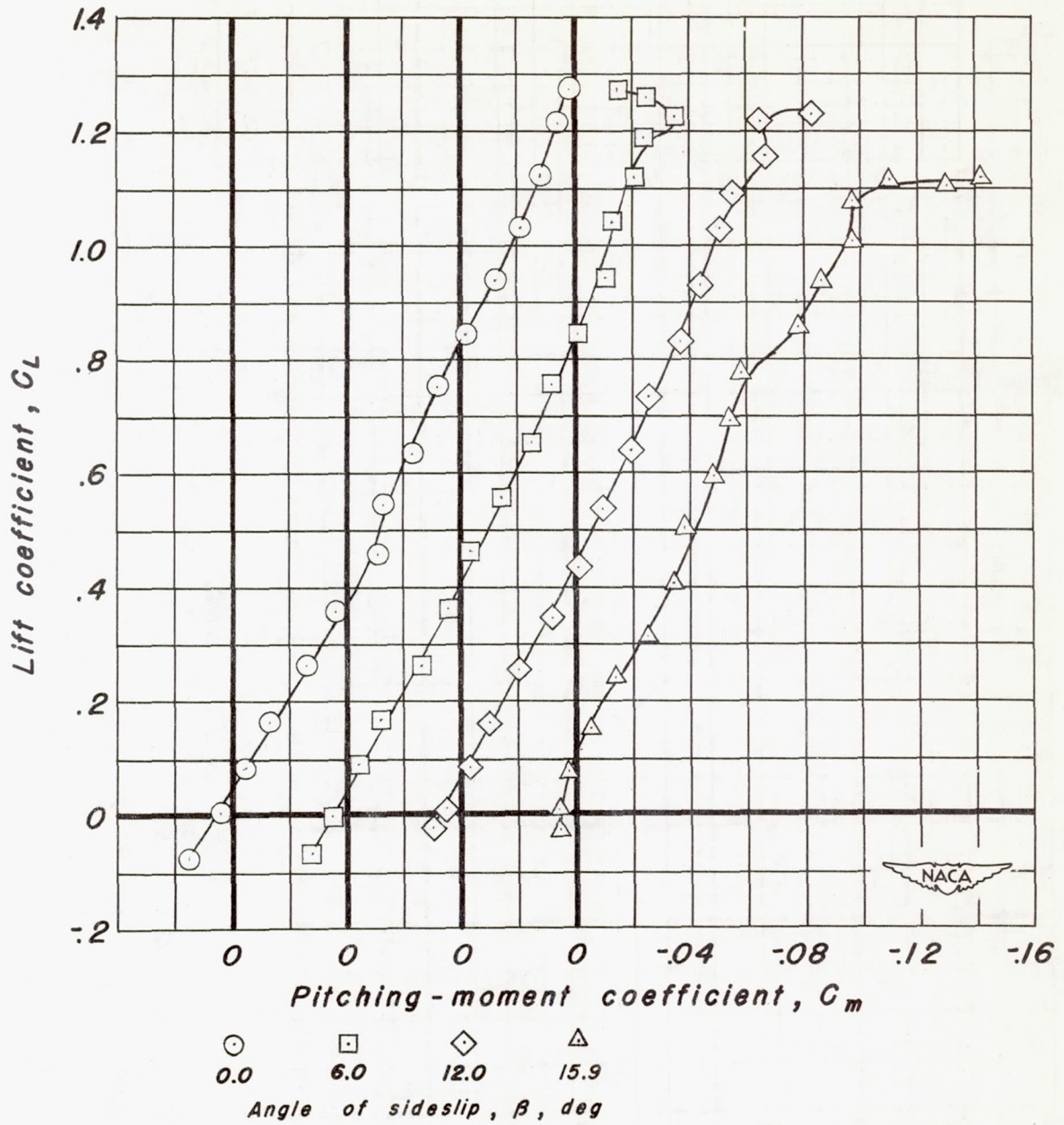
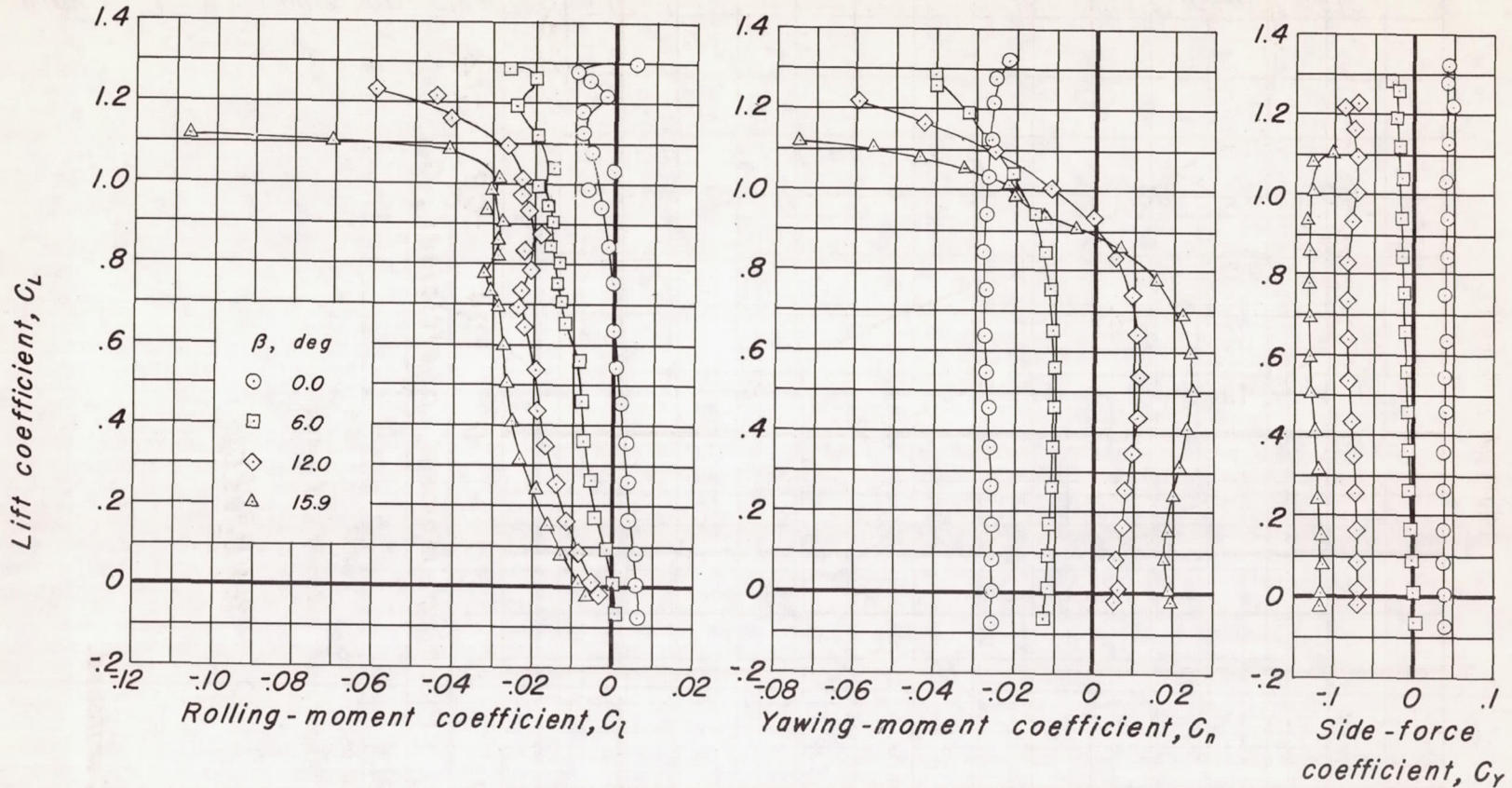
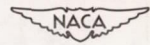
(c) C_L vs C_m .

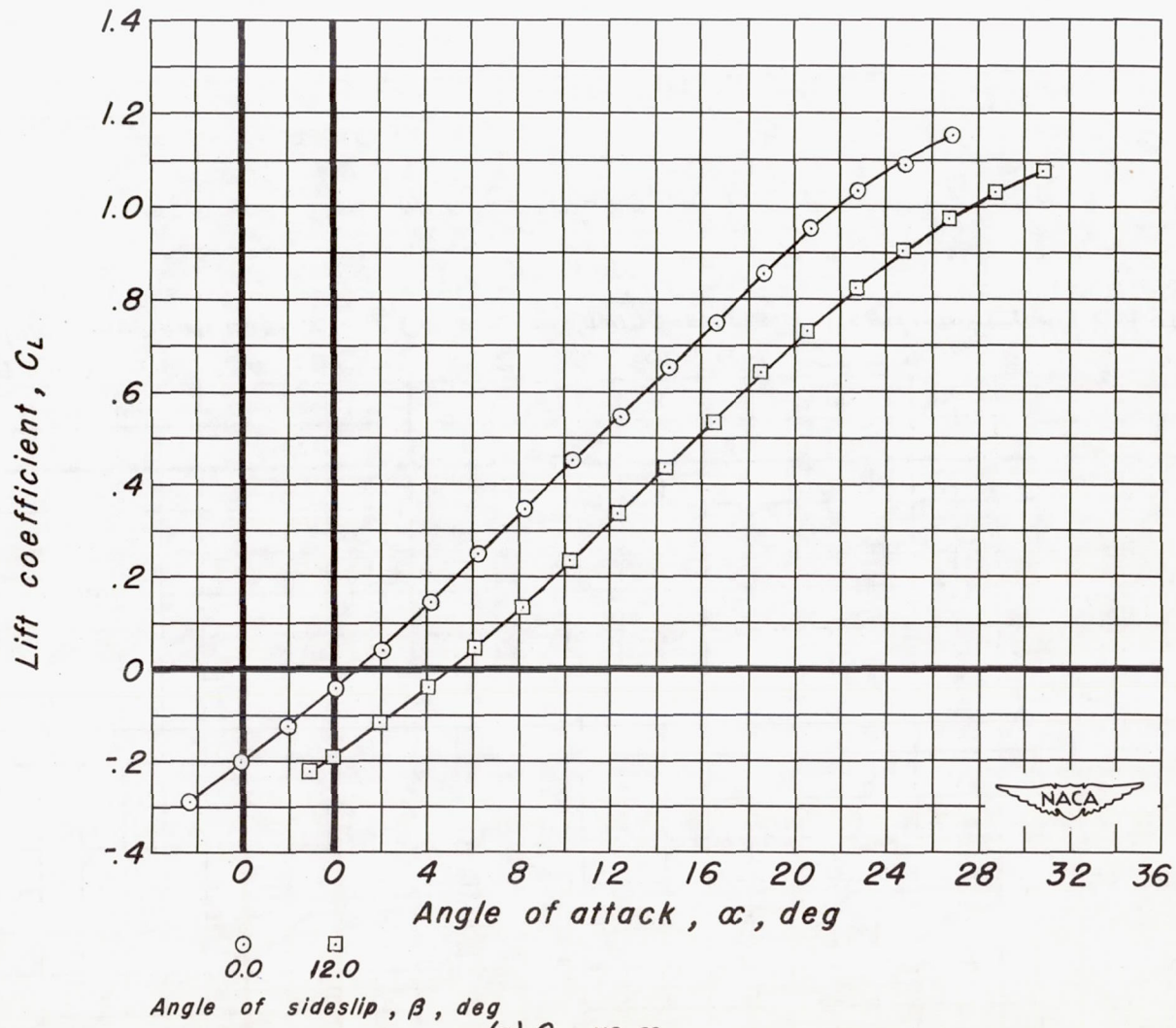
Figure 18.— Continued.



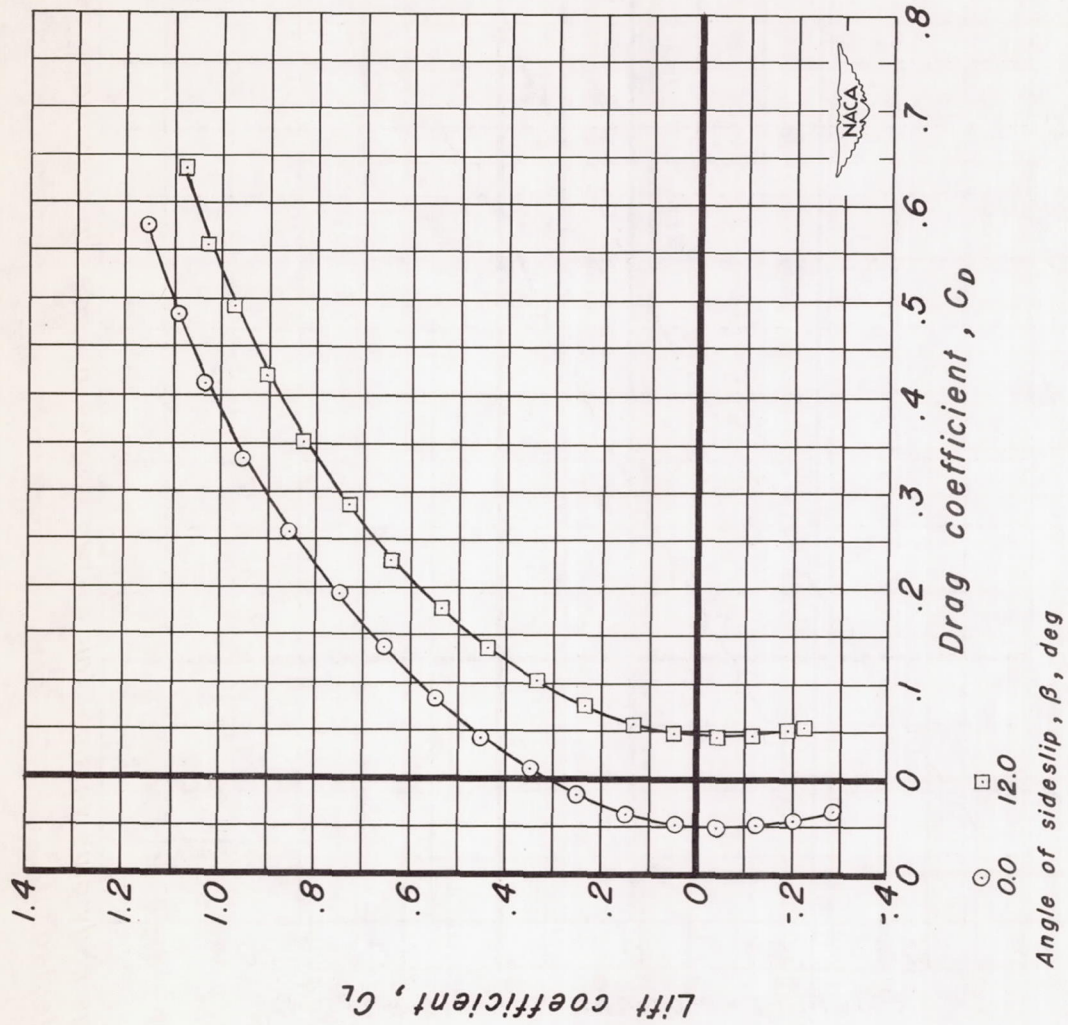
(d) C_L vs C_l , C_n and C_Y .

Figure 18.— Concluded.



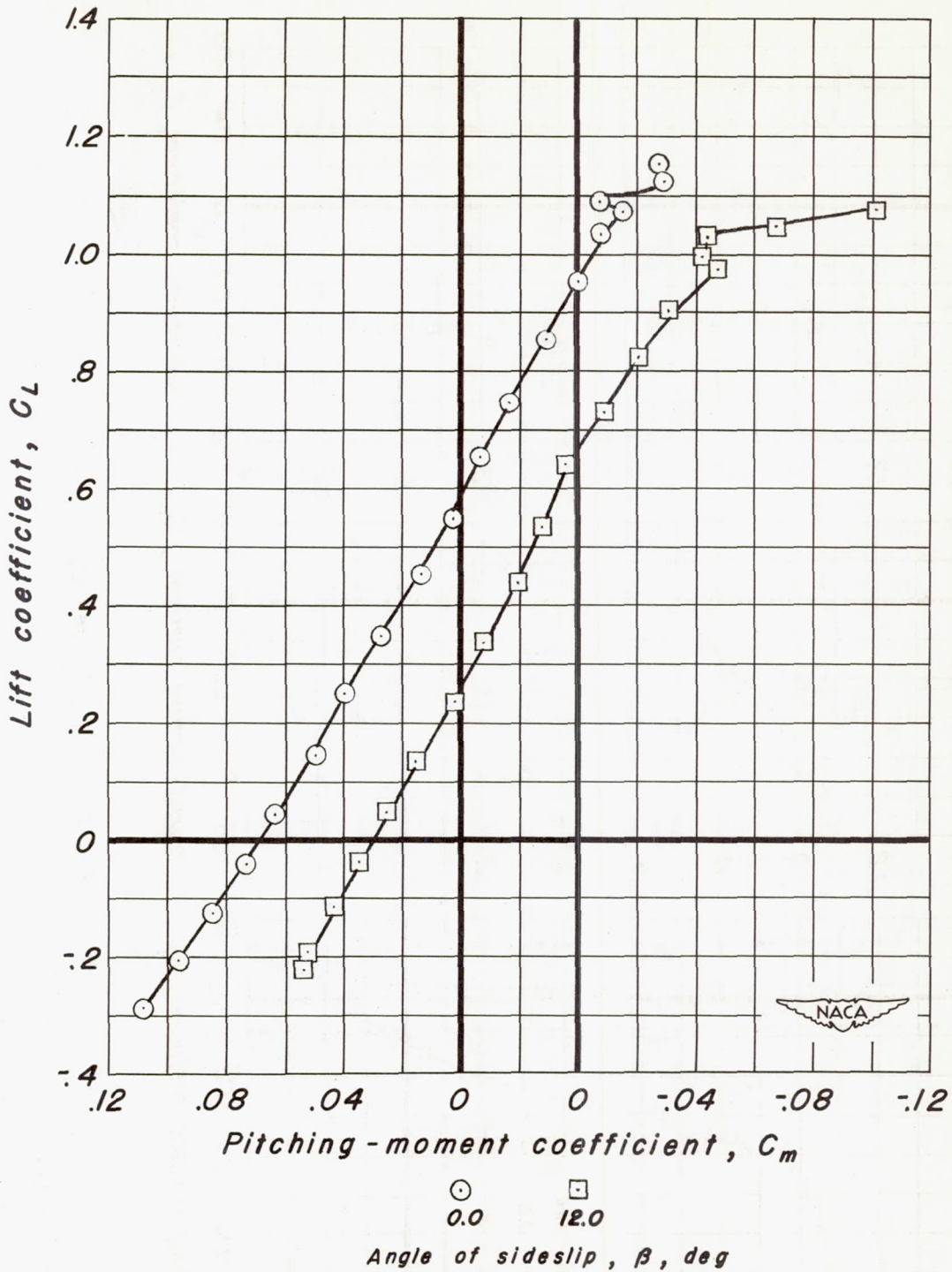


(a) C_L vs α .
Figure 19.— Wing plus body plus vertical tail at two angles of sideslip with flaps deflected -20.7° and rudder deflected 10° .



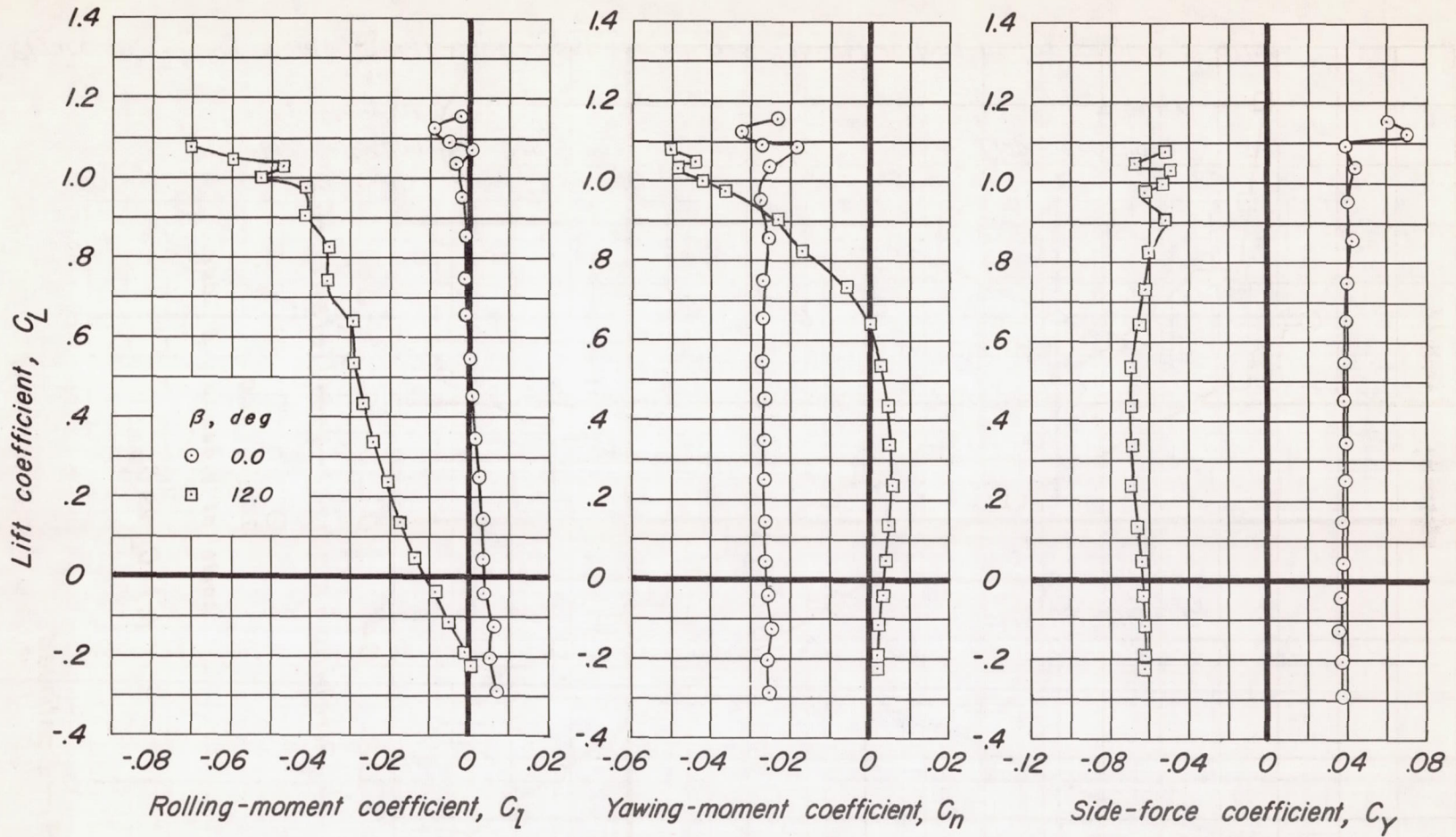
(b) C_L vs C_D .

Figure 19.- Continued.



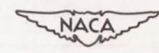
(c) C_L vs C_m .

Figure 19.— Continued.



(d) C_L vs C_l , C_n and C_y .

Figure 19. - Concluded.



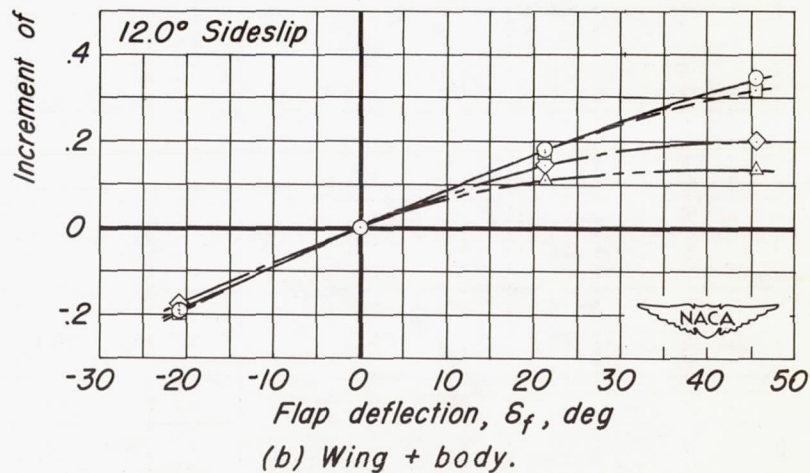
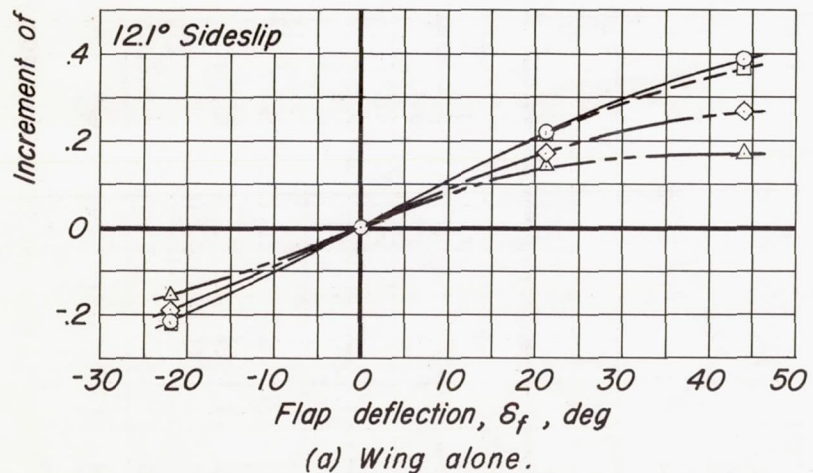
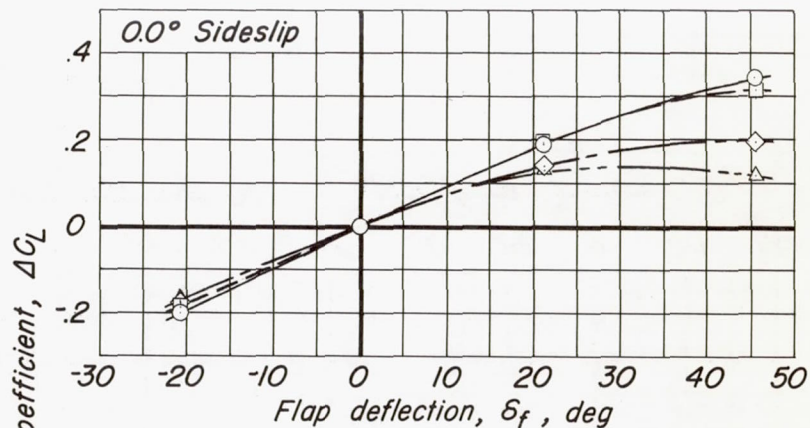
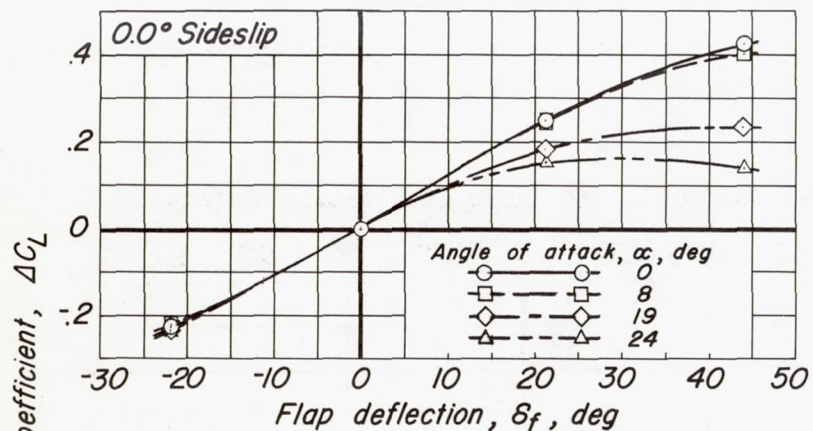
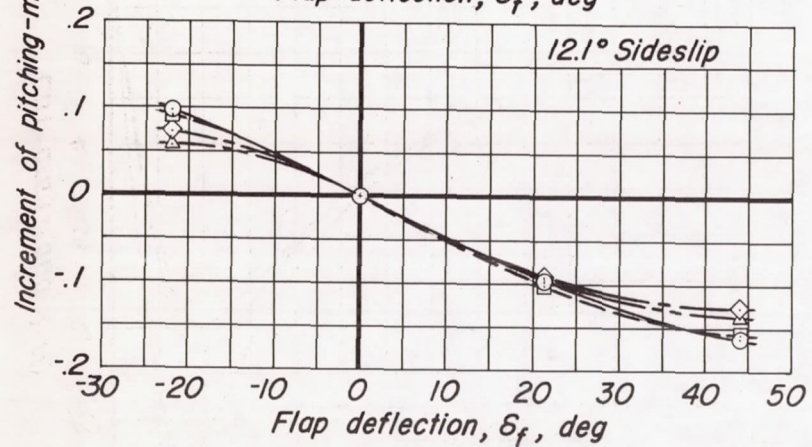
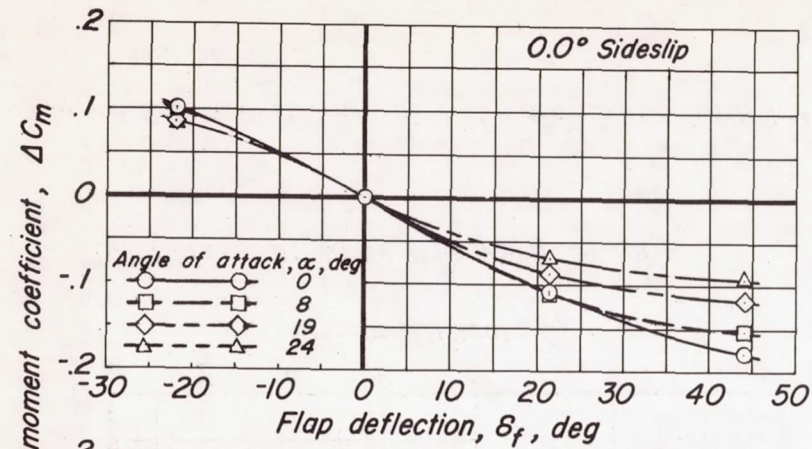
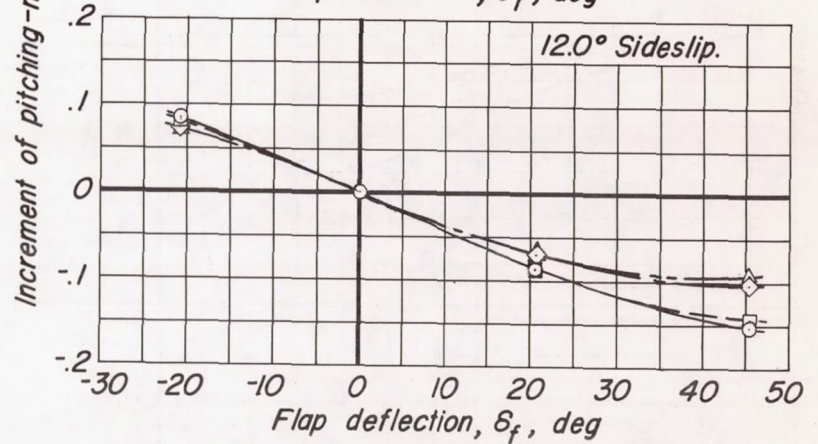
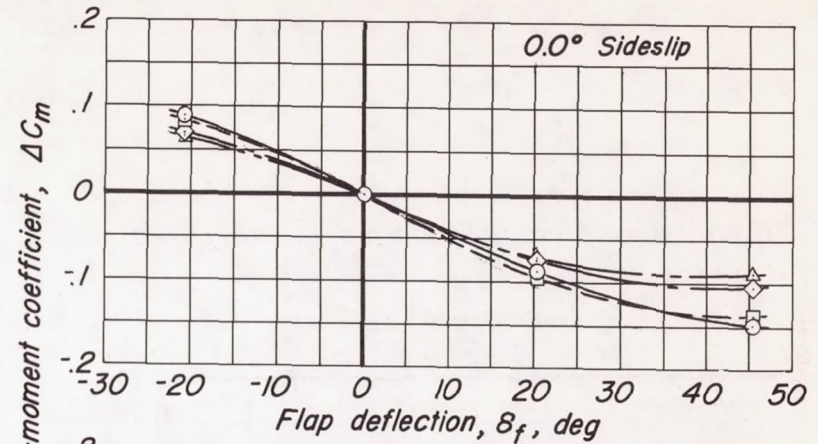


Figure 20.— Increments of lift coefficient for various flap deflections at four angles of attack.



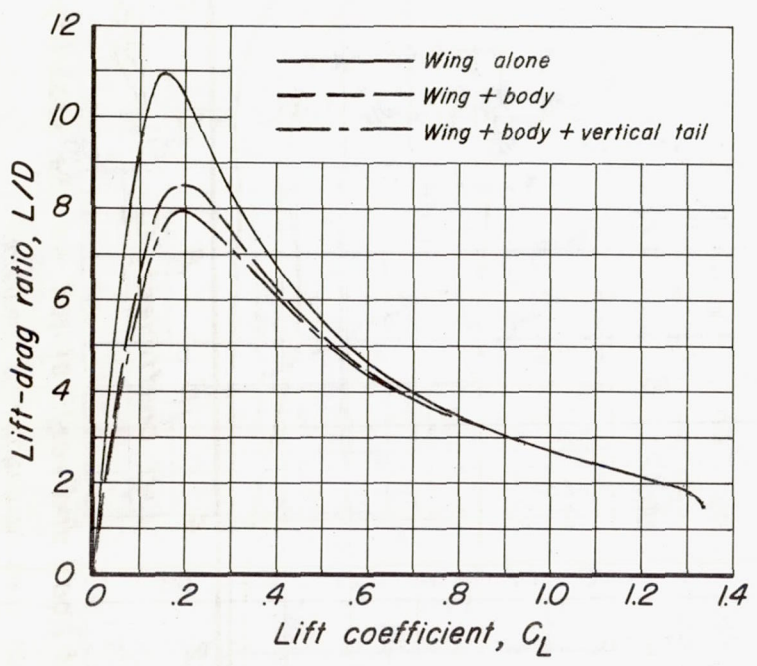
(a) Wing alone.



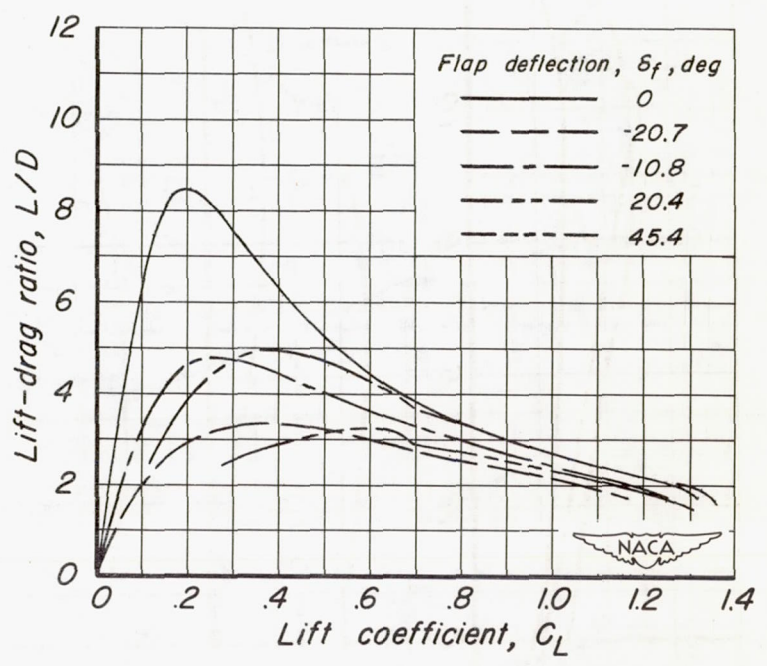
(b) Wing + body.



Figure 21.- Increments of pitching-moment coefficient for various flap deflections at four angles of attack.



(a) Effect of body and vertical tail.



(b) Effect of deflecting flaps ; wing + body.

Figure 22.— Variation of lift-drag ratio with lift coefficient.

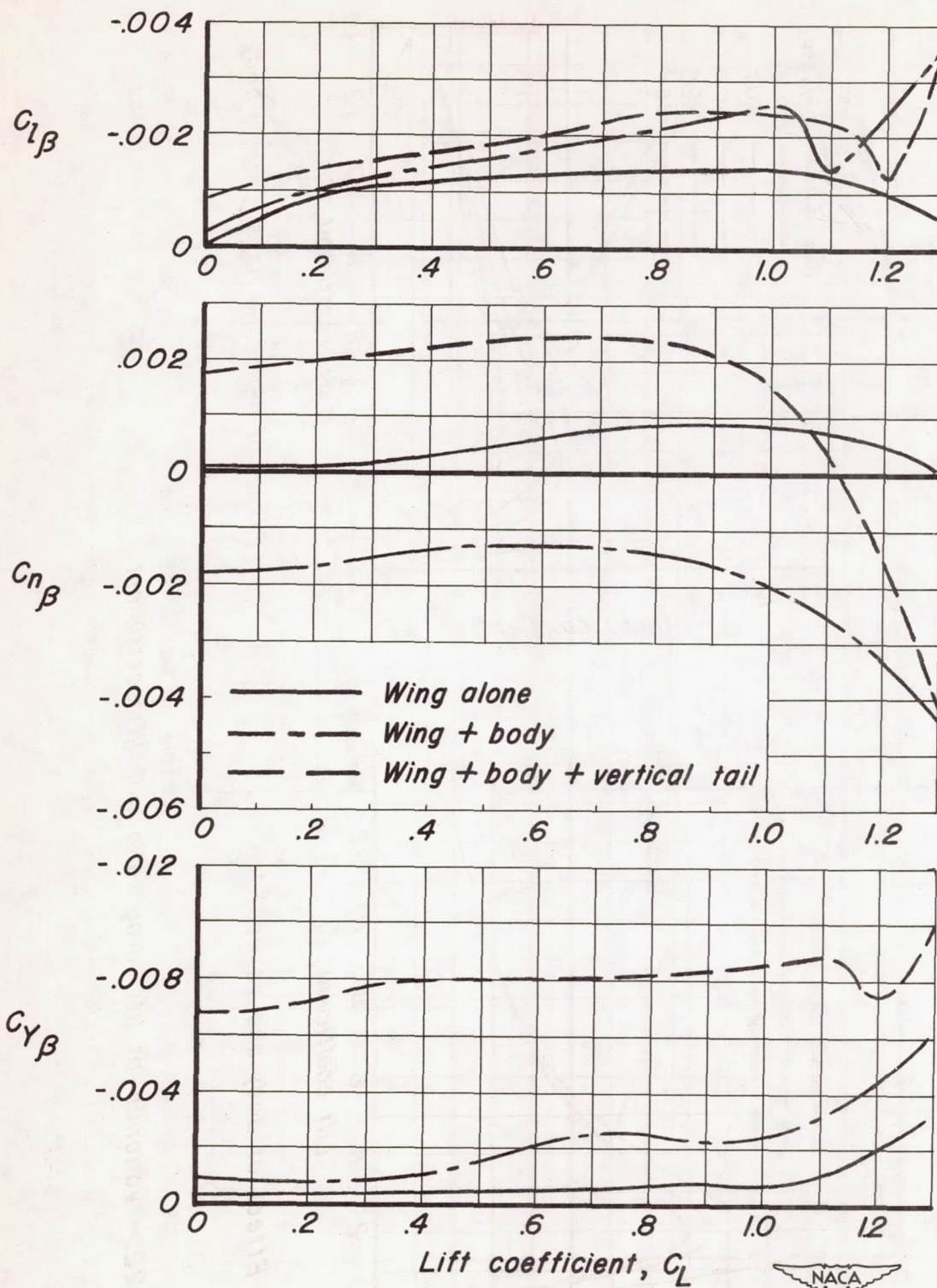
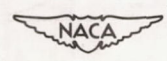


Figure 23. - Effect of body and vertical tail on the stability derivatives.



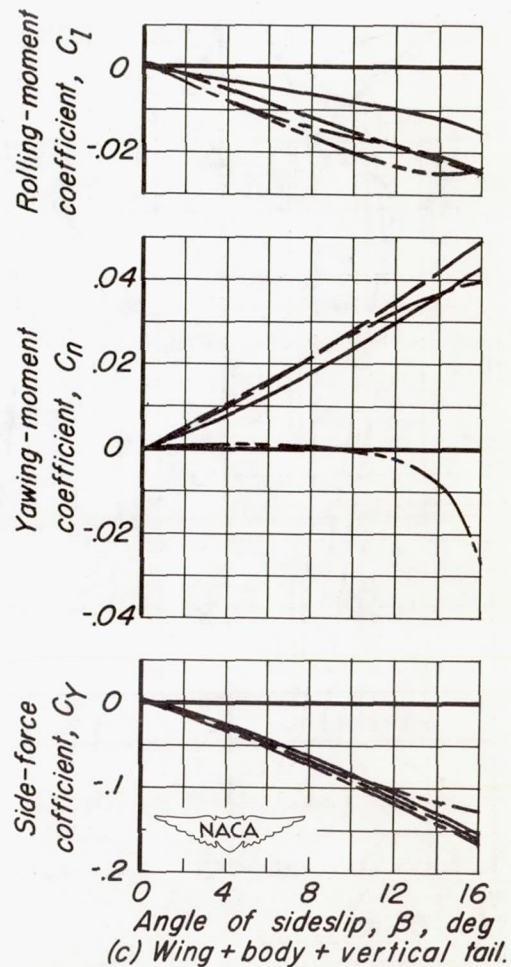
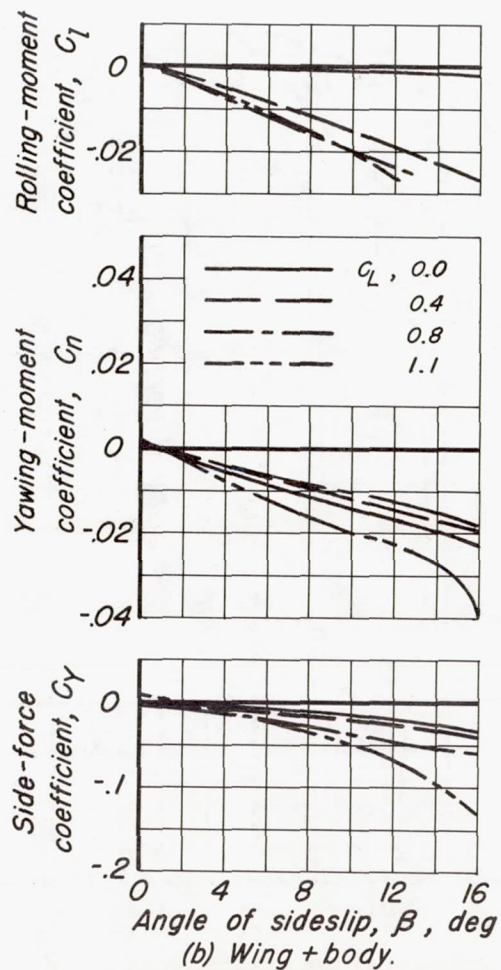
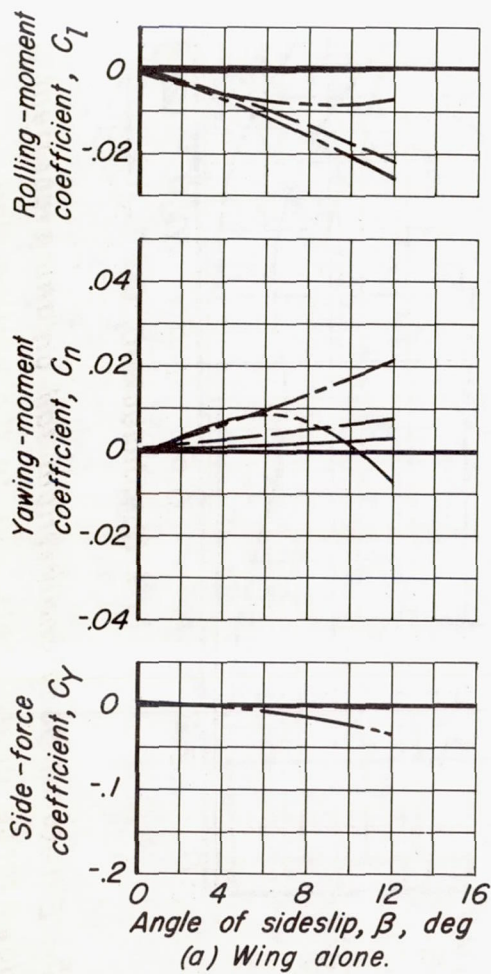


Figure 24. — Variation of rolling-moment, yawing-moment, and side-force coefficients with sideslip at four lift coefficients.

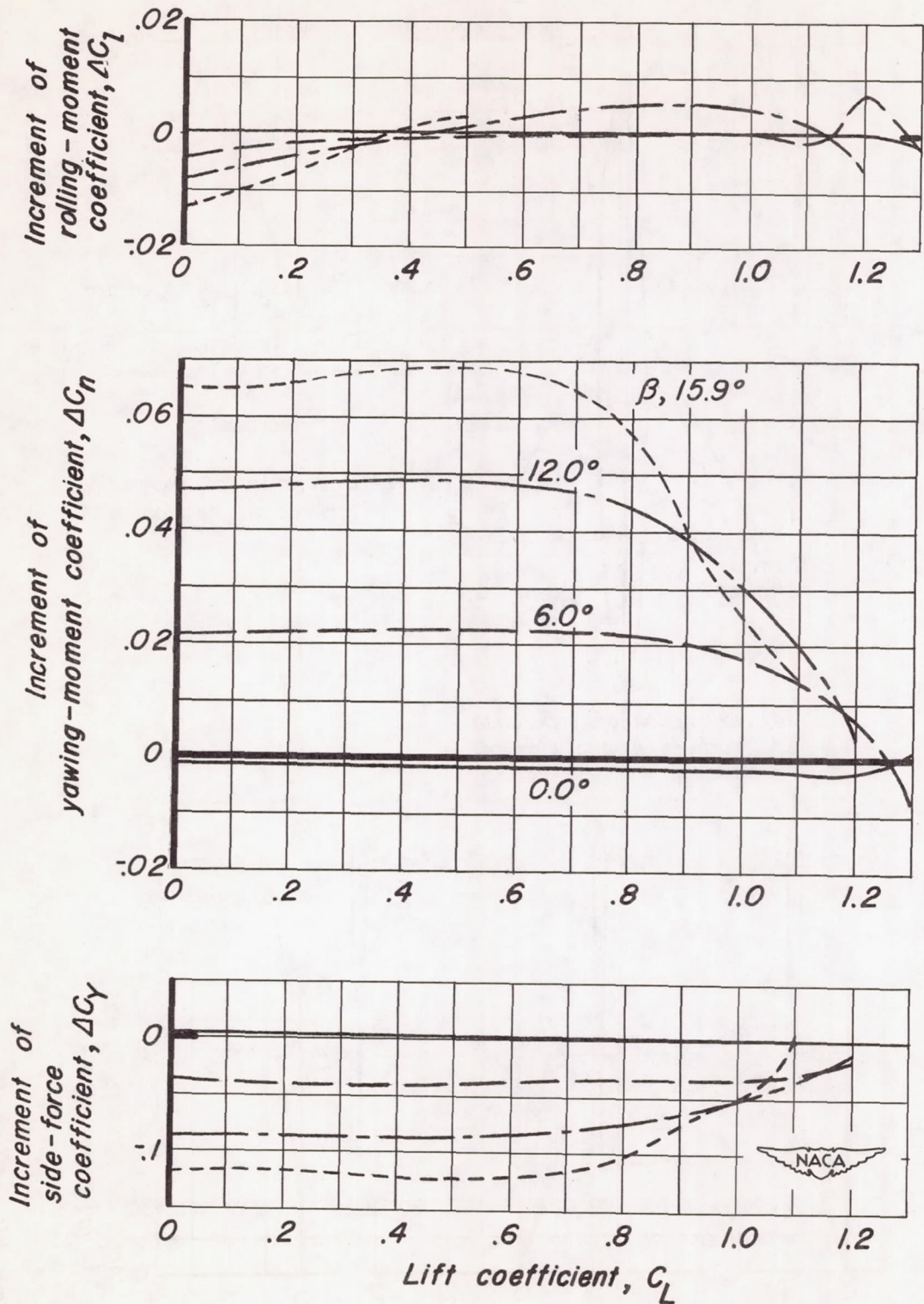
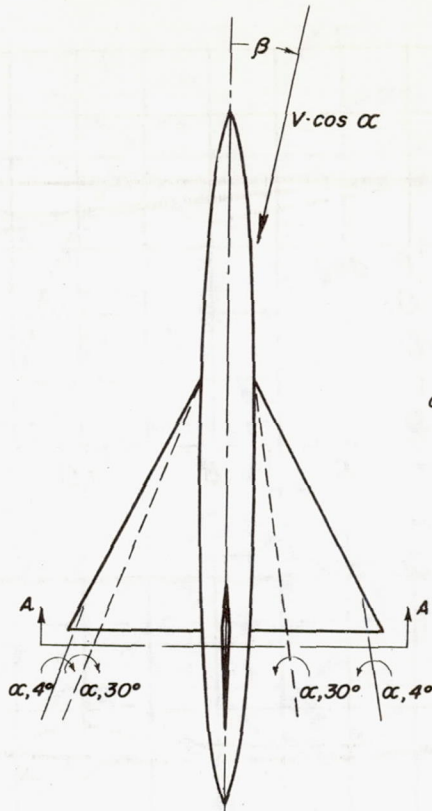
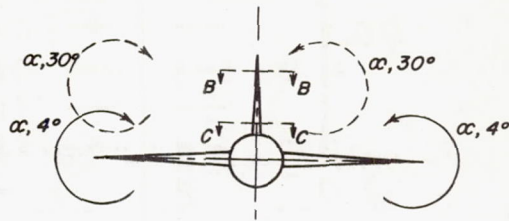


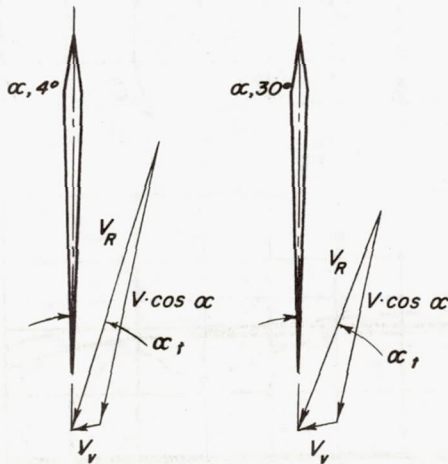
Figure 25.— Increments of rolling-moment, yawing-moment, and side-force coefficients due to the vertical tail.



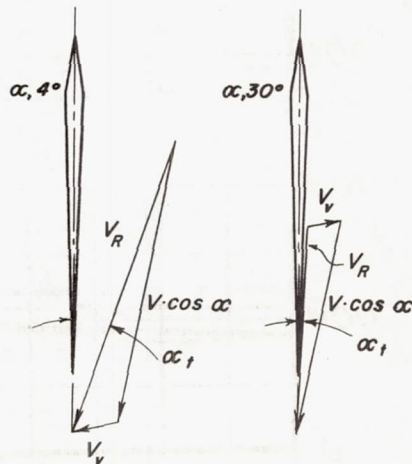
(a) Orientation of separation vortices in plan view of model.



(b) Orientation of separation vortices at section A-A.



(c) Velocity-vector diagram for vertical tail at section B-B.



(d) Velocity-vector diagram for vertical tail at section C-C.



Figure 26.— Influence of separation vortices on the angle of attack of the vertical tail surface.

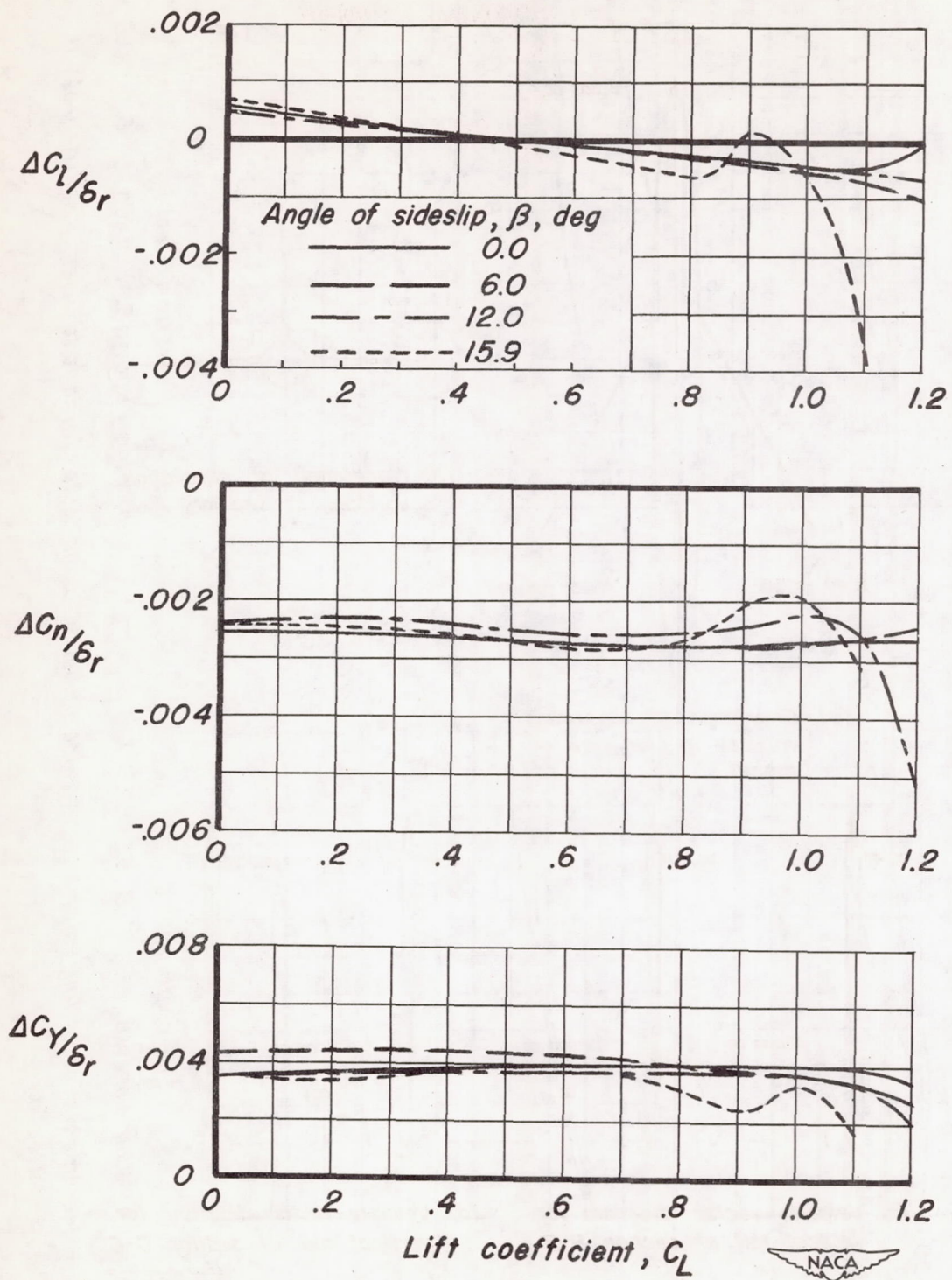
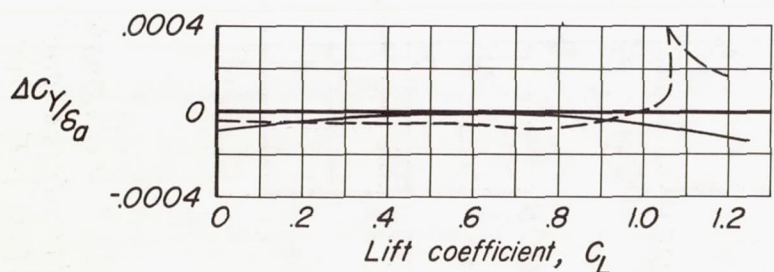
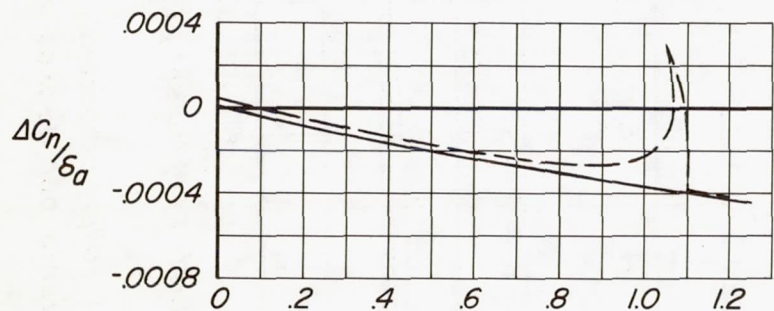
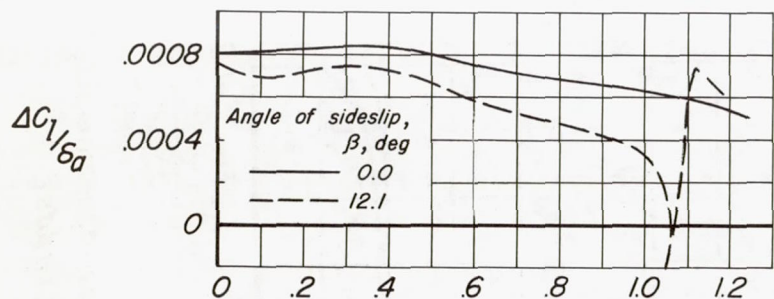
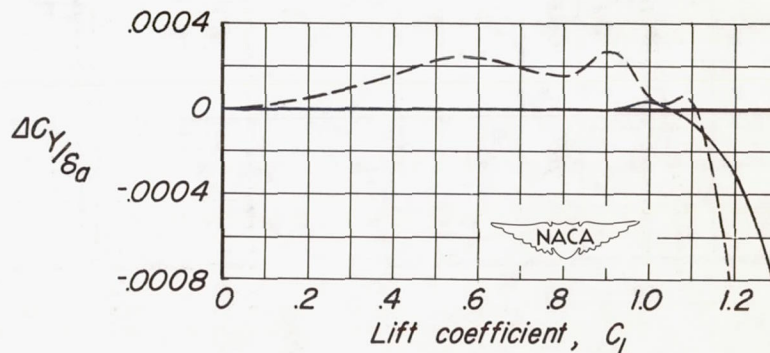
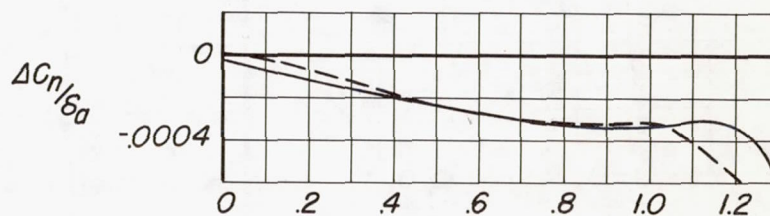
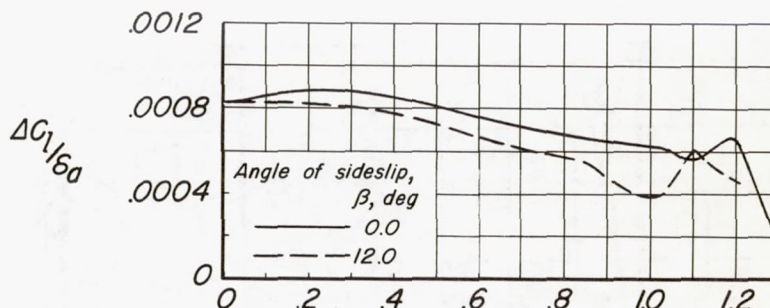


Figure 27. — Increments of rolling-moment, yawing-moment, and side-force coefficients per degree of rudder deflection; $\delta_r = 10^\circ$.



(a) Wing alone ($\delta_{aL} = +11.7^\circ$ & $\delta_{aR} = -11.3^\circ$).



(b) Wing + body ($\delta_{aL} = +10.8^\circ$ & $\delta_{aR} = -10.8^\circ$).

Figure 28. — Increments of rolling-moment, yawing-moment, and side-force coefficients per degree of total aileron deflection.